

D35 – UAS Data Analysis Report

Temporal Monitoring of Riparian Vegetation Condition in Desert Ecosystems



Prepared for:
Clark County, Nevada – Desert Conservation Program

January 3, 2022

Prepared by:
Alta Science and Engineering, Inc.
1220 Big Creek Road, Suite A
Kellogg, Idaho 83837
alta-se.com

Contents

Section 1	Introduction.....	1
1.1	Purpose and Need.....	2
1.2	Site Description.....	4
Section 2	Field Data Collection.....	6
Section 3	Methods.....	7
3.1	Data Processing	7
3.2	Data Analysis.....	8
Section 4	Selected Analysis Examples.....	9
4.1	Cover – land cover classification.....	9
4.2	Cover and Height – convex hulls with maximum heights.....	14
4.3	Height and Density – Leaf Area Density (LAD)	15
4.4	Greenness – NDVI / MSAVI.....	17
Section 5	Paired Sensor Comparisons with Discussion.....	19
5.1	ALS and TLS Comparison	19
5.2	Multispectral imagery and RGB imagery	21
5.3	Summary and Conclusions	25
Section 6	References	28

Tables

Table 1.	Data analyses conducted for each sensor	8
Table 2.	Land cover classes used in land cover classification.	10
Table 3.	Land cover classification model performance using random forest supervised classification.	11
Table 4.	Land cover type classification errors. Cell values are counts of training locations of a true land cover type and their predicted land cover type.	13
Table 5.	Vegetation indices used in this study for assessing the cover and ‘greenness’ of vegetation.....	18
Table 6.	Green vegetation and bare soil areas based on interpretation of NDVI and MSAVI vegetation indices.	18
Table 7.	Comparison of width, discreteness, resolution, analysis advantages, and cost for multispectral sensors and RGB digital cameras.....	22
Table 8.	Relative level of quality achieved by each sensor for each analysis/attribute. Some analyses have substantially higher quality results when >1 sensor’s data are combined.....	25
Table 9.	General comments for RGB, multispectral, ALS, and TLS sensor data collection and subsequent data analysis	26

Figures

Figure 1. Study Area Location and Data Extents	5
Figure 2. Landcover classification results from Model 6, including PC1 + PC2 + PC3 + PC4 + PC5 + NDSI + NDWI + CHM + Blue index.	12
Figure 3. Individual detected convex hulls for TP 3, using the ALS-derived canopy model and symbolized using RGB-interpreted plant species information.	14
Figure 4. Area and height of convex canopy hulls by species (or species mix) at TP 3.....	15
Figure 5. Illustration showing the Leaf Area Density (LAD calculation). Taken from Almeida et al., 2019.....	16
Figure 6. LAD calculation for TP1, TP2, and TP3, calculated from ALS data.	16
Figure 7. Leaf Area Density (LAD) for plot 3, aligned with TLS point cloud data to illustrate the LAD calculation and interpretation.	17
Figure 8. NDVI (a) and MSAVI (b) image comparison of greenness for approximately 43 ha of the study site.	19
Figure 9. TLS and ALS point cloud comparison at target plot 1.	21
Figure 10. Red, green, and blue spectral sensitivity comparison for commercial RGB digital cameras and multispectral sensors.....	23
Figure 11. Site Imagery illustrating differences in the RGB and multispectral sensors.	24

Appendices

Appendix A Ground based data collection field sheets and photo log	A
Appendix B Quality Assurance / Quality Control (QA/QC) information for UAS sensor data processing	B

Acronyms and Abbreviations

ALS	Areal Laser Scanner
Alta	Alta Science & Engineering, Inc.
AMMP	Adaptive Management and Monitoring Plan
Aridlands	Aridlands, LLC
ANOVA	Analysis Of Variance
BGO	Biological Goals and Objectives
CHM	Canopy Height Model
CRR	Canopy Relief Ration
DCP	Desert Conservation Program
DLS	Downward Light Sensor
DSM	Digital Surface Model
FAA	Federal Aviation Administration
GCP	Ground control points
GNSS	Global Navigation Satellite System
GSD	Ground Sampling Distance
LAD	Leaf Area Density
LAI	Leaf Area Index
LiDAR	Light Detection and Ranging
MSAVI	Modified Soil-Adjusted Vegetation Index
MSHCP	Multiple Species Habitat Conservation Plan
NDSI	Normalized Difference Salinity Index
NDVI	Normalized Difference Vegetation Index
NDWI	Normalized Difference Water Index
NIR	Near Infrared
OPUS	Online Positioning User Service
PC	Principal Component
QA/QC	Quality Assurance / Quality Control
RF	Random Forest
RGB	Red, Green, Blue
RMSE	Root Mean Square Error
RTK	Real-Time Kinematic
TBC	Trimble Business Center
TLS	Terrestrial laser scanner

TP	Target Plot
UAS	Unmanned Aircraft System
USFWS	U. S. Fish and Wildlife Service
VI	Vegetation Indices

Units

cm	centimeter
ha	hectare
m	meter
m ²	square meter
mg/kg	milligrams per kilogram
mm	millimeter

Section 1 Introduction

Quantifying vegetation metrics has long been a focus of management and monitoring of avian habitats. Habitat quality, as reflected in vegetation conditions, provides the underpinning of animal species' occurrence and population performance over time. Thus an important component of maintaining avian populations of interest is maintaining habitat quality. In the eastern Mojave desert, riparian vegetation conditions have been declining over the past >30 years in response to long-term drought and invasive species (Albano et al. 2020).

Concomitantly, Mojave bird communities have collapsed over the past 100 years, both declining in species richness and occupied area (Iknayan and Beissinger 2018). To address these declines, planning for conservation actions requires knowledge of if, where, and how vegetation metrics are changing. Monitoring vegetation condition in these riparian areas is thus critical, both for monitoring the vegetation communities themselves and for monitoring habitat quality for resident avian populations.

Historically, vegetation conditions have been assessed via field-intensive and expensive survey methods (Sankey et al. 2018). More recently, technological advancements are enabling habitat quantification at finer resolutions, larger spatial scales, and for reduced costs (Gómez-Sapiens et al. 2021). In particular, the use of multispectral imagery and Light Detection and Ranging (LiDAR) are being deployed to improve the scale and accuracy of vegetation metrics (Acebes et al. 2021). For example, recent work has tested the ability of multispectral imagery and LiDAR to identify and map fuel class types (García et al. 2011), to classify shrubs and trees in grassland ecosystems (Hellesen and Matikainen 2013), and to identify individual plant species (Sankey et al. 2018, Dashti et al. 2019, Gómez-Sapiens et al. 2021).

The application of multispectral imagery and LiDAR to quantifying animal habitats is fairly recent and has primarily focused on the structure of avian habitats in temperate forests (Bakx et al. 2019, Acebes et al. 2021). This reflects the ease with which LiDAR can quantify canopy structure in forests (Bakx et al. 2019, Burns et al. 2020). Less common is the application of multispectral imagery and LiDAR to quantify habitat quality in dryland riparian areas. Part of the challenge of dryland riparian areas is bright background soil and juxtaposed heterogeneous vegetation types, which has hindered older methods using simple red-green-blue imagery. The application of multispectral imagery and LiDAR can help overcome these challenges by providing information both on multiple bands of spectral reflectance (reflecting species and water balance attributes) and on structural components of heterogeneous dryland vegetation communities (Dashti et al. 2019, Grijseels et al. 2021). For example, monitoring restoration success in dryland riparian habitats can be effectively done at the level of vegetation species groups using both multispectral imagery and LiDAR (Gómez-Sapiens et al. 2021). In some cases, multispectral imagery and LiDAR can identify target desert plant species with an accuracy of 84-89% (Sankey et al. 2018).

While several studies have looked at applications of multispectral and LiDAR data to aspects of dryland vegetation, studies focusing on avian habitat are primarily limited to shrub-grasslands such as the sagebrush steppe (Zabihi et al. 2019). There is currently a lack of understanding of how off-the-shelf technologies can be used to quantify avian habitat in dryland riparian ecosystems. Nonetheless, developing modern cost-effective monitoring methods for dryland riparian avian habitat is a pressing need for conservation of local and regional avian populations. Here, we evaluated the utility of multispectral and LiDAR data to quantify dryland riparian avian habitat in a dryland riparian ecosystem in the eastern Mojave desert. The goal was to evaluate the types of habitat and vegetation metrics that can be obtained and to discuss the costs and benefits of different sensor types given the data they can collect.

1.1 Purpose and Need

The Clark County Desert Conservation Program (DCP) manages Endangered Species Act compliance on behalf of Clark County and the cities of Boulder City, Henderson, Las Vegas, North Las Vegas, Mesquite, and the Nevada Department of Transportation (collectively, the Permittees) through implementation of the Clark County Multiple Species Habitat Conservation Plan (MSHCP) and associated Section 10(a)(1)(B) incidental take permit. The MSHCP was developed to support the incidental take permit, allowing for the “take” of current or future federally listed threatened or endangered species under the Endangered Species Act (RECON 2001). The key purpose of the MSHCP is to balance long-term conservation and recovery of species and habitat within Clark County and the beneficial land use of the growing human population within Clark County (RECON 2001).

Condition K of the incidental take permit stipulates that take of covered avian species is conditioned upon the acquisition of private lands in desert riparian habitats along the Muddy and Virgin rivers and the Meadow Valley Wash (U.S. Fish and Wildlife Service [USFWS] 2001). To comply with this permit condition, the DCP has acquired properties with riparian habitat along the Virgin and Muddy Rivers in Clark County, Nevada.

In addition to acquiring land, the DCP is tasked with monitoring avian habitat quality in acquired desert riparian habitats. The word “quality”, associated with “habitat”, occurs frequently throughout Chapter 2 of the MSHCP (RECON 2001). For example, in Section 2.4.2.2 – Conservation Planning Principles (pg 2-57), the MSHCP states that the reserve system should preserve “the quality of habitat sufficient to allow for...resident species.” Further, in Section 2.6 – Covered Species, Evaluation Species, and Watch List Species (pg 2-173), the MSHCP states that “Multiple species planning efforts...will be evaluated as to the extent to which the plan provides for the quality of natural habitat.” The importance of general habitat quality within the MSHCP is clear, as is the biological importance of habitat quality for covered species. As habitat quality declines, individuals and populations of covered species have fewer resources necessary to maintain their populations, and thus populations will decline. Given both of these factors, the DCP chose to include monitoring habitat quality as an important component of monitoring covered species populations themselves.

Both species and habitat monitoring are integral to informing on achievement of DCP’s Biological Goals and Objectives (BGOs; TerraGraphics 2016). Further, the Adaptive Management and Monitoring Plan (AMMP; TerraGraphics 2017) was developed to lay out the techniques to monitor covered species and the general quality of their habitats and to incorporate the results from this monitoring in a process to ensure that should populations or habitat quality decline, mechanisms are in place to detect those declines and evaluate their causes. At the time of the development of the AMMP, however, the protocols for monitoring general habitat quality (both riparian and desert upland) remained unspecified.

The BGOs and the AMMP are anticipated to be updated in 2022 and one of the focus areas for the update (among other updates) is to establish a protocol for long-term riparian property monitoring within the AMMP. This pilot project was designed to test current and upcoming remote sensing technologies on DCP property to understand whether they should be integrated into long-term habitat quality monitoring within the AMMP. Desired characteristics for DCPs long-term riparian monitoring include:

- Adaptive methods. Monitoring technologies will change over time and methods and measure attributes should be translatable to future methods.
- Cost-effectiveness.

- Straight-forward analysis.
- Comparability to other data sets. The ability to directly compare DCP long-term monitoring data to data collected under other institutions and programs is beneficial for several reasons: 1) Providing context in the case that DCP habitat conditions show a marked-decrease in condition, 2) Ability to combine with larger data sets to interpret trends in habitat, 3) Using established methods increases cost-effectiveness and repeatability.
- Nested and opportunistic monitoring. There may be instances where short-term or project effectiveness monitoring can inform on upland and riparian habitat condition (for example, using low-altitude Unmanned Aircraft System [UAS] aerial imagery or LiDAR to monitor seedling growth and establishment). These types of data should be opportunistically nested into long-term monitoring data and analysis.
- Measuring attributes that will inform on habitat quality for MSHCP-covered riparian species. This is a particular challenge because the six focal riparian species listed in Section 1.2 have diverging habitat requirements. For example, the yellow-billed cuckoo requires a dense canopy >5 meters (m) tall with a diverse vertical structure, whereas the vermilion flycatcher requires open habitat with scattered trees and does not tolerate a dense understory or canopy. Designing a monitoring strategy with the aim of identifying quality habitat for all MSHCP-covered avian species is not possible because what may be good habitat for one species is unsuitable habitat for another.

This pilot project was a first step in the process of selecting a final long-term riparian monitoring protocol. Our approach to test the available remote sensing technologies was to select a study area with generally representative species and vegetation density of all DCP-owned riparian properties.

We evaluated and selected attributes that are common to long-term riparian vegetation monitoring and that influence habitat quality for MSHCP-covered avian species:

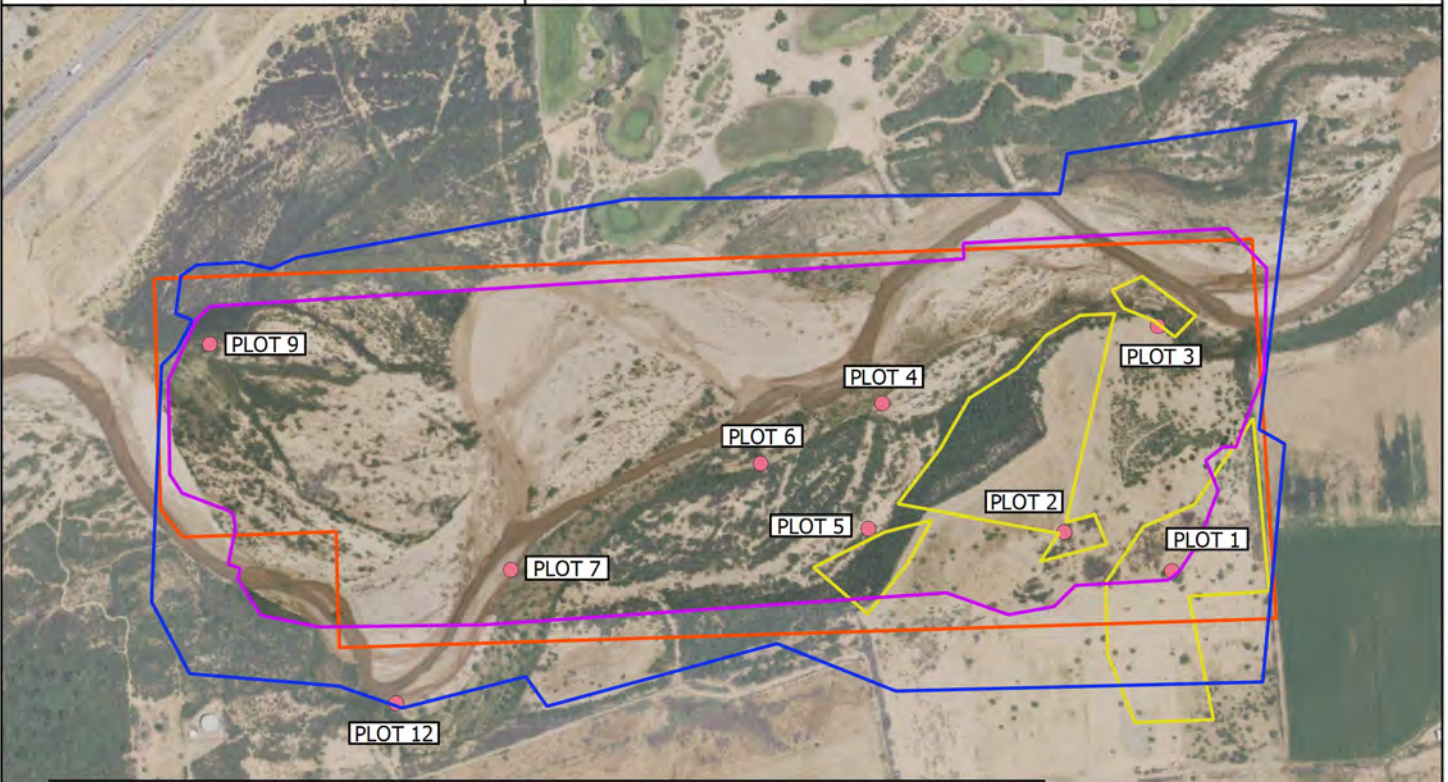
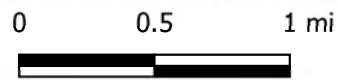
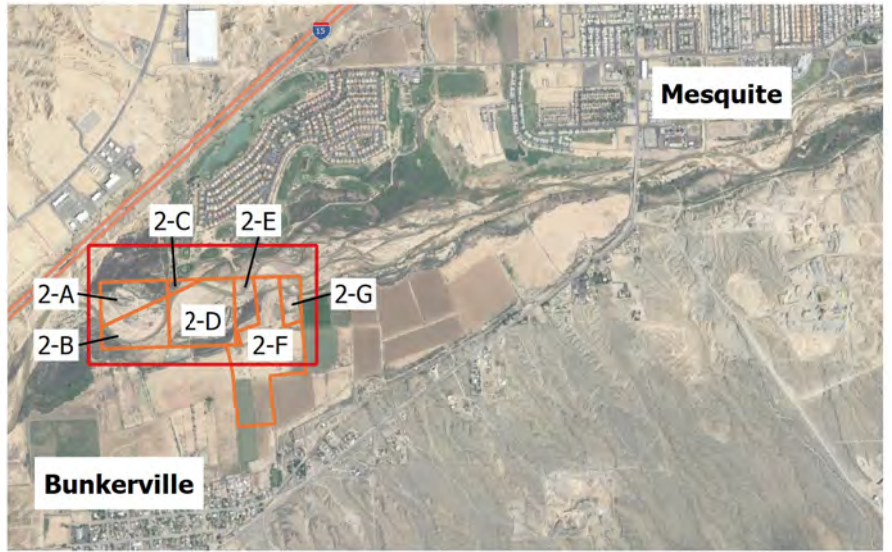
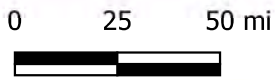
- Cover—Specific measurements or attributes include total cover, composition of herbaceous, woody, bare ground, rock, surface water, etc., as well as cover by functional group, (key) species, and understory vs. overstory.
- Height—Specific measurements or attributes may include overall/average height and height by canopy level.
- Vegetation density—Specific measurements or attributes may include Leaf Area Index (LAI), Leaf Area Density (LAD), Canopy Relief Ration (CRR), Chlorophyll, Normalized Difference Vegetation Index (NDVI)/Modified Soil-Adjusted Vegetation Index (MSAVI), stem count, or similar.
- Vigor/Greenness—Specific measurements or attributes may include live vs stressed vs dead plants, NDVI/MSAVI/TriTGI (visible bands)
- Other metrics such as river bank and floodplain slopes and heights were discussed and are desirable for a long-term monitoring program, but are not as directly related to avian habitat and are not the specific focus of this pilot project.

Several of the attributes listed above are commonly derived from remotely sensed data.

1.2 Site Description

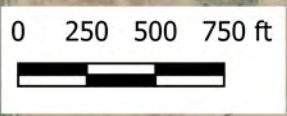
Clark County owns 545.5 acres distributed across sixteen parcels in five locations in the lower Virgin River watershed that contain riparian areas. The study area is comprised of a portion of these parcels at the 'Bunkerville East' location. Bunkerville East consists of 153.54 acres in seven parcels labeled 2-A through 2-G (Figure 1). The parcels are located in the town of Bunkerville across from the southwest corner of the Casablanca Golf Course in Mesquite, Nevada. Bunkerville East includes the active floodplain of the Virgin River, with the river cutting through the site from east to west. Both riparian and upland vegetation are present throughout the study area. A historic levee is also present on the south side of the Virgin River. Additional description of these parcels is included in the *Riparian Reserves Management Plan* (Alta 2021).

The following MSHCP-covered species have been observed on the Virgin River riparian properties (including Bunkerville East) since 2017 (SWCA 2017a, SWCA 2017b, SWCA 2019): southwestern willow flycatcher (*Empidonax traillii extimus*), yellow-billed cuckoo (*Coccyzus americanus*), blue grosbeak (*Passerina caerulea*), Arizona Bell's Vireo (*Vireo bellii arizonae*), summer tanager (*Piranga rubra*), vermilion flycatcher (*Pyrocephalus rubinus*), and phainopepla (*Phainopepla nitens*). Crissal thrasher (*Toxostoma crissale*), an evaluation species, was also observed.



Legend

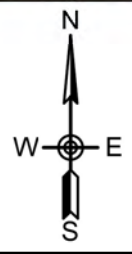
Aerial LiDAR	Multi-Spectral Extents	Ground-Based Plot
RGB Imagery	Terrestrial Laser	



DRAWN BY:
S. MOROSKY

PROJECT MANAGER:
T. HARJU

DATE:
10/13/2021



**OVERVIEW &
DATA EXTENTS
CLARK COUNTY, NV**

Section 2 Field Data Collection

Alta Science & Engineering, Inc. (Alta), Aridlands LLC (Aridlands), and DCP staff collected UAS aerial visible spectrum imagery (Red, Green, Blue [RGB imagery]), UAS aerial multispectral imagery, UAS aerial LiDAR, terrestrial LiDAR, and ground-based vegetation data at the project area on April 7 and 8, 2021. Figure 1 illustrates the footprint for each sensor and the location of ground control plots. Sensors used and data collected included:

- UAS RGB imagery (red, green, and blue bands). A 20MP RGB camera (1" CMOS sensor) was flown on a DJI Phantom 4 Pro V2 quadcopter at an altitude of 80 m to achieve an average ground sampling distance (GSD) of 2.2 centimeters (cm) over approximately 107 acres. This data was collected because (a) it can be used to augment the LiDAR and multispectral data, (b) it collects the highest resolution data, (c) it is the lowest cost and most available type of sensor, and (d) to evaluate whether this type of sensor might be adequate to collect data to characterize riparian vegetation and bird habitats.
- UAS multispectral imagery. A MicaSense RedEdge-MX multispectral sensor was flown on a Draganfly Commander quadcopter at an altitude of 110 m, achieving an average GSD of 7.36 cm over approximately 52 hectares (ha) (128.5 acres; April 7, 2021) and 53 ha (131 acres; April 8, 2021). The RedEdge is a 5-band sensor that collects reflectance data in discrete and narrow wavelength bands that provide information about plant physiological status and are comparable to the wavelength bands collected by Landsat and Sentinel satellite platforms: blue (475±16 nm), green (560±13 nm), red (668±7 nm), red edge (717±6 nm), and near infrared (842±28 nm).
- UAS LiDAR (hereafter Areal Laser Scanner [ALS]). A single return Velodyne LiDAR sensor with 32 individual lasers was flown at a 60m altitude and averaged 86 ground returns per square meter (maximum of approximately 500 ground returns per square meter).
- Terrestrial laser scanner (TLS). A Trimble SX10 robotic total station and laser scanner was deployed at four select locations to collect 360-degree terrestrial scans. Returns ranged from 280 to 120,000 points per square meter in areas within close proximity to where the TLS was stationed. Approximately 15 acres were covered using the TLS.
- Ground control points (GCP). A Trimble R8 Base Station with 1-cm Root Square Men Error (RMSE) accuracy was set up. Nine ground control points were placed throughout the study area and surveyed using a Trimble R10 Real-Time Kinematic (RTK) rover. In addition, A CHC Global Navigation Satellite System (GNSS) Base Station was set on a surveyed point to collect position data for use in ALS trajectory processing. GCPs are used to improve the absolute accuracy in location and measurements (distance, area, height) of all collected data. GCPs were dispersed primarily through the southeastern two-thirds of the study area because the Virgin River restricted access to the northwestern portion of the study area.
- Qualitative vegetation plots. Vegetation species and distributions were characterized at each of the nine GCP locations. Locations were selected to include a broad range of vegetation cover (e.g, predominantly bare ground, dense woody cover, dense herbaceous cover, widely spaced shrubs). The square plots varied in area, from approximately 200 to 576 square meters (m²) (average = 340 m²), with dimensions typically limited by the ability of field crews to penetrate the vegetation. The objectives for these assessments were to identify common species, and mixed species stands, to

parameterize models for land cover characterization. Data collected included a sketch of the plot, including location of the ground control point and individual plants with species identified. Areas that were mixed species were noted as such with the dominant species listed first. Photographs were taken at each plot. Data sheets and a photo log are included as Appendix A.

The ALS, multispectral imagery, and RGB imagery sensors collected data over a slightly different footprint ranging from 107 acres to 130 acres. When ALS, multispectral imagery, and RGB imagery footprints were overlapped, a total of 103 acres was captured by all three sensors and was used as the base footprint for analysis. Appendix B includes additional instrument and quality assurance/quality control QA/QC information.

Section 3 Methods

Methods can be separated into two distinct steps: 1) data processing, and 2) data analysis.

3.1 Data Processing

Data processing differs for each sensor. The processing steps and chosen software varies by sensor type and included Pix4D, Waypoint Inertial Explorer, ScanLook PC, Trimble Business Center (TBC), and Global Mapper.

Pix4D was used to process both the RGB imagery and the multispectral imagery. Multispectral imagery was collected during two overlapping missions (Figure 1). The first mission (April 7, 2021) covered 52 ha and consisted of 3,560 images (730 images per band) and included 7 GCPs. The second mission (April 8, 2021) covered 53 ha and consisted of 2,995 images (599 per band) and included 5 GCPs. Processing and creation of radiometrically calibrated, georectified reflectance orthomosaics for each mission was completed using Pix4Dmapper (ver. 4.6.4). Additional processing outputs from Pix4DMapper included: (a) point cloud classification (to improve digital terrain model generation), (b) a 3D textured mesh, (c) a raster digital surface model, and (d) merged geotiff orthomosaic and reflectance maps. Radiometric calibration of each image was accomplished using sun irradiance and sun angle data collected by a MicaSense Downward Light Sensor (DLS; mounted on the top of the drone) and attached as EXIF data to each image, as well as pre- and post-flight captures of a calibrated reflectance panel.

The RGB imagery was collected during a single multi-flight mission (Figure 1). As with the multispectral imagery, processing and creation of a georectified orthomosaic was completed using Pix4Dmapper. Additional processing outputs included: (a) point cloud classification, (b) a 3D textured mesh, (c) a raster digital surface model (i.e., “structure from motion”), and (d) a merged geotiff orthomosaic. No radiometric calibration was completed or necessary.

The ground control points (RTK data) were Online Positioning User Service (OPUS) corrected to georectify site-wide survey control.

ALS data underwent trajectory processing using Waypoint Inertial Explorer and the CHC Base data. This step precisely locates the ALS sensor throughout the flight for ALS data accuracy. Next the ALS data were overlain on the Trajectory using ScanLook PC. Global Mapper was used for ground classification of the ALS Point Cloud. The points classified as ‘ground’ were then vertically rectified using the survey ground control points. After the ALS data was rectified it was used to build a Digital Surface Model (DSM) for further analysis.

TLS data were processed using the point cloud add-on to TBC. This resulted in georectified point clouds and 360-degree photographs at each location that were used for further analysis.

The relevant processing steps described above for ALS were built into the TBC process for the TLS and do not require separate processing steps for the user.

3.2 Data Analysis

Data analysis was completed using FUSION, ArcMap, QGIS, and Program R (v4.1.0). Several analyses had initial processing or classification steps conducted in FUSION and final statistical modeling and graphs or images completed in Program R or ArcMap. Table 1 shows distinct analyses and the software and packages used in analysis for each sensor's data. Complete code for all analyses exceeds 100 pages and is available upon request.

Most analyses were limited to a 20m x 50m rectangle randomly situated to include each of the ground-based vegetation plots to limit the computational time. In the future, select analyses that inform or promote DCP's conservation projects can be scaled up to the entire study area. The purpose of the analyses listed in Table 1 is limited to the pilot-project level and are designed to test the ability of each sensor's data in conditions unique to DCP's property to see if they are appropriate for long-term monitoring.

Table 1. Data analyses conducted for each sensor

	Analysis	Analysis Software and Packages	Sensor Type		
			RGB	MS	ALS / TLS
Cover	Supervised land cover classification	R - randomForest package	X	X	
	NDVI/MSAVI	QGIS/GRASS – r.reclass function		X	
	Individually detected hull area	FUSION –ConopyModel, then R-lidR package			X
	Cover	FUSION - Gridmetrics			X
	Canopy Relief Ratio (CRR)	FUSION - Gridmetrics			X
	Initial classification (Surface water, bare ground, rocks, etc)	Global Mapper or FUSION			X
Height	Maximum height from hulls	See Hull Area analysis, above.			X
	Structure from Motion (SFM)	Global Mapper (RGB) / PIX4D (MS)	X	X	
Density	Leaf Area Index (LAI)	R - RStoolbox and Raster packages		X	
	Leaf Area Density (LAD)	R - lidR package			X
	Chlorophyll (GCI and MCARI)	R - RStoolbox and Raster packages		X	
	Stem Count	FUSION –ConopyModel, then R-lidR package			X
Greenness	NDVI/MSAVI	R - RStoolbox and Raster packages		X	
	Live vs dead	Calculated as part of the land cover classification (green vs. brown)			
Other	Terrain modeling - DEM / DTM	Global Mapper / FUSION			X
	Surface modeling - DSM	Global Mapper (RGB) / PIX4D (MS)	X	X	

Section 4 Selected Analysis Examples

Each analysis listed in Table 1, above, was performed because they inform at least one of the overarching attributes that are expected to be part of the DCPs long-term riparian monitoring program (see Section 1.1, above). The purpose of this pilot study was to focus on which sensors produce the most applicable data for use in long-term monitoring and that meet the desired characteristics listed in Section 1.1, above. To this end, we selected a sample of the analyses listed in Table 1 to illustrate how each sensor's data may be used, and how the quality of analyses increase with the use of additional sensors data.

4.1 Cover – land cover classification

Primary sensor used for this analysis: Multispectral sensor

Secondary sensor/data used as additional information: Ground-based data sheets and photos were relied on to create the training data.

Land cover classification is the assignment of pieces of a landscape to one of a set of user-defined discrete mutually exclusive bins (e.g., bare ground, vegetated, or water). Identifying the dominant land cover type across a landscape is an important part of identifying and monitoring individual habitats and general habitat quality. For example, long-term trends from a dryland mixed tree, shrub, bare ground, and water riparian ecosystem to a bare ground and water riparian ecosystem would reflect an obvious decline in avian habitat ecology for most species.

Land cover classification, like any classification system, is inherently imperfect but can be a useful way to understand how landscapes are configured. Accuracy of land cover classifications are partially an effect of input data accuracy, spatial resolution, and accuracy of the prediction algorithm. Here, we tested the ability of the sensors described in Section 2 to delineate 17 land cover types (Table 2) within the pilot project area, and validated the land cover classifications using the qualitative vegetation methods described in Section 2.

Table 2. Land cover classes used in land cover classification.

Basic	Acceptable	Really Good	Great	Highest detail	
1	2	3	4	5	
Vegetation	Photosynthesizing (green leaves)	Shrubs	Desirable	ATLE	Quailbush (GRN)
				BASA4	Mule-fat (GRN)
				ER spp	Rabbitbrush (GRN)
				PLSE	Arrowweed (GRN)
		Trees	Desirable	PRGLT	Honey mesquite (GRN)
				SAGO	Goodding's willow (GRN)
	Trees	Desirable	Undesirable	TARA	Tamarisk (GRN)
			Undesirable	PRPU	Screwbean mesquite
	Undesirable	PRGLT		Honey mesquite (BRN)	
		Undesirable	TARA	Tamarisk (BRN)	
Dead	Woody (logs, etc)		WOOD		
	Herbaceous				
Soils and other ground cover	Dry soil	Bright		DRY	
		Less bright			
	Wet soil (mud)			MUD	
	Salt encrusted surfaces			SALT	
	Rock (and concrete)			RCK	
Open water				WATR	
Shadow				SHAD	

Supervised classification involves combining 'training' data with the input data to train the statistical model on how to classify sites based on the associations of the input data with the training data. For example, one might tell the program that locations A, B, and C are known to be vegetated, bare ground, and water, respectively. The program then uses the combinations of values of the input data at locations A, B, and C to assign all locations in the analysis area to one of these groups based on each location's combinations of values of input data. The predicted land cover class is then compared to the training cover class to evaluate accuracy of the predictions. Different types of input data are expected to result in varying levels of prediction accuracy.

We tested the ability of six supervised classification models to classify the pilot project area into 17 land cover classes using random forest (RF) analyses (Table 3). The six models ranged from simple (original 5-band multispectral data only) to increasingly complex versions involving multiple principal components (PCs) and derived imagery metrics (e.g. Normalized Difference Water Index, NDWI). PCs are new variables that are linear recombinations of related values from a set of input variables. PCs maximize the common information across the input variables in the newly recombined variables. They are then interpreted by the analyst based on the contributions of each input variable on each recombined variable. We used PCs of the 5-band multispectral data to extract physical and biological information from the bands. For example, the first and most important principal component of 5-band multispectral data usually captures most of the variation in the data set and represents differentiation of bare ground versus vegetation (Schirrmann et al. 2016). All supervised classification analyses were performed using the randomForest package in Program R.

Table 3. Land cover classification model performance using random forest supervised classification.

Model number	Model	Overall Accuracy ^a	Kappa ^b	No. of Parameters ^c
6	PC1 + PC2 + PC3 + PC4 + PC5 + NDSI + NDWI + CHM + Blue index ^d	0.894	0.886	9
5	PC1 + PC2 + PC3 + NDSI + NDWI + CHM + Blue index	0.874	0.864	7
4	Blue + Green + Red + Red-edge + NIR + NDSI + NDWI + CHM + Blue index ^e	0.853	0.841	9
3	PC1 + PC2 + PC3 + PC4 + PC5	0.817	0.803	5
1	Blue + Green + Red + Red-edge + NIR	0.771	0.754	5
2	PC1 + PC2 + PC3	0.749	0.729	3

^aThe percentage of correctly classified land cover types.

^bOverall accuracy adjusted by imbalanced frequency of cover type occurrence.

^cNumber of predictive parameters (i.e., model complexity).

^dPrincipal Component X (PCX); Normalized Difference Salinity Index (NDSI); Normalized Difference Water Index (NDWI); Canopy Height Model (CHM); Blue light band (Blue Index)

^eMultispectral light bands: Blue, Green, Red, Red-edge, and Near Infrared (NIR)

We found that more complicated models (i.e., higher number of predictive parameters) performed better at predicting land cover types, ranging from an overall accuracy of 0.749 (frequency-adjusted accuracy kappa = 0.729) for a model with only the first three principal components to an overall accuracy of 0.894 (kappa = 0.886) for the model with all five principal components plus four additional imagery metrics (Table 3; Kedia et al. 2021). Performance of the best model was very good, with ~89% of test locations having a correct land cover assignment by the random forest algorithm.

Not all landcover cover types were equally predicted accurately. The accuracy of predicting the training data for Model 6 (the best performing model, overall accuracy of 0.894) is shown in Table 3. Green quailbush (*Atriplex lentiformis*, ATLE-GRN), mud (MUD), and water (WATR) were most accurately predicted, with zero classification errors (Table 4). Several cover types also had < 5% error rates, including green mule-fat (*Baccharis salicifolia*, BASA4-GRN), brown honey mesquite (*Prosopis glandulosa* var. *torreyana*, PRGLT-BR), brown screwbean mesquite (*Prosopis pubescens*, PRPU-BR), green Goodding's willow (*Salix gooddingii*, SAGO-GRN), and salt (SALT). Rock (RCK) and wood (WOOD) cover types were least accurately classified, with 20.9% and 31.2% of training cells, respectively, misclassified as another cover type (Table 4). The final from Model 6 results are shown in Figure 2.

This analysis was selected as an example for several reasons: 1) land cover classification is common in habitat monitoring and will likely be a required element of DCPs long-term monitoring plan; 2) because it performed better than other analyses at quantifying and classifying cover (see section 4.2, below); and 3) the analysis is unique and has potential to contribute to the scientific community and inform on methods and data that may be used by others to perform land cover classification in similar ecosystems.

Figure 2. Landcover classification results from Model 6, including PC1 + PC2 + PC3 + PC4 + PC5 + NDSI + NDWI + CHM + Blue index.

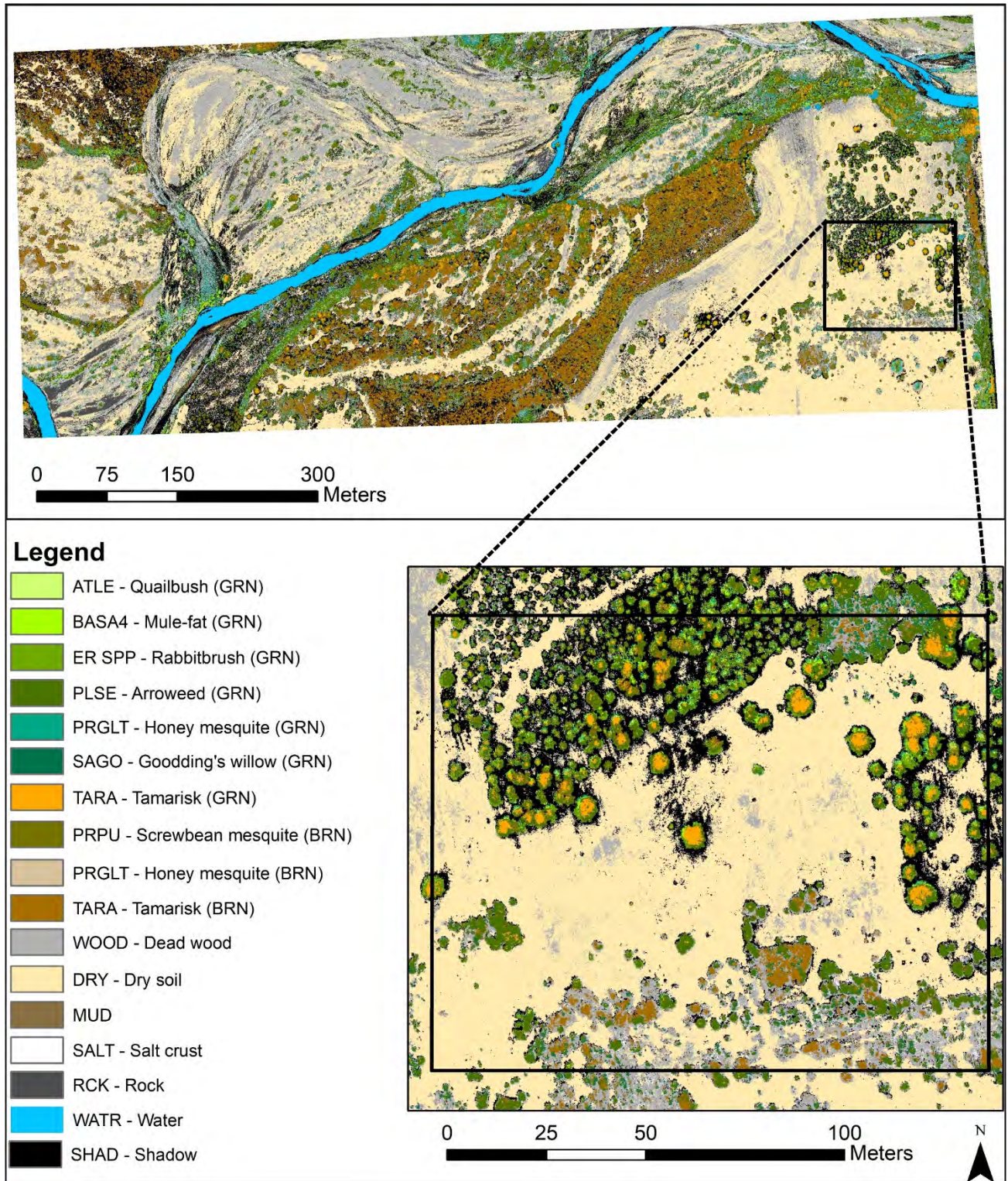


Table 4. Land cover type classification errors. Cell values are counts of training locations of a true land cover type and their predicted land cover type.

True land cover type	Predicted land cover type ^a																	Error ^b
	ATLE-GRN	BASA4-GRN	DRY	ER SPP-GRN	MUD	PLSE-GRN	PRGLT-BR	PRGLT-GRN	PRPU-BR	RCK	SAGO-GRN	SALT	SHAD	TARA-BR	TARA-GRN	WATR	WOOD	
ATLE-GRN	15	0	0	0	0	0	0	0	0	0	0	0	0	0	0	0	0	0.000
BASA4-GRN	0	41	0	0	0	0	1	0	0	0	0	0	0	0	0	0	0	0.024
DRY	0	0	55	0	0	0	0	0	0	3	0	0	0	0	0	0	2	0.083
ER SPP-GRN	0	1	0	42	0	0	1	1	0	0	0	0	0	0	0	0	0	0.067
MUD	0	0	0	0	21	0	0	0	0	0	0	0	0	0	0	0	0	0.000
PLSE-GRN	0	2	0	0	0	62	0	0	2	0	3	0	0	0	4	0	0	0.151
PRGLT-BR	0	0	0	0	0	0	23	0	1	0	0	0	0	0	0	0	0	0.042
PRGLT-GRN	0	0	0	0	0	0	0	13	1	0	0	0	0	0	0	0	1	0.133
PRPU-BR	0	0	0	0	0	1	1	0	60	0	0	0	0	1	0	0	0	0.048
RCK	0	0	1	0	0	0	0	0	0	34	4	1	0	1	0	0	2	0.209
SAGO-GRN	0	0	0	0	0	1	0	0	1	0	99	0	0	0	2	0	1	0.048
SALT	0	0	0	0	0	0	0	0	0	0	0	27	0	0	0	0	1	0.036
SHAD	0	0	1	0	0	0	0	0	2	0	0	0	70	0	0	0	1	0.054
TARA-BR	0	0	0	0	0	1	0	0	2	0	0	0	2	56	0	0	4	0.138
TARA-GRN	0	0	0	0	0	1	0	0	0	0	4	0	0	0	68	0	0	0.068
WATR	0	0	0	0	0	0	0	0	0	0	0	0	0	0	0	75	0	0.000
WOOD	0	1	5	0	0	1	0	0	1	0	3	3	5	5	0	0	53	0.312

^aPredicted land cover types: quailbush, green (*Atriplex lentiformis*, ATLE-GRN); mule-fat, green (*Baccharis salicifolia*, BASA4-GRN); dry soil (DRY); rabbitbrush, green (*Ericameria* spp., ER SPP-GRN); mud (MUD); arrowweed, green (*Pluchea sericea*, PLSE-GRN); honey mesquite, brown (*Prosopis glandulosa* var. *torreyana*, PRGLT-BR); honey mesquite, green (*P. glandulosa* var. *torreyana*, PRGLT-GRN); screwbean mesquite, brown (*Prosopis pubescens*, PRPU-BR); rock (RCK); Goodding's willow, green (*Salix gooddingii*, SAGO-GRN); salt (SALT); shade (SHAD); tamarisk saltcedar, brown (*Tamarix ramosissima*, TARA-BR); tamarisk saltcedar, green (*T. ramosissima*, TARA-GRN); water (WATR); and wood (WOOD).

^bProportion of training cells misclassified as an incorrect land cover type.

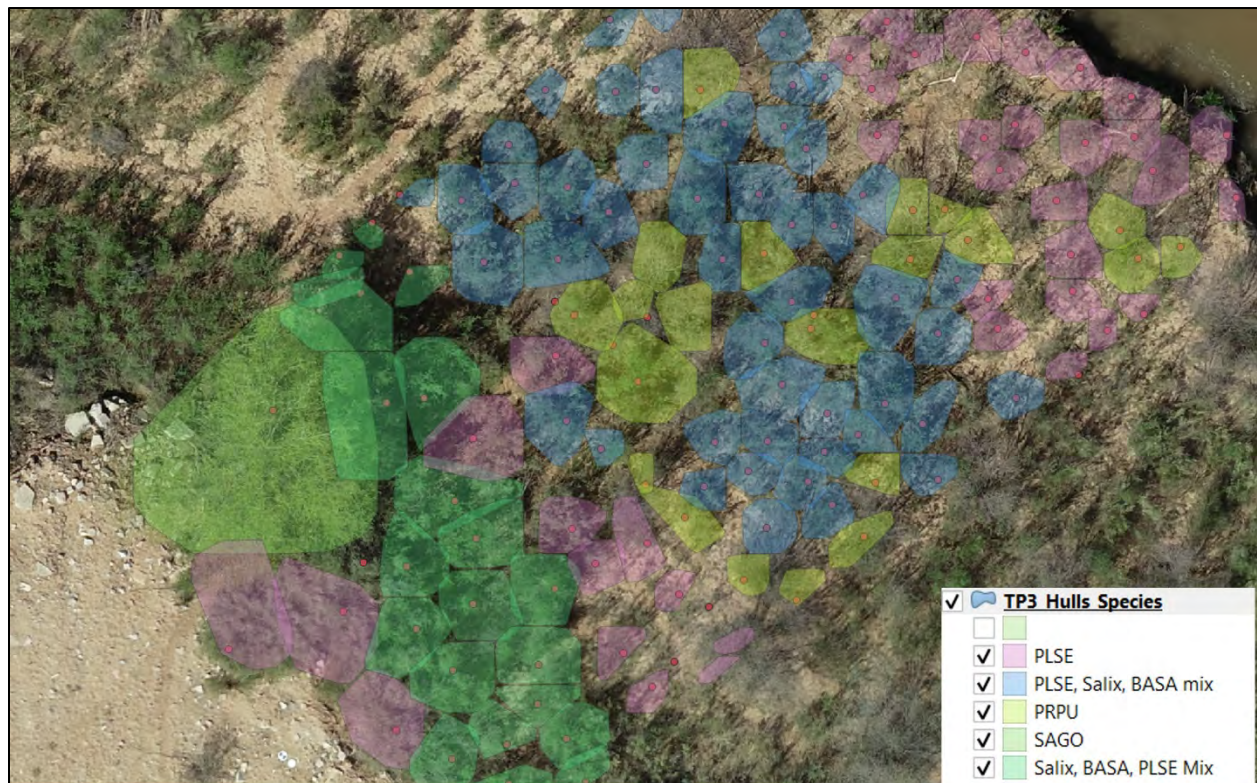
4.2 Cover and Height – convex hulls with maximum heights

Primary sensor used for this analysis: ALS / TLS

Secondary sensor/data used as additional information: RGB imagery, ground-based data sheets and photos.

Canopy hulls with associated maximum heights were calculated for individual plants using a two-stage approach. First, a canopy model was generated in FUSION using point cloud data (ALS or TLS data) and was then analyzed for each target plot using the lidR package in Program R to generate individual tree detected hulls with maximum heights. The aerial coverage of each resulting plant hull can quantify total cover. To expand this analysis further, the resulting plant hulls were overlaid with species polygons that were identified using the RGB imagery paired with the field data sheets and photos taken during field work. Figure 3 shows an example of the ALS plant hulls at target plot 3 (TP3) with RGB-interpreted species information applied to them.

Figure 3. Individual detected convex hulls for TP 3, using the ALS-derived canopy model and symbolized using RGB-interpreted plant species information.

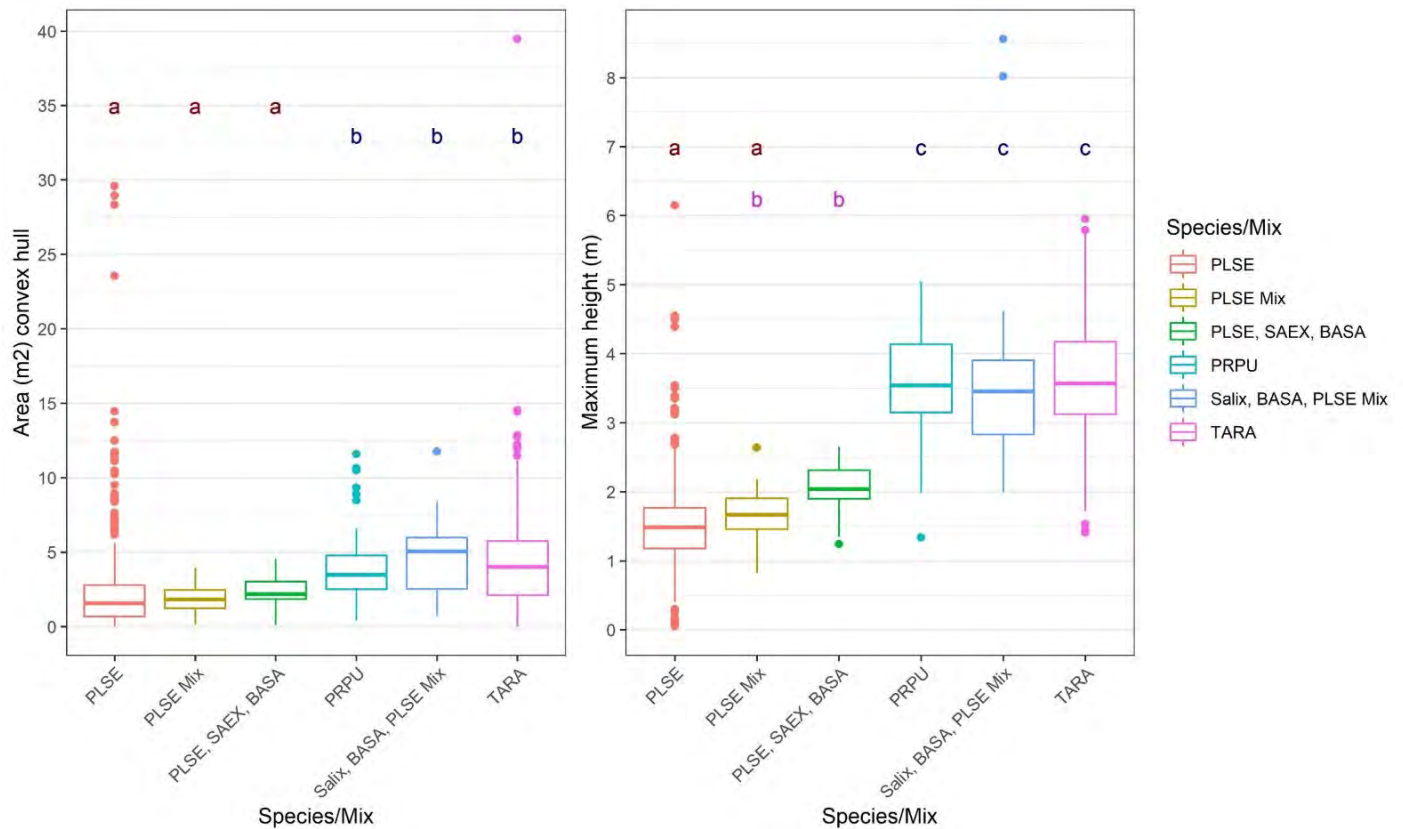


NOTE: species codes in the legend are defined in Table 2 (Section 4.1)

The canopy hulls and heights were calculated using only the ALS or TLS data; however, resulting metrics such as convex hull area or height did not successfully predict vegetation species. The RGB imagery paired with ground-based data was essential to identifying species and interpreting trees versus shrubs. After applying the species data derived from the RGB imagery combined with the field data and photos, we performed an Analysis of Variance

(ANOVA) with Tukey's Honest Squared Distance post-hoc tests to identify statistically significant groupings (Figure 4).

Figure 4. Area and height of convex canopy hulls by species (or species mix) at TP 3



Notes: Species codes with shared letters (a,b,c) are not statistically different; species codes without shared letters indicate statistically significant groupings ($p < 0.05$). Species codes are defined in section 4.1.

Statistical analysis was able to differentiate some groups of species (or species mixes), but the groupings didn't necessarily match functional groups or other natural ecological groupings. For example, the area of the convex hull differentiated between arrowweed (PLSE; or mixed dominated by arrowweed) and other species groups but could not differentiate between the trees (screwbean mesquite; PRPU), tamarisk (TARA), and other shrub mixes. The maximum height graph shows similar groupings but did not completely differentiate between species or functional groups (Figure 4). Additional refining of this analysis would be needed before it could be relied on for long-term monitoring.

This analysis was selected as an example because it has potential to address two overarching attributes—*Cover and Height*, and illustrates the benefits of combining data from multiple sensors. If this analysis should be selected for use in long-term monitoring, additional refinement in statistical analysis may be needed to find the optimal methods for species and/or functional group identification. Generally speaking, the method appears to be most useful for a trees in a forest and not optimal for desert riparian areas.

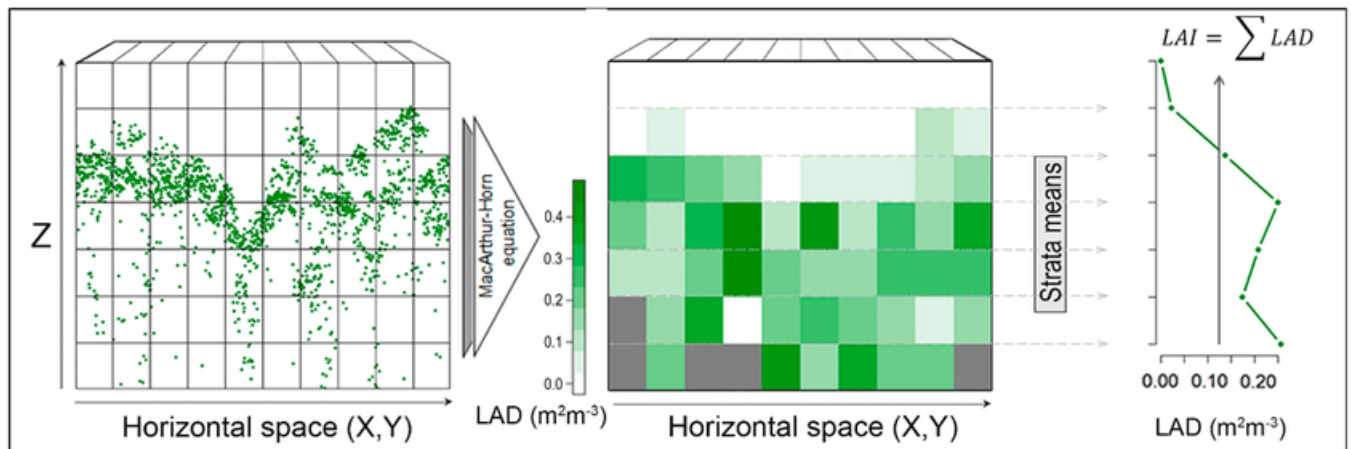
4.3 Height and Density – Leaf Area Density (LAD)

Primary sensor used for this analysis: ALS / TLS

Secondary sensor/data used as additional information: None

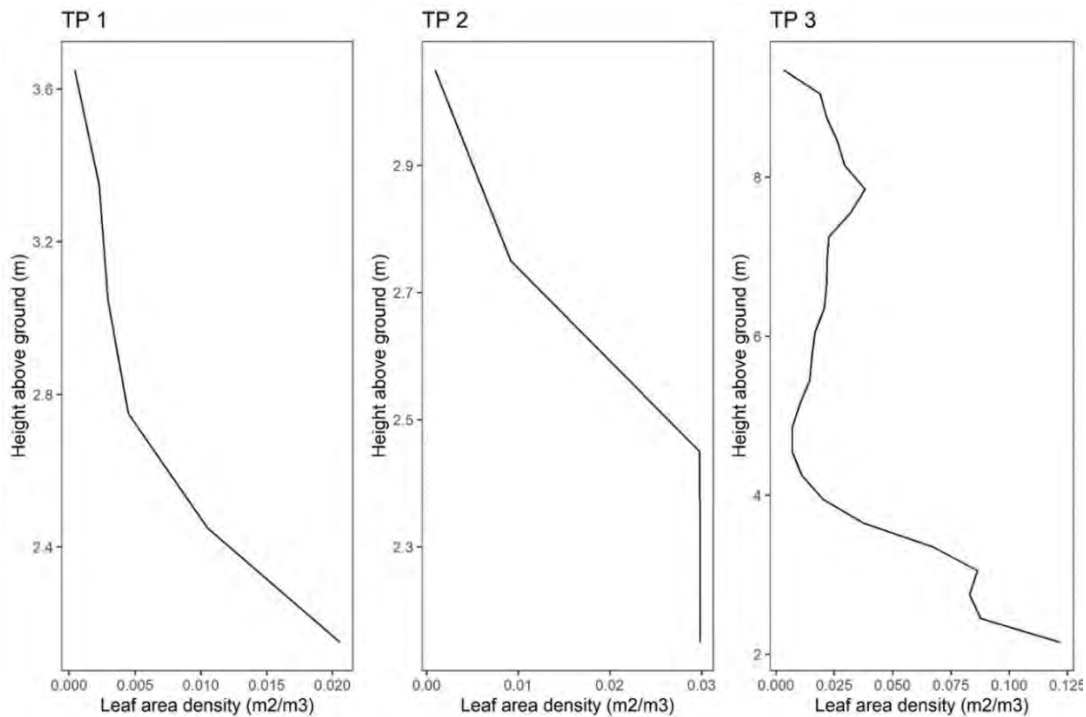
LAD is calculated using point cloud data (ALS or TLS) and is an index of leaf area per unit of volume. Figure 5 illustrates how the calculation transforms point clouds into a LAD plot. The LAD calculation provides quantitative measures of canopy height and density, as well as an illustrative view of canopy levels and overall vegetation structure.

Figure 5. Illustration showing the Leaf Area Density (LAD calculation). Taken from Almeida et al., 2019.



LAD was calculated using ALS data for all target plots (TPs) and TLS data for select areas near target plots 1, 2, and 3 (see Section 5.1 for ALS and TLS comparison) using the lidR package in program R. Figure 6 shows the resulting LAD plots for TP 1, TP 2, and TP 3.

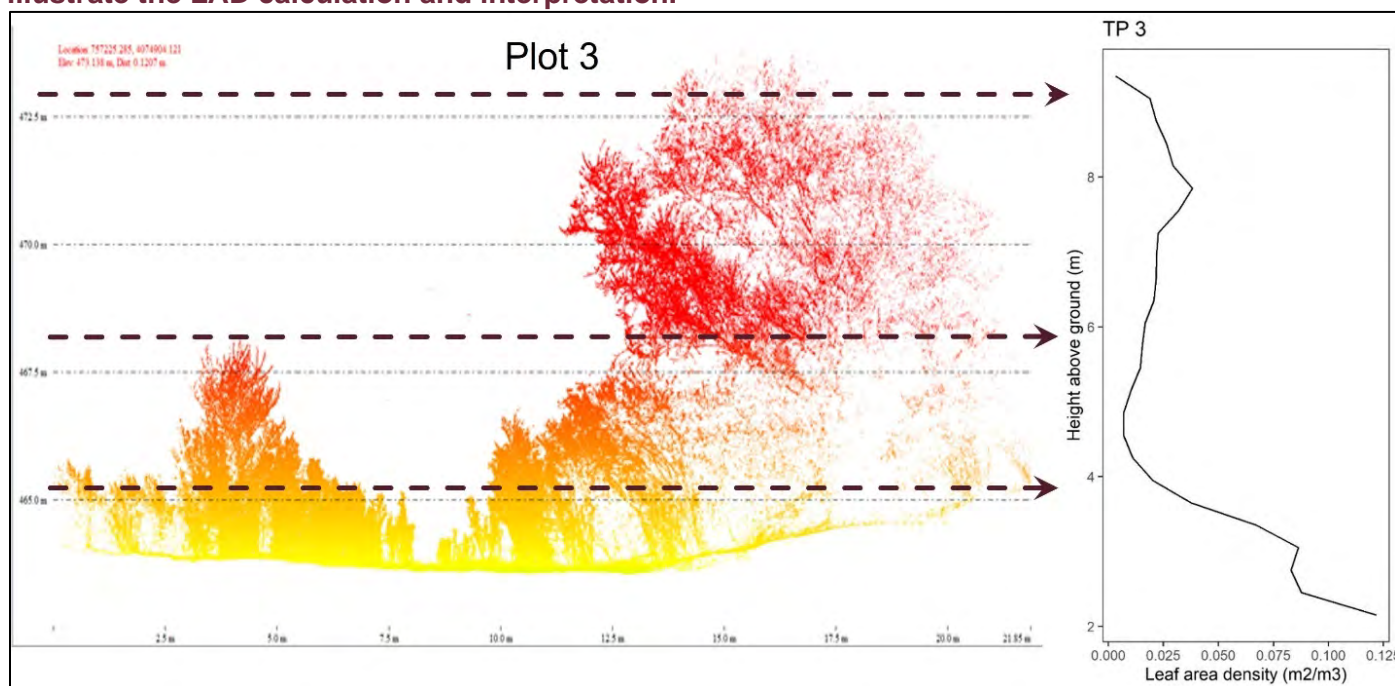
Figure 6. LAD calculation for TP1, TP2, and TP3, calculated from ALS data.



Note: The X-axis (leaf area density) and Y-axis (vegetation height) differ on each panel.

To illustrate how to interpret and use LAD, Figure 7 aligns the LAD plot from target plot 3 with a snapshot of the TLS point cloud from the same plot.

Figure 7. Leaf Area Density (LAD) for plot 3, aligned with TLS point cloud data to illustrate the LAD calculation and interpretation.



Note: Dotted arrow lines represent cross sections of vegetation being summed together in the LAD plot. This figure is for illustrative purposes only. The cross sections on the TLS point cloud data represent only a portion of the plot that the LAD calculation was performed on.

Using the TP 3 LAD plot as an example, we can see that there is relatively high leaf area density near the ground, decreasing to its lowest density at approximately 4-5m above the ground, and increasing again at approximately 8m above the ground. This indicates there are two canopy layers at this plot, one being shrubs < 4m tall and the other being trees with a canopy height of approximately 7- 9m tall.

This analysis was selected as an example to highlight because it has the ability to address two overarching attributes— *Height and Density*, using only one sensor.

4.4 Greenness – NDVI / MSAVI

Many vegetation indices (VIs) for detecting and quantifying green vegetation have been developed since the 1960s (Xue and Su 2017). One of the most commonly used VIs is the NDVI, developed in 1974 (Rouse et al. 1974). This index compares the surface reflectance of portions of the red and near infrared (NIR) spectra (Table 5) and exploits the fact that the healthy green portions of plants strongly absorb red wavelengths and strongly reflect NIR wavelengths. We selected this VI to assess vegetation cover during this study largely because it is commonly known and easy to interpret.

Many of the VIs introduced since NDVI were developed to address specific known shortcomings in NDVI. One of its shortcomings is that the index is greatly influenced by soil reflectance when vegetation cover is low. The MSAVI was thus developed, and subsequently improved, in 1994 (Qi et al. 1994a, b). MSAVI and MSAVI2 also use the fact that plants reflect red and NIR wavelengths in characteristic ways and is superior to other soil adjusted indices in that no

foreknowledge or assumptions about soil brightness and vegetation cover are required. Since we observed large areas of bare soil at the study site, we selected this index to evaluate whether it might be more accurate for describing vegetation cover.

Table 5. Vegetation indices used in this study for assessing the cover and ‘greenness’ of vegetation.

Vegetation Index	Symbol	Definition	Reference
Normalized Difference VI	NDVI	$\frac{NIR - Red}{NIR + Red}$	Rouse et al. 1974
Modified Soil Adjusted VI	MSAVI2	$0.5 * \left[(2NIR + 1) - \sqrt{(2NIR + 1)^2 - 8(NIR - R)} \right]$	Qi et al. 1994b

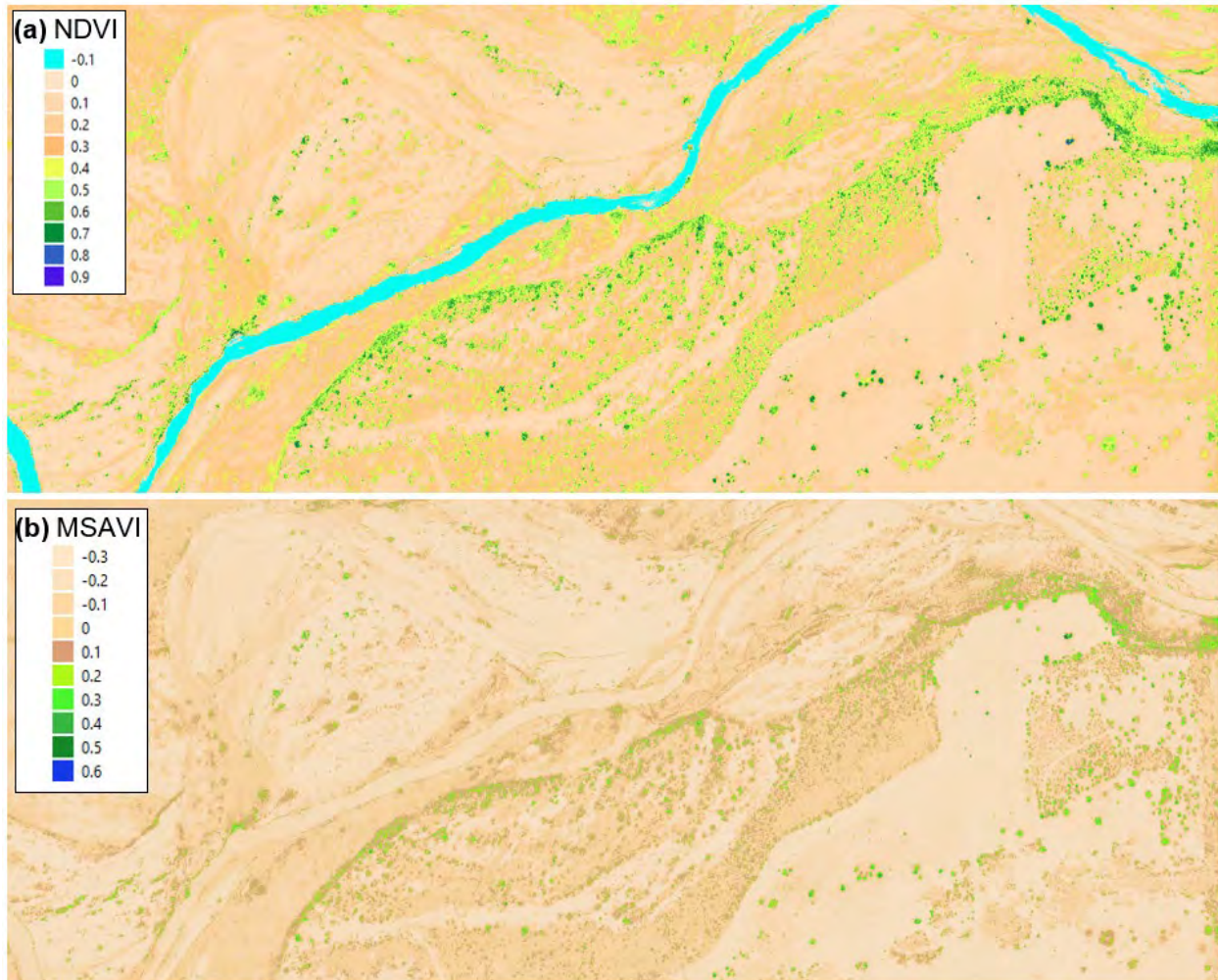
The two indices differ in their specific results for the amount of green vegetation cover (Table 6, Figure 8), but agree that bare ground is the predominant land cover and green vegetation cover likely represents less than 5% of the area.

Table 6. Green vegetation and bare soil areas based on interpretation of NDVI and MSAVI vegetation indices.

Substrate	NDVI		MSAVI	
	Value range	Area (ha)	Value range	Area (ha)
Bare soil & open water	≤ 0.3	33.78	≤ 0.1	41.03
Mixed soil, plants, etc	0.3 – 0.5	7.58	n/a	
Green vegetation	> 0.5	1.72		
Sparse green vegetation	n/a		0.1 – 0.3	1.95
Dense green vegetation			>0.3	0.07

The largest model disagreement is due to intermediate values of NDVI being of an indeterminate land cover class. An evaluation of which VI is more accurate would require groundtruthing those areas where there is disagreement in the “green vegetation” classes, as well as an evaluation of what the “mixed” NDVI pixels represent.

Figure 8. NDVI (a) and MSAVI (b) image comparison of greenness for approximately 43 ha of the study site.



Notes: Green and blue represent plant covered pixels; tan colors represent bare ground (and open water in [b]); cyan is open water in (a); yellow and yellow-green pixels indicate mixtures of green plants, woody and senescent plant parts, and/or bare ground. See Table 6 for areal extent of each category and how the indices are interpreted.

Section 5 Paired Sensor Comparisons with Discussion

5.1 ALS and TLS Comparison

ALS and TLS sensors produce the same type of data and can be used interchangeably in analyses. The differences in the data lie in how they are collected. ALS data is collected from the air, in this case a UAS drone flying at 60 m above the ground. TLS data is collected from a stationary point on a tripod with a base that allows the sensor to rotate both vertically and horizontally to collect data from a 360-degree globe view. Primary limitations when comparing the two sensor's data sets are:

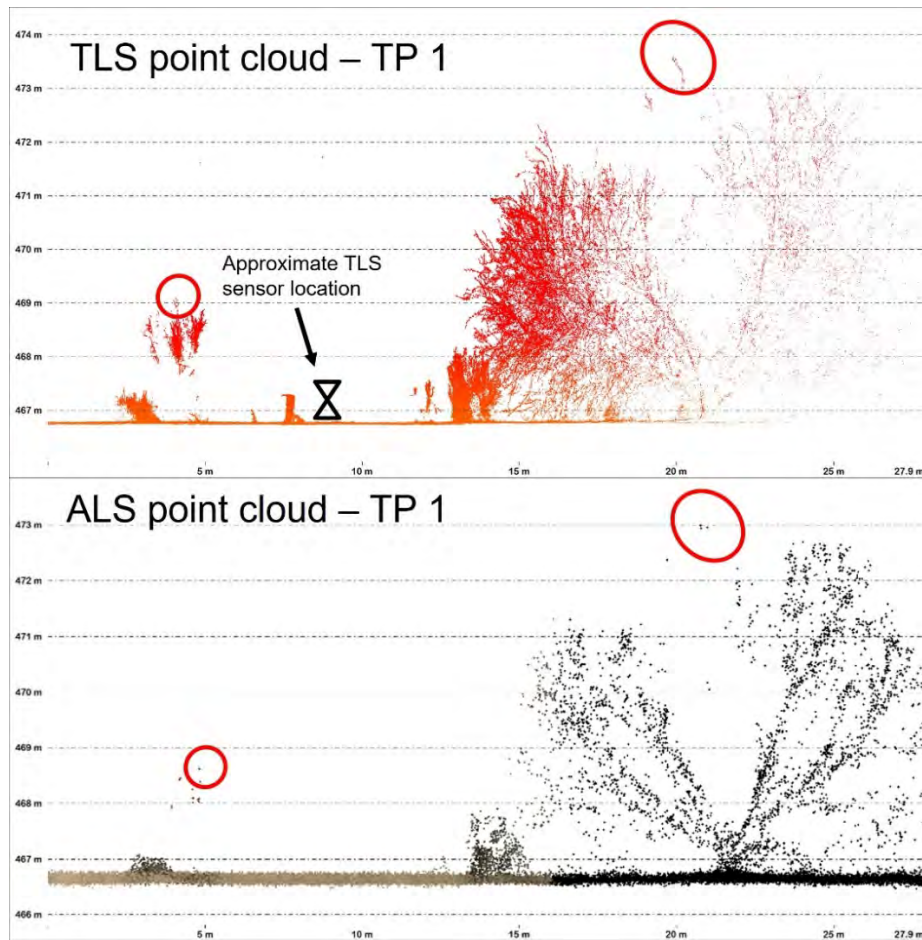
- ALS data is sparser because its sensor is in a constant state of movement (average of 80 points per m² with a maximum approximately 100 points per m² for ALS compared to 280 - 120,000 points per m² for TLS data), and

- TLS data covers a relatively small footprint from each tripod location. The TLS laser is limited to returns on surfaces that it can reach; once the laser cannot penetrate through the vegetation, no data is returned. In flat, sparsely vegetated areas the TLS ranges further than in hilly and/or densely vegetated plots. At our study site, the TLS was positioned at 4 locations and totaled approximately 15 acres of coverage, over half of which did reach the ground surface through the vegetation.

From a practical and field data collection standpoint, primary limitations of each sensor are:

- The ALS sensor requires more expertise during field data collections in that a Federal Aviation Administration (FAA) part 107 certification is required to fly a drone commercially, and field data collection may be limited by weather.
- The TLS sensor is stationary and must be disassembled and hauled to each plot location. Height and location accuracy and repeatability of the TLS is directly related to its tie into location points. Additional control points, similar to those described in Section 2, are set for each TLS plot. This is both time consuming and requires additional equipment being hauled across the field site. The TLS instrument comes with the sensor for the control point, but the survey unit for accurate positioning is separate. If access is limited, it may become impractical to carry the equipment from plot to plot.

Our analyses used ALS and TLS data separately to compare and contrast the two sets of data when possible. In general, the quality of data was similar in locations that had adequate TLS data. Figure 9 serves two illustrative purposes for comparing and contrasting the ALS and TLS data; it is used to compare maximum plant height data as well as point cloud density.

Figure 9. TLS and ALS point cloud comparison at target plot 1.

Note: Red circles indicate maximum heights of individual plants.

Notable comparisons on Figure 9 include:

- TLS and ALS maximum plant heights are similar and indicate similar data quality.
- ALS point cloud density is more consistent throughout the example cross-section; albeit generally less dense than the TLS point clouds.
- TLS point cloud data is extremely dense close to the sensor and rapidly decreases point density with distance through vegetation.

5.2 Multispectral imagery and RGB imagery

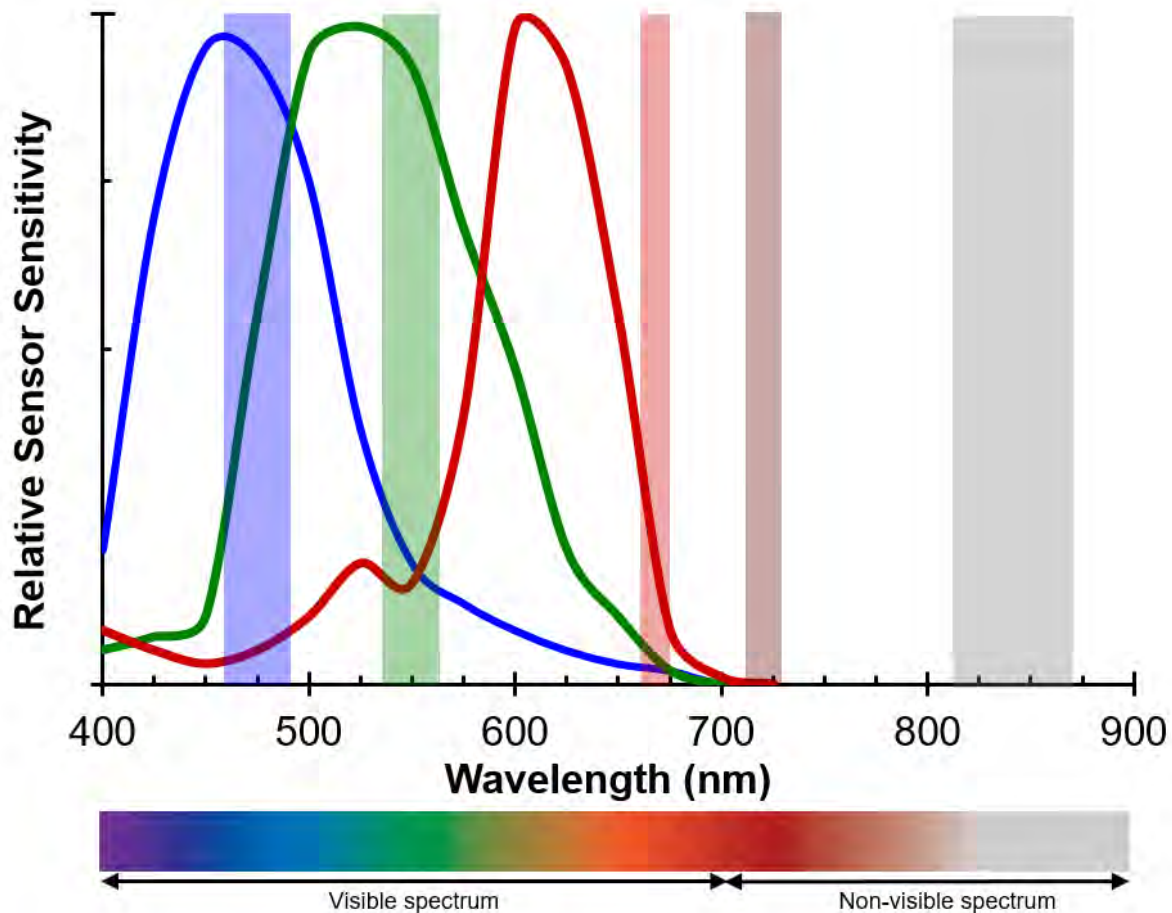
Both multispectral sensors and RGB cameras can be used to collect quantitative data that indicate the amount of visible light being reflected off the surface of plants, soils, and other substrates. Important differences between them are described in Table 7, and include the width and discreteness of spectral sensitivity, the dimensions of the focal plane (in both pixels and millimeters [mm]) and thus resolution, how their data can be used in long-term monitoring analyses, as well as costs. A comparison of the spectral sensitivity and width for each band is illustrated in Figure 10 and highlights the discreet nature of the multispectral bands versus the continuous nature that more resembles the human eye for RGB digital camera.

Table 7. Comparison of width, discreteness, resolution, analysis advantages, and cost for multispectral sensors and RGB digital cameras.

	Multispectral Sensor (MicaSense RedEdge-MX is used here as an example)	RGB Digital Camera (1" CMOS chip carried by a DJI Phantom 4 Pro V2 is used here as an example)
Width of each band (nm) with discussion on discreteness	<p>Blue = 475± 16 nm Green = 560±13 nm Red = 668±7 nm Red-Edge (not visible) = 717±6 nm Near-infrared (not visible) = 842±28 nm</p> <p>Spectral sensitivity is discreet for each band (shown as vertical bars in Figure 10) and for visible RGB bands do not match the three cones in the human eye, making the resulting image appear flat or otherwise "unnatural".</p>	<p>Blue = 400-700 nm Green = 400-700 nm Red = 400-700 nm</p> <p>Spectral sensitivities overlap 100% for each band, but are nominally sensitive to each 'red', 'green', and 'blue' wavelengths (shown as curves with peaks for each of the RGB bands in Figure 10). The overlap in spectral sensitivity very closely matches that of the human eye and resulting images appear richer and more "natural".</p>
Resolution as a function of dimensions of the focal plane	<p>1.2 megapixels per band, resulting in a GSD of 6.82 cm/pixel (focal plane is 1280 x 960 pixels) at an altitude of 100 m. This resolution is lower than what is achieved using an RGB digital camera.</p>	<p>20 megapixels total, resulting in a GSD of 2.73 cm/pixel (focal plane is 5472 x 3648 pixels) at an altitude of 100 m. This resolution is higher than what can be achieved using a multispectral sensor.</p>
Generalized comparison for analysis	<p>Multispectral sensors have three primary advantages over RGB digital cameras for long-term vegetation monitoring analysis purposes:</p> <ol style="list-style-type: none"> 1) Each of the five spectral bands are "tuned" to specifically provide information on physiological status of plants (e.g., chlorophyll concentration, cell water content, cell wall thickness). 2) The sensor is typically paired with another sensor that adjusts for sun angle and allows quantitative comparison given different light conditions between collection periods. 3) the sensor measures two non-visible spectral bands that the RGB cannot collect data on. All five spectral bands may be analyzed separately or together, which broadens the range of analysis possible. 	<p>RGB digital cameras have two primary advantages over the multispectral sensor:</p> <ol style="list-style-type: none"> 1) The images produced appears natural and rich to the human eye. This advantage is important when using imagery to aid in interpretation of analyses using other sensors (multispectral imagery, ALS, etc). 2) A much higher resolution can be obtained, even from inexpensive cameras, that allows for improved recognition of small objects and easier identification of species during manual interpretation of the imagery.
Equipment costs	<p>~\$5,000, not including the cost of drone, mounting equipment, etc.</p>	<p>~\$1,500, including cost of drone, mounting equipment, etc.</p>

A comparison of the spectral sensitivity and width for each of the bands is illustrated in Figure 10 and highlights the discreet nature of the multispectral bands versus the continuous nature that more resembles the human eye for RGB digital camera. Although both sensors collect red, green, and blue wavelengths, the RGB digital camera collects the complete (continuous) spectrum, whereas multispectral sensors collect smaller, discrete wavelengths.

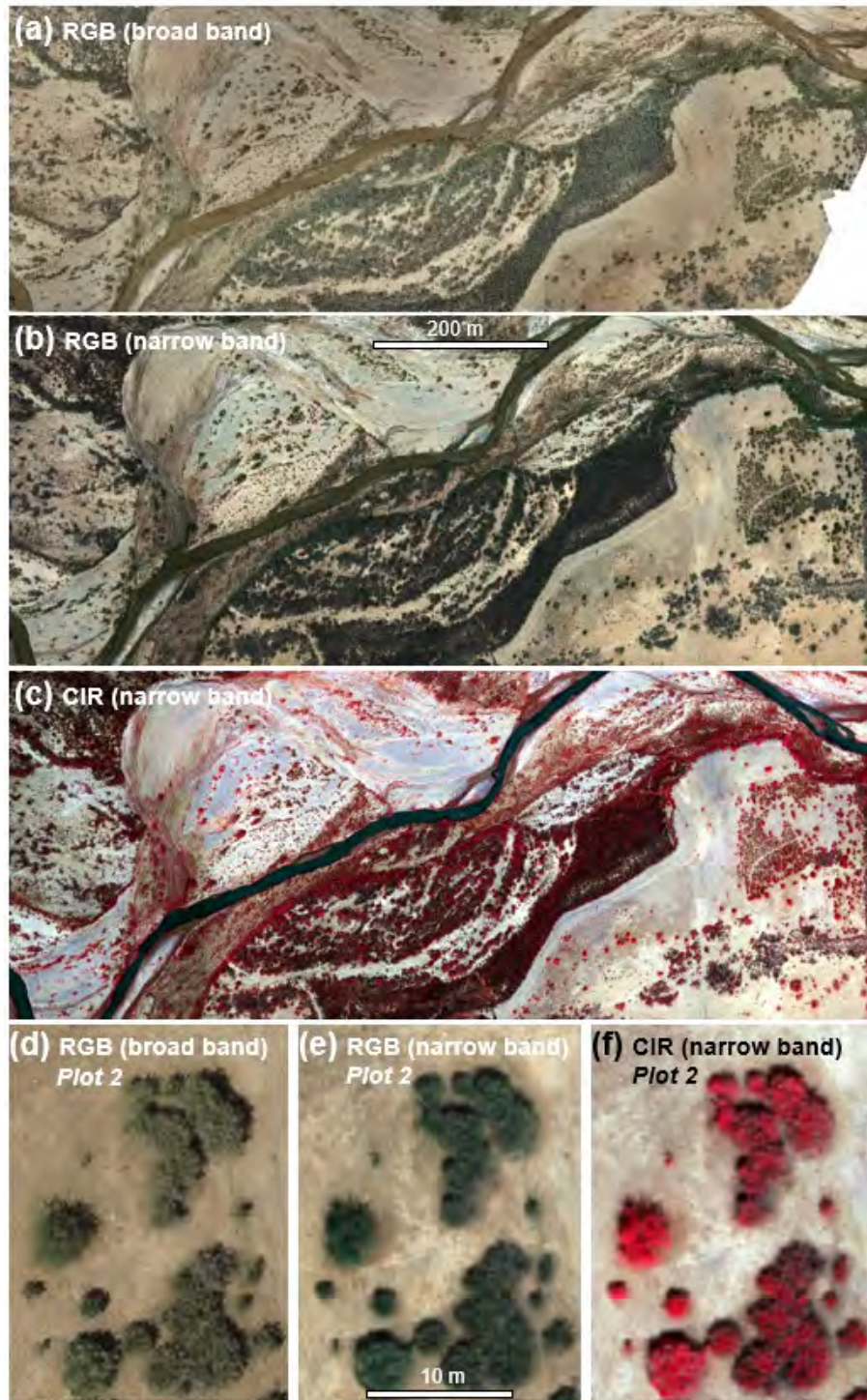
Figure 10. Red, green, and blue spectral sensitivity comparison for commercial RGB digital cameras and multispectral sensors.



Note: Typical broad and overlapping spectral sensitivity curves of commercial digital cameras (lines) for blue, green, and red bands compared with the narrow and discrete sensitivities for a multispectral sensor (bars) for blue, green, red, red edge, and near infrared bands. Camera curves redrawn from multiple sources, including Pagnutti et al. 2017.

To further illustrate the difference in RGB visual interpretation between multispectral imagery and RGB digital camera imagery, Figure 11 shows the color differences within the study area.

Figure 11. Site Imagery illustrating differences in the RGB and multispectral sensors.



Notes: (a) Full color image from the RGB camera – note the diverse shades of green and red.
(b) Composite image from the narrow blue, green, and red bands of the multispectral sensor – note how many of the bare soil areas have blue-green tints.
(c) Composite image from the narrow green, red, and near infrared bands of the multispectral sensor – this is referred to as “false color” since the reflectance bands are arbitrarily assigned colors (NIR → red, red → green, green → blue).
(d) through (e) are zoomed in to plot 2 to more closely illustrate the visual differences between an RGB digital camera (d) and a multispectral image (e) and (f).

It is common to pair data from a multispectral sensor and a RGB digital camera, collected at the same or similar time to enhance analyses. The multispectral imagery has several analysis advantages over the RGB imagery, but simply cannot match the RGB interpretability to the human eye. The decision to collect both data from both sensors often comes down to cost; the cost of maintaining and deploying a RGB digital camera on a drone is relatively inexpensive and may be offset by efficiencies gained during analysis and interpretation time.

5.3 Summary and Conclusions

Each sensor that was tested at the Bunkerville East site had strengths and weaknesses for how they can be used in a long-term monitoring program focused on avian riparian habitat. The example analyses described in Section 4 are intended to illustrate a variety of data produced from each sensor, as well as show differing levels of analysis complexity and success (or applicability) to long-term desert riparian habitat monitoring. All proposed attributes are listed in Table 7 (same as those listed in Table 2), with notation indicating the quality achieved by each sensor for each attribute.

The last two rows of Table 7 provide a generalized rating of cost and complexity. Section 1.1 described DCPs desired characteristics for a long-term monitoring program and included 'cost efficiency' and 'straightforward analysis'. The desired characteristics will play a large role in final selection of sensors and methods used in long-term monitoring on DCP properties. For the purposes of this pilot study, we provide a comparison for each sensor relative to each other.

Table 8. Relative level of quality achieved by each sensor for each analysis/attribute. Some analyses have substantially higher quality results when >1 sensor's data are combined.

General Attribute	Specific Attribute / Analysis	Sensor Type		
		MS	ALS/TLS	RGB
Cover	Vegetation and ground composition	Quant	Quant	Qual
	Total Cover	Quant	Quant (CRR)	Qual
	Cover by group and/or species	Quant	Qual	Qual
	understory vs overstory	NA	Quant	NA
Height	Overall/average height	Qual	Quant	Qual
	Height by canopy level	NA	Quant	NA
Vegetation Density	LAI/CH/LAD/TGI	Quant (LAI, CH)	Quant (LAD)	NA
	NDVI/MSAVI	Quant	NA	NA
Vigor/ Greenness	NDVI/MSAVI/TGI (visible bands)	Quant	NA	NA
	Live vs stressed vs dead	Qual?	NA	Qual
Other	Slopes/bank height	Qual	Quant	Qual
Rating: Generalized Cost – data collection and processing		\$\$\$	\$\$\$/\$\$	\$
Rating: Analysis complexity (straightforward = 1, complex = 3)		3	2/2	1

Note: The ratings for analysis complexity is based on the specialized knowledge required to perform the analyses. For example, if an analysis could be performed in an easy to obtain program (e.g. ArcMap or Program R), using widely available methods with step-by-step instructions, we would consider the analysis straightforward; whereas, if methods are not well defined yet and/or the analysis requires a high degree of interpretation and statistical knowledge, the analysis would be considered complex.

Overall, the RGB imagery does not calculate any of the attributes to a quantitative level and has the least stand-alone utility for long-term monitoring; however, it is invaluable as a companion data source to other sensors. The ALS and TLS sensors have the ability to quantitatively calculate specific attributes for all of the overarching attributes (e.g., *Cover*, *Height*, etc.) with the exception of *Vigor/Greenness*. The multispectral sensor has the ability to quantitatively calculate specific attributes with *Cover*, *Vegetation Density*, and *Vigor/Greenness* general attributes, but not *Height*, or any of the *Other* attributes that require accurate surface modeling, such as floodplain height or river bank slope.

Overall comments based on the success and ease data collection and analysis are listed in Table 9.

Table 9. General comments for RGB, multispectral, ALS, and TLS sensor data collection and subsequent data analysis

Sensor	Positive	Negative
RGB	<ul style="list-style-type: none"> Easiest and cheapest to collect Best at identifying species, etc. as a companion for most analyses 	<ul style="list-style-type: none"> Has the least ability of any sensor to accomplish relevant analyses on its own and most/all analyses that it can be used for are qualitative only.
Multispectral	<ul style="list-style-type: none"> The only multi-dimensional sensor, which means it is the only sensor that performs well for species and/or functional group differentiation and for plant vigor analyses 	<ul style="list-style-type: none"> Surfaces and height measurements are very coarse and not likely to have the quality required for long-term monitoring programs High processing power required for larger areas
ALS	<ul style="list-style-type: none"> Best at calculating overall surfaces and heights Secondary ability to calculate density, which was unexpected 	<ul style="list-style-type: none"> High processing power required for larger areas Requires additional data (RGB interpretation of field data) to identify species
TLS	<ul style="list-style-type: none"> Highest level of detail (point density) collected 	<ul style="list-style-type: none"> Short range for data collection at each plot severely limits its use in analyses. Bulky to transport from plot to plot without vehicle access Requires additional data (RGB interpretation of field data) to identify species.

Regardless of which sensor(s) are used to collect remotely sensed data, a moderate-to-high amount of field data is required to inform analyses (i.e., for use as training data or to delineate species on the RGB imagery), as well as to validate results.

The use of remote-sensed data to quantify vegetative conditions for the purpose of evaluating and monitoring habitat quality is a rapidly developing field. Even so, the use of such data for quantifying avian habitat in desert riparian ecosystems is nascent, particularly for high resolution data across small areas such as those managed by DCP. We found that some aspects of avian

habitat were well-captured in this study, such as using multispectral data to classify the project area into 17 land cover classes, multispectral data to quantify vegetative vigor, and using ALS to quantify vertical variation in plot-level canopy structure. Other metrics performed poorly, such as the use of ALS to identify individual plant species or species assemblages. For updating the AMMP to include guidance on how to monitor desert riparian habitat quality over time, the methods, results, and pros and cons can be used to develop a monitoring strategy that best achieves the goals of the DCP.

Section 6 References

- Acebes, P., Lillo, P., and Jaime-González, C. 2021. Disentangling LiDAR contribution in modelling species-habitat structure relationships in terrestrial ecosystems worldwide – a systematic review and future directions. *Remote Sensing* 13:3447.
- Albano, C. M., McGwire, K. C., Hausner, M. B., McEvoy, D. J., Morton, C. G., and Huntington, J. L. 2020. Drought sensitivity and trends of riparian vegetation vigor in Nevada, USA (1985-2018). *Remote Sensing* 12:1362.
- Almeida, D., et. al. 2019. Optimizing the Remote Detection of Tropical Rainforest Structure with Airborne Lidar: Leaf Area Profile Sensitivity to Pulse Density and Spatial Sampling. *Remote Sensing* 11:92. doi:10.3390/rs11010092.
- Alta Science & Engineering, Inc. (Alta), 2021. Riparian Reserves Management Plan. Version 1.3. Prepared for Clark County Desert Conservation Program. July 2021.
- Bakx, T. R. M., Koma, Z., Seijmonsbergen, A. C., and Kissling, W. D. 2019. Use and categorization of Light Detection and Ranging vegetation metrics in avian diversity and species distribution research. *Diversity and Distributions* 25:1045-1059.
- Burns, P., et al. 2020. Incorporating canopy structure from simulated GEDI lidar into bird species distribution models. *Environmental Research Letters* 15:095002.
- Dashti, H., et al. 2019. Regional scale dryland vegetation classification with an integrated lidar-hyperspectral approach. *Remote Sensing* 11:2141.
- García, M., Riaño, D., Chuvieco, E., Salas, J., and Danson, F. M. 2011. Multispectral and LiDAR data fusion for fuel type mapping using Support Vector Machine and decision rules. *Remote Sensing of Environment* 115:1369-1379.
- Gómez-Sapiens, M., Schlatter, K. J., Meléndez, Á., Hernández-López, D., Salazar, H., Kendy, E., and Flessa, K. W. 2021. Improving the efficiency and accuracy of evaluating aridland riparian habitat restoration using unmanned aerial vehicles. *Remote Sensing in Ecology and Conservation* 7:488-503.
- Grijseels, N. H., Buchert, M., Brooks, P. D., and Pataki, D. E. 2021. Using LiDAR to assess transitions in riparian vegetation structure along a rural-to-urban land use gradient in western North America. *Ecohydrology* 14:e2259.
- Hellesen, T., and Matikainen, L. 2013. An object-based approach for mapping shrub and tree cover on grassland habitats by use of LiDAR and CIR orthoimages. *Remote Sensing* 5:558-583.
- Ikanyan, K. J., and Beissinger, S. R. 2018. Collapse of a desert bird community over the past century driven by climate change. *Proceedings National Academy of the Sciences* 115:8597-8602.
- Kedia, A. C., Kapos, B., Liao, S., Draper, J., Eddinger, J., Updike, C., and Frazier, A. 2021. An integrated spectral-structural workflow for invasive vegetation mapping in an arid region using drones. *Drones* 5:19.
- Pagnutti, M., Ryan, R., Cazenavette, G., Gold, M., Harlan, R., Leggett, E., Pagnutti, J. 2017. Laying the foundation to use Raspberry pi 3 V2 camera module imagery for scientific and engineering purposes. *Journal of Electronic Imaging* 26:013014. [https://1w2yci3p7wwa1k9jld1jygd-wpengine.netdna-ssl.com/wp-content/uploads/2019/10/SAT_MX_MXblue-Spectrum2.2.jpg] [https://doi.org/10.1117/1.JEI.26.1.013014].

- Qi, J., Kerr, Y., and Chehbouni, A. 1994a. External factor consideration in vegetation index development. *Proceedings of Physical Measurements and Signatures in Remote Sensing*. ISPRS, 723-730.
- Qi, J., Chehbouni, A., Huete, A.R., Kerr, Y.H., and Sorooshian, S. 1994b. A modified soil adjusted vegetation index. *Remote Sensing of Environment* 25:119-128.
- RECON. 2001. Final Clark County Multiple Species Habitat Conservation Plan and Environmental Impact Statement for Issuance of a Permit to Allow Incidental Take of 79 Species in Clark County, Nevada, September 2000.
- Rouse Jr., J.W., Haas, R., Schell, J., and Deering, D. 1974. Monitoring vegetation systems in the Great Plains with ERTS. *NASA Special Publication* 1:309-317.
- Sankey, T. T., McVay, J., Swetnam, T. L., McClaran, M. P., Heilman, P., and Nichols, M. 2018. UAV hyperspectral and lidar data and their fusion for arid and semi-arid land vegetation monitoring. *Remote Sensing in Ecology and Conservation* 4:20-33.
- Schirrmann, M., Giebel, A., Gleiniger, F., Pflanz, M., Lentschke, J., and Dammer, K-H. 2016. Monitoring agronomic parameters of winter wheat crops with low-cost UAV imagery. *Remote Sensing* 8:706.
- SWCA. 2017a. Point-Count Surveys on Riparian Properties - Final Project Report.
- SWCA. 2017b. Federally Listed Bird Surveys on Three Riparian Reserve Units in Clark County, Nevada – Final Project Report.
- SWCA. 2019. Avian Surveys on MSHCP Properties 2019 Final Project Report. Prepared for the Desert Conservation Program. September 2019. TerraGraphics. 2016. Biological Goals and Objective for the Clark County, NV Multiple Species Habitat Conservation Plan – Final.
- TerraGraphics Environmental Engineering, Inc. (TerraGraphics). 2016. Biological Goals and Objectives for the Clark County, NV Multiple Species Habitat Conservation Plan - Final. June 22, 2016.
- TerraGraphics. 2017. Adaptive Management and Monitoring Plan. Prepared for Clark County Desert Conservation Program. January 19, 2017.
- U.S. Fish and Wildlife Service (USFWS). 2001. Clark County Desert Conservation Plan Permit PRT 801045.
- Xue, J., and B. Su. 2017. Significant remote sensing vegetation indices: a review of developments and applications. *Journal of Sensors*.
- Zabihi, K., Driese, K. L., G. B. Paige, and A. K. Hild. 2019. Application of ground-based lidar and gap intercept measurements to quantify a shrub configuration metric within greater sage-grouse nesting habitat. *Western North American Naturalist* 79:4.

Appendix A
Ground based data collection field sheets and photo log

Fine-Scale Riparian Monitoring Demonstration Project (Desert Conservation Program - SAP)

1
Plot

VR1
Location

SL, TH, CR
Observers

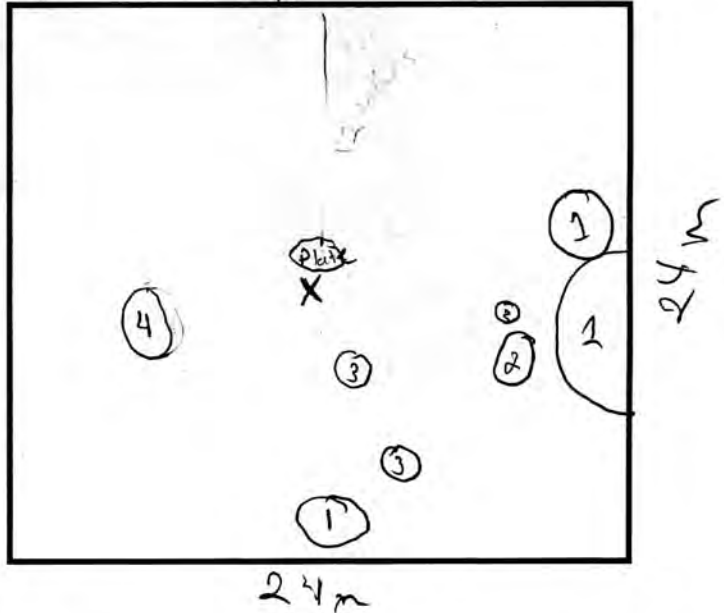
4/8/2021
Date

In the box below sketch a) the location of the target marker, b) the direction of magnetic north, c) the dimensions of the plot, and d) the approximate locations and sizes of plants within the plot

Species

- 1 PRGLT
- 2 ATLE
- 3 Rabbit Brush
- 4 PLSE
- 5
- 6
- 7
- 8
- 9
- 10
- 11
- 12

Notes: ATLE along the North west edge



2
Plot

VR2
Location

Smc, TH, CR
Observers

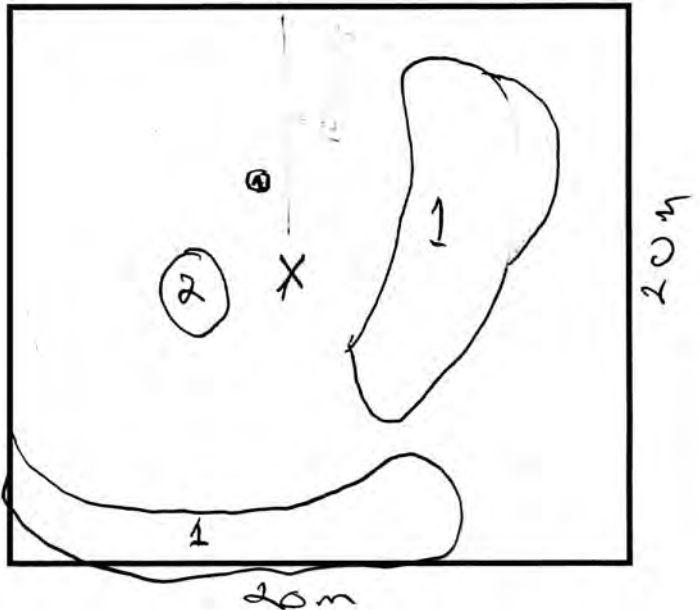
4/8/2021
Date

In the box below sketch a) the location of the target marker, b) the direction of magnetic north, c) the dimensions of the plot, and d) the approximate locations and sizes of plants within the plot

Species

- 1 PLSE
- 2 TARA
- 3
- 4
- 5
- 6
- 7
- 8
- 9
- 10
- 11
- 12

Notes: NO plants; North had NO veg for ~100m



Fine-Scale Riparian Monitoring Demonstration Project (Desert Conservation Program - SAP)

3
Plot

VR3
Location

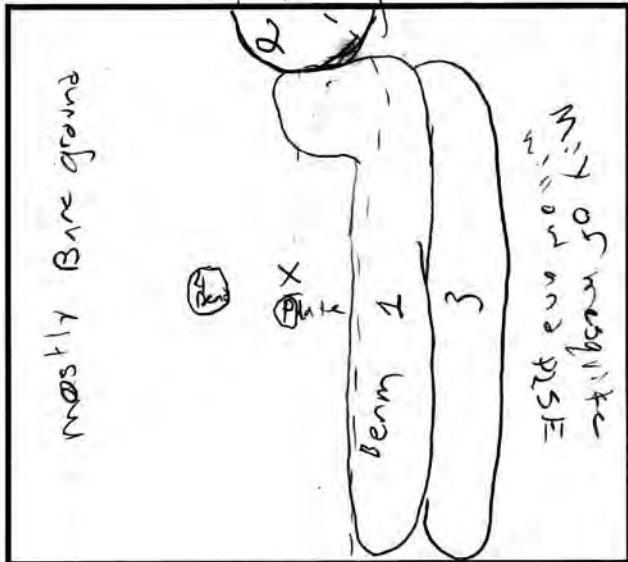
SC, TH, CW
Observers

4/8/21
Date

In the box below sketch a) the location of the target marker, b) the direction of magnetic north, c) the dimensions of the plot, and d) the approximate locations and sizes of plants within the plot

Species

- 1 PLSE
- 2 SAGO
- 3 Salix spp.
- 4 TARA
- 5 PRPU
- 6
- 7
- 8
- 9
- 10
- 11
- 12



Notes: Dashed line is the Berm with mix of species Below the Berm

4
Plot

VR4
Location

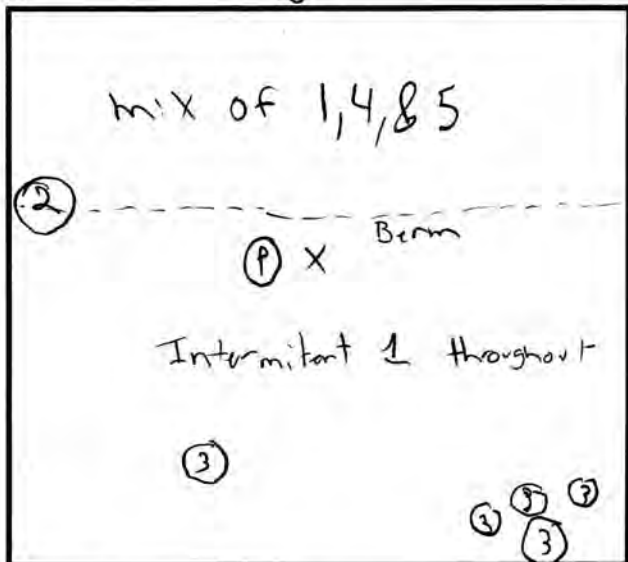
SC, TH, CW
Observers

4/8/2021
Date

In the box below sketch a) the location of the target marker, b) the direction of magnetic north, c) the dimensions of the plot, and d) the approximate locations and sizes of plants within the plot

Species

- 1 DLSE
- 2 PRPU
- 3 SAGO
- 4 SA ET
- 5 BASA
- 6
- 7
- 8
- 9
- 10
- 11
- 12



Notes: Sandy Soil, Dotted line denotes Drop off Berm

Fine-Scale Riparian Monitoring Demonstration Project (Desert Conservation Program - SAP)

5
Plot

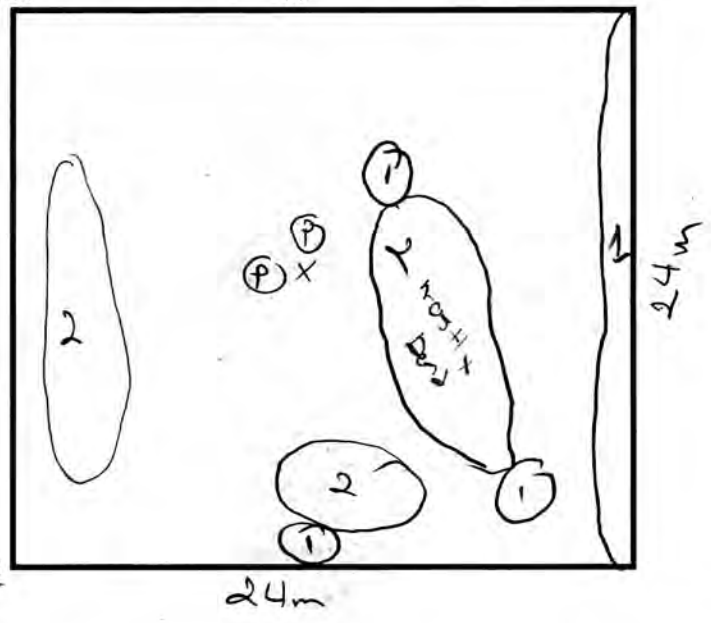
VRS
Location

SL, TH, CW
Observers

4/8/2021
Date

	Species
1	TARA
2	PLSE
3	
4	
5	
6	
7	
8	
9	
10	
11	
12	

In the box below sketch a) the location of the target marker, b) the direction of magnetic north, c) the dimensions of the plot, and d) the approximate locations and sizes of plants within the plot



Notes: Sandy Soil throughout
intermittent PLSE

6
Plot

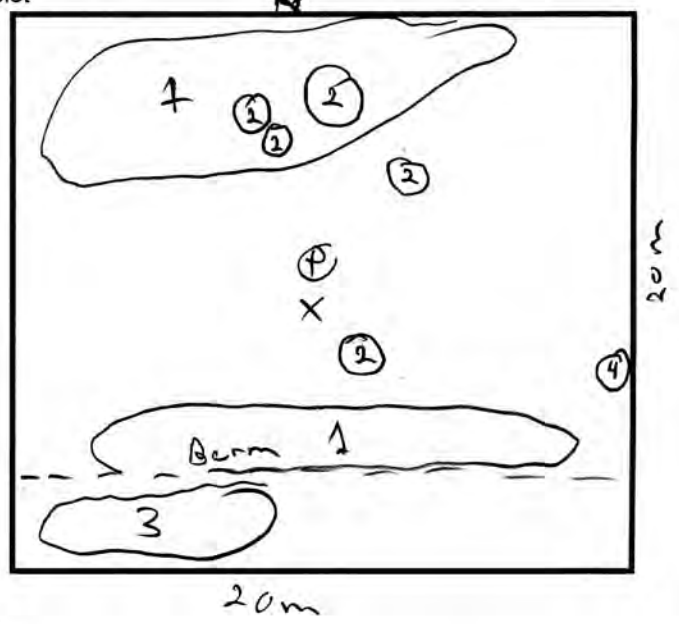
VRG
Location

SL, TH, LW
Observers

4/8/2021
Date

	Species
1	PLSE
2	PRPV
3	TARA
4	SAGO
5	
6	
7	
8	
9	
10	
11	
12	

In the box below sketch a) the location of the target marker, b) the direction of magnetic north, c) the dimensions of the plot, and d) the approximate locations and sizes of plants within the plot



Notes: SAGO Not in good shape
Dotted line indicates Berm
PLSE interspersed throughout

Fine-Scale Riparian Monitoring Demonstration Project (Desert Conservation Program - SAP)

7
Plot

VR7
Location

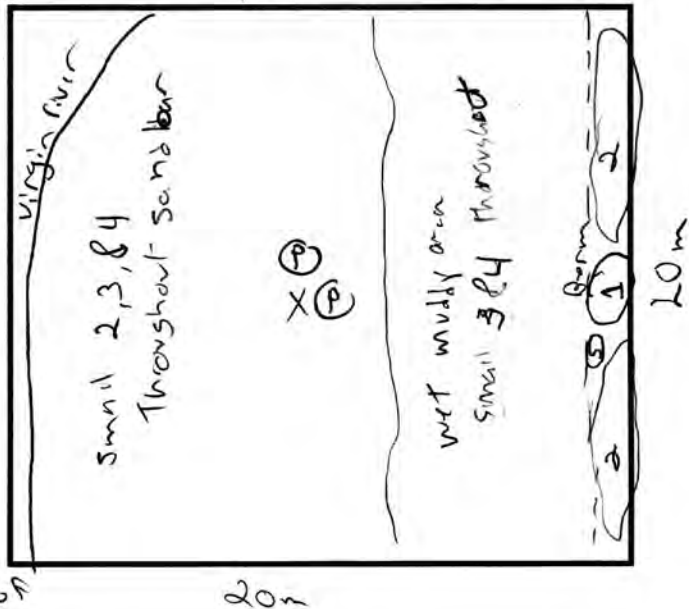
SC, TH, CW
Observers

4/8/21
Date

Species

- 1 PRPU
- 2 PLSF
- 3 BASA
- 4 TARA
- 5 willow sp
- 6
- 7
- 8
- 9
- 10
- 11
- 12

In the box below sketch a) the location of the target marker, b) the direction of magnetic north, c) the dimensions of the plot, and d) the approximate locations and sizes of plants within the plot



Notes: Dotted line indicates Berm
Small individuals Throughout west of the Berm

Plot

Location

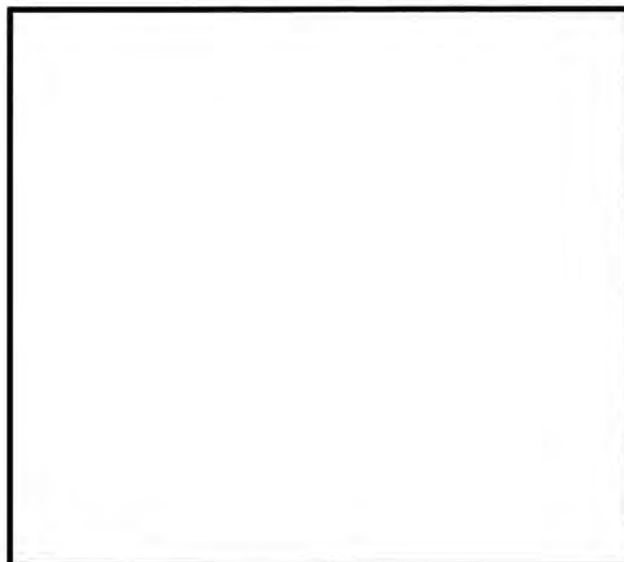
Observers

Date

Species

- 1
- 2
- 3
- 4
- 5
- 6
- 7
- 8
- 9
- 10
- 11
- 12

In the box below sketch a) the location of the target marker, b) the direction of magnetic north, c) the dimensions of the plot, and d) the approximate locations and sizes of plants within the plot



Notes:

Fine-Scale Riparian Monitoring Demonstration Project (Desert Conservation Program - SAP)

12
Plot

YR 12
Location

SC, TH, CW
Observers

4/7/2021
Date

- Species
- 1 PRPU
 - 2 Willow spp
 - 3 PLSE
 - 4 BASA
 - 5
 - 6
 - 7
 - 8
 - 9
 - 10
 - 11
 - 12

In the box below sketch a) the location of the target marker, b) the direction of magnetic north, c) the dimensions of the plot, and d) the approximate locations and sizes of plants within the plot



Notes: The bright green lush seedlings are BASA whole area pretty sandy

9
Plot

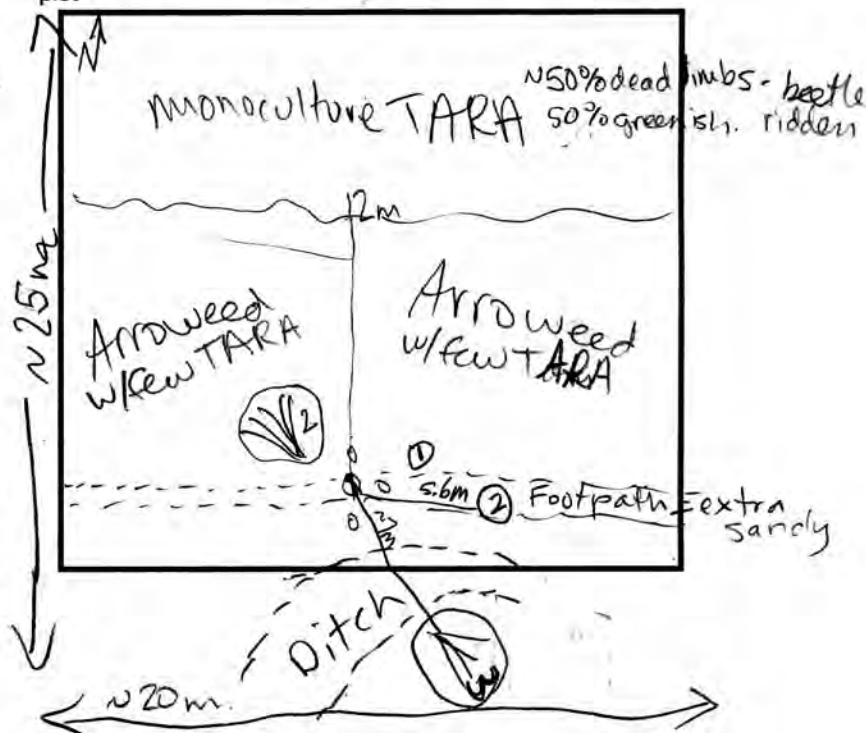
YR 9
Location

SC, TH, CW
Observers

4/7/2021
Date

- Species
- 1 TARA
 - 2 PRPU
 - 3 SAGO
 - 4 PLSE
 - 5
 - 6
 - 7
 - 8
 - 9
 - 10
 - 11
 - 12

In the box below sketch a) the location of the target marker, b) the direction of magnetic north, c) the dimensions of the plot, and d) the approximate locations and sizes of plants within the plot



Notes: whole area pretty sandy - footpath - on a SWFL survey trail (black + white ribbons)

Photo 1



Plot 1, DCP Staff collecting data, honey mesquite and rabbitbrush plants

Photo 2



Plot 1, Susan Firor with TLS set up, arrowweed in back

Photo 3



Plot 2, TLS set up, facing south

Photo 4



Plot 2, facing north, tamarisk on left

Photo 5



Plot 3, Goodings willow on left, old berm with concrete evident

Photo 6



Plot 4, Goodings willows

Photo 7



Plot 4, looking downriver, mix of salix and mule fat on the right

Photo 8



Plot 5, facing approximately south (away from river), arrowweed in front, tamarisk in back.

Photo 9



Plot 6, arrowweed with screwbean mesquite

Photo 10



Plot 6, arrowweed with tamarisk in back

Photo 11



Plot 7, facing river, tamarisk and mule fat seedlings

Photo 12



Plot 7, facing approximately south, away from river. Mule fat is bright green.

Photo 13



Plot 9, screwbean mesquite on right, goodings willow in back, arrowweed throughout.

Photo 14



Plot 9, screwbean mesquite in front, arrowweed throughout, tamarisk in back throughout.

Photo 15



Plot 12, facing downriver

Photo 16



Plot 12, facing upriver, mixed seedlings

Appendix B
Quality Assurance / Quality Control (QA/QC) information for UAS sensor data processing

- !** **Important:** Click on the different icons for:
- ?** Help to analyze the results in the Quality Report
 - i** Additional information about the sections

💡 Click [here](#) for additional tips to analyze the Quality Report

Summary



Project	VR-ms-20210407
Processed	2021-05-11 01:23:47
Camera Model Name(s)	RedEdge-M_5.5_1280x960 (Blue), RedEdge-M_5.5_1280x960 (Green), RedEdge-M_5.5_1280x960 (Red), RedEdge-M_5.5_1280x960 (NIR), RedEdge-M_5.5_1280x960 (Red edge)
Rig name(s)	«RedEdge-M»
Average Ground Sampling Distance (GSD)	7.36 cm / 2.90 in
Area Covered	0.522 km ² / 52.2229 ha / 0.20 sq. mi. / 129.1125 acres
Time for Initial Processing (without report)	23m:51s

Quality Check



? Images	median of 10000 keypoints per image	✓
? Dataset	3560 out of 3560 images calibrated (100%), 2 images disabled	✓
? Camera Optimization	0.34% relative difference between initial and optimized internal camera parameters	✓
? Matching	median of 6105.66 matches per calibrated image	✓
? Georeferencing	yes, 7 GCPs (7 3D), mean RMS error = 0.114 m	✓

? Preview

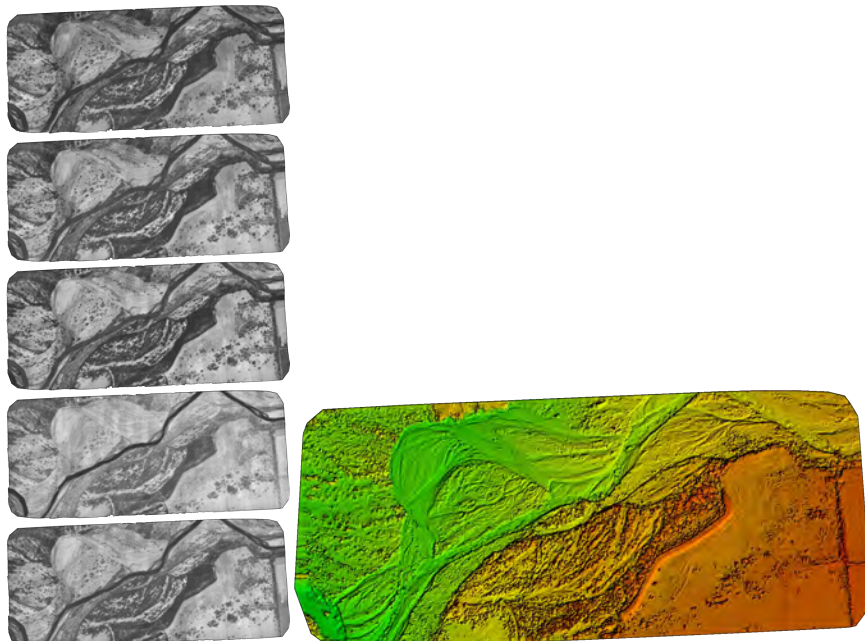


Figure 1: Orthomosaic and the corresponding sparse Digital Surface Model (DSM) before densification.

Calibration Details



Number of Calibrated Images	3560 out of 3562
Number of Geolocated Images	3562 out of 3562

Initial Image Positions

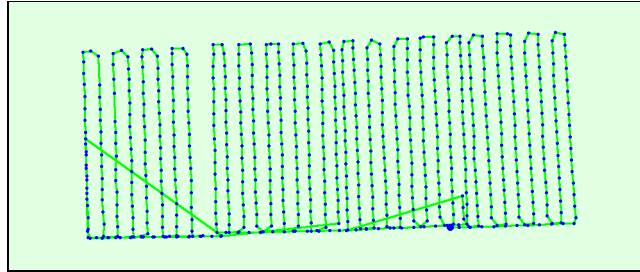
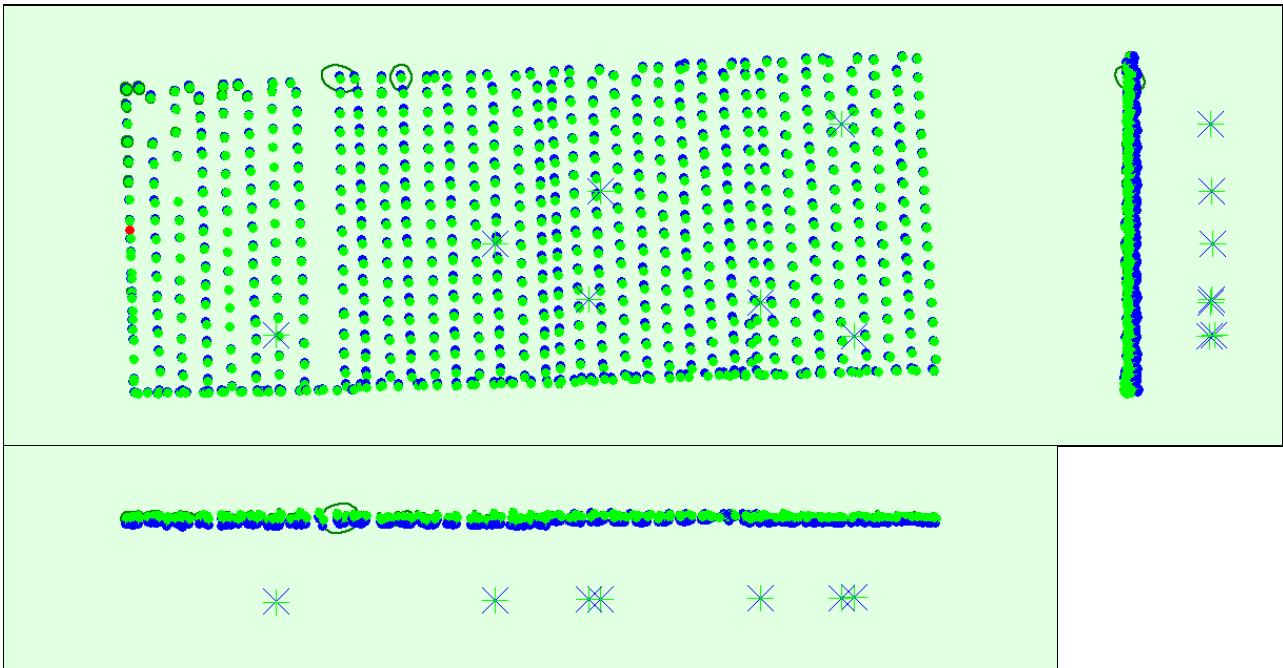


Figure 2: Top view of the initial image position. The green line follows the position of the images in time starting from the large blue dot.

Computed Image/GCPs/Manual Tie Points Positions



Uncertainty ellipses 100x magnified

Figure 3: Offset between initial (blue dots) and computed (green dots) image positions as well as the offset between the GCPs initial positions (blue crosses) and their computed positions (green crosses) in the top-view (XY plane), front-view (XZ plane), and side-view (YZ plane). Red dots indicate disabled or uncalibrated images. Dark green ellipses indicate the absolute position uncertainty of the bundle block adjustment result.

Absolute camera position and orientation uncertainties



	X[m]	Y[m]	Z[m]	Omega [degree]	Phi [degree]	Kappa [degree]
Mean	0.029	0.037	0.041	0.019	0.014	0.004
Sigma	0.010	0.010	0.008	0.005	0.004	0.004

Overlap



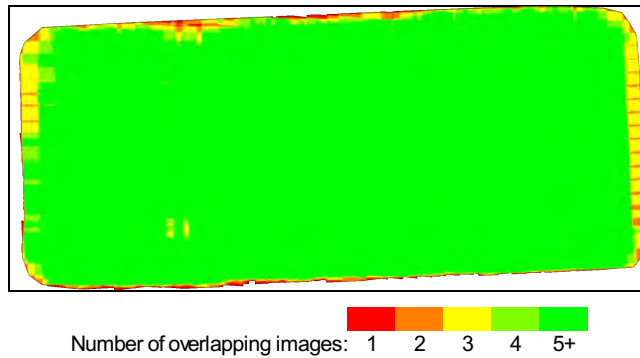


Figure 4: Number of overlapping images computed for each pixel of the orthomosaic. Red and yellow areas indicate low overlap for which poor results may be generated. Green areas indicate an overlap of over 5 images for every pixel. Good quality results will be generated as long as the number of keypoint matches is also sufficient for these areas (see Figure 5 for keypoint matches).

Bundle Block Adjustment Details

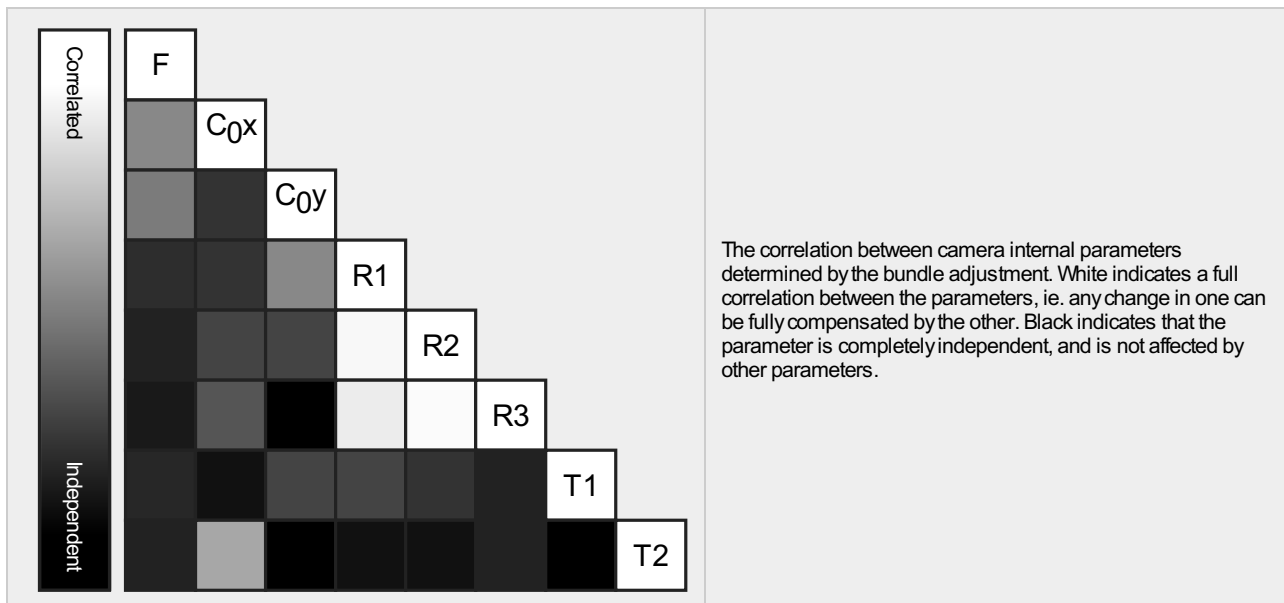
Number of 2D Keypoint Observations for Bundle Block Adjustment	5959450
Number of 3D Points for Bundle Block Adjustment	1387144
Mean Reprojection Error [pixels]	0.211

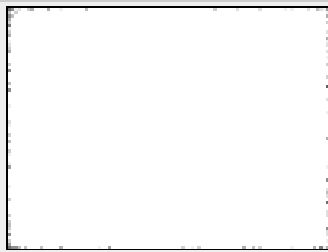
Internal Camera Parameters

RedEdge-M_5.5_1280x960 (Blue). Sensor Dimensions: 4.800 [mm] x 3.600 [mm]

EXIF ID: RedEdge-M_5.5_1280x960

	Focal Length	Principal Point x	Principal Point y	R1	R2	R3	T1	T2
Initial Values	1446.530 [pixel] 5.424 [mm]	669.584 [pixel] 2.511 [mm]	489.632 [pixel] 1.836 [mm]	-0.114	0.232	-0.214	0.001	-0.000
Optimized Values	1455.876 [pixel] 5.460 [mm]	669.631 [pixel] 2.511 [mm]	489.795 [pixel] 1.837 [mm]	-0.097	0.149	-0.040	0.000	0.000
Uncertainties (Sigma)	0.460 [pixel] 0.002 [mm]	0.164 [pixel] 0.001 [mm]	0.172 [pixel] 0.001 [mm]	0.001	0.006	0.013	0.000	0.000





The number of Automatic Tie Points (ATPs) per pixel, averaged over all images of the camera model, is color coded between black and white. White indicates that, on average, more than 16 ATPs have been extracted at the pixel location. Black indicates that, on average, 0 ATPs have been extracted at the pixel location. Click on the image to see the average direction and magnitude of the re-projection error for each pixel. Note that the vectors are scaled for better visualization. The scale bar indicates the magnitude of 1 pixel error.

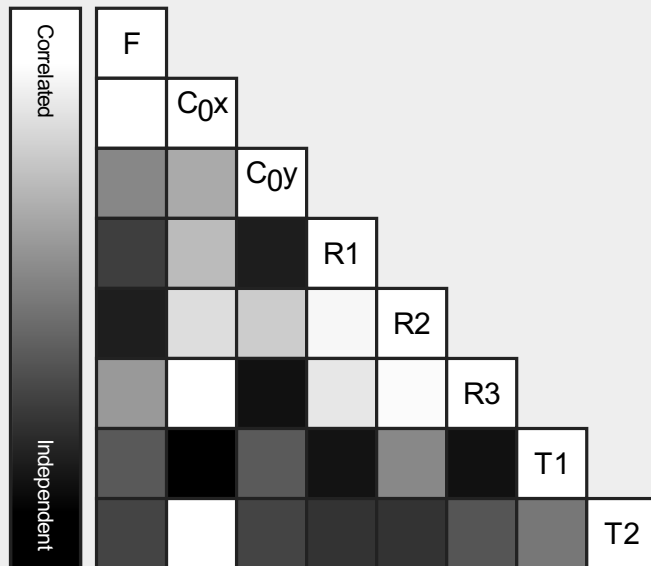
Internal Camera Parameters

RedEdge-M_5.5_1280x960 (Green). Sensor Dimensions: 4.800 [mm] x 3.600 [mm]

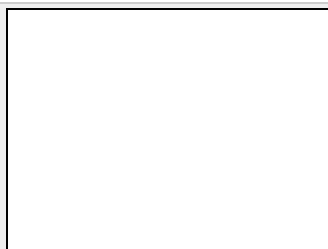


EXIF ID: RedEdge-M_5.5_1280x960

	Focal Length	Principal Point x	Principal Point y	R1	R2	R3	T1	T2
Initial Values	1446.530 [pixel] 5.424 [mm]	654.936 [pixel] 2.456 [mm]	480.704 [pixel] 1.803 [mm]	-0.119	0.237	-0.215	0.000	-0.000
Optimized Values	1443.560 [pixel] 5.413 [mm]	655.672 [pixel] 2.459 [mm]	481.059 [pixel] 1.804 [mm]	-0.101	0.148	-0.032	-0.000	0.000
Uncertainties (Sigma)	0.454 [pixel] 0.002 [mm]	0.112 [pixel] 0.000 [mm]	0.141 [pixel] 0.001 [mm]	0.000	0.002	0.004	0.000	0.000



The correlation between camera internal parameters determined by the bundle adjustment. White indicates a full correlation between the parameters, ie. any change in one can be fully compensated by the other. Black indicates that the parameter is completely independent, and is not affected by other parameters.



The number of Automatic Tie Points (ATPs) per pixel, averaged over all images of the camera model, is color coded between black and white. White indicates that, on average, more than 16 ATPs have been extracted at the pixel location. Black indicates that, on average, 0 ATPs have been extracted at the pixel location. Click on the image to see the average direction and magnitude of the re-projection error for each pixel. Note that the vectors are scaled for better visualization. The scale bar indicates the magnitude of 1 pixel error.

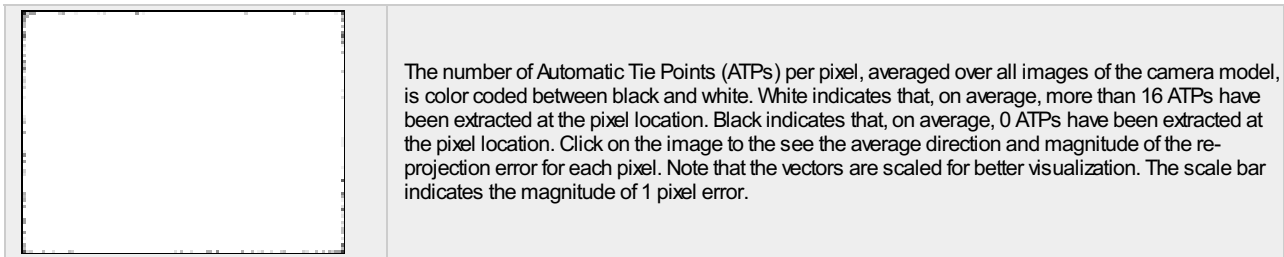
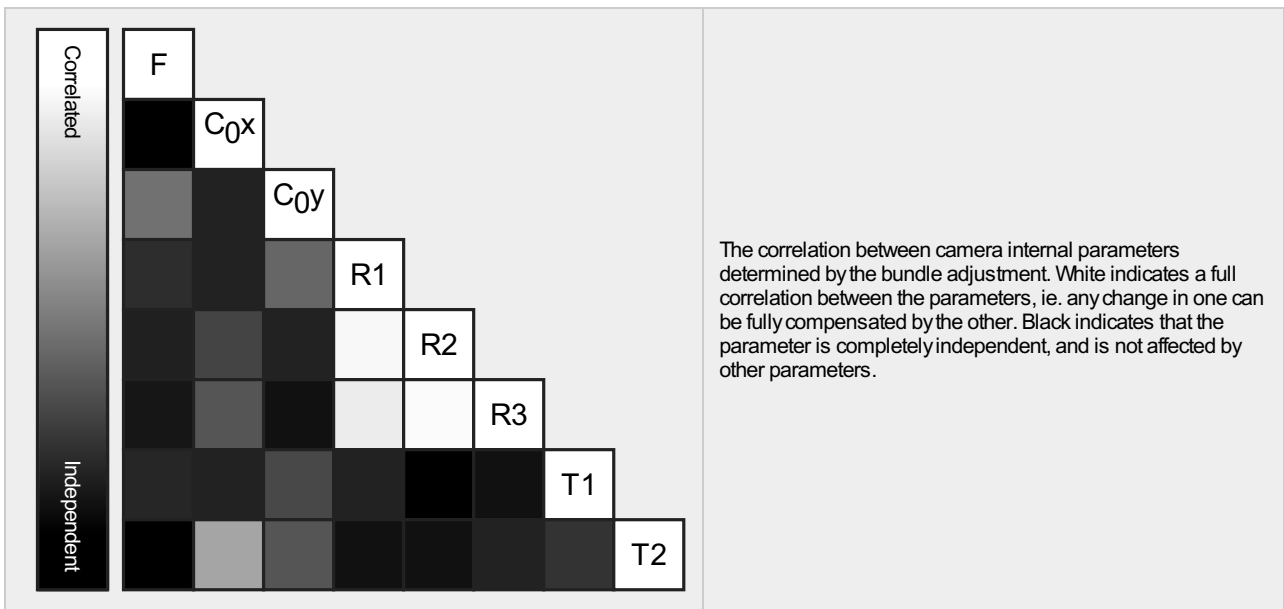
Internal Camera Parameters

RedEdge-M_5.5_1280x960 (Red). Sensor Dimensions: 4.800 [mm] x 3.600 [mm]



EXIF ID: RedEdge-M_5.5_1280x960

	Focal Length	Principal Point x	Principal Point y	R1	R2	R3	T1	T2
Initial Values	1446.530 [pixel] 5.424 [mm]	659.416 [pixel] 2.473 [mm]	484.059 [pixel] 1.815 [mm]	-0.118	0.233	-0.219	0.001	-0.000
Optimized Values	1451.964 [pixel] 5.445 [mm]	660.752 [pixel] 2.478 [mm]	485.341 [pixel] 1.820 [mm]	-0.099	0.139	-0.019	0.000	0.000
Uncertainties (Sigma)	0.460 [pixel] 0.002 [mm]	0.163 [pixel] 0.001 [mm]	0.169 [pixel] 0.001 [mm]	0.001	0.006	0.013	0.000	0.000



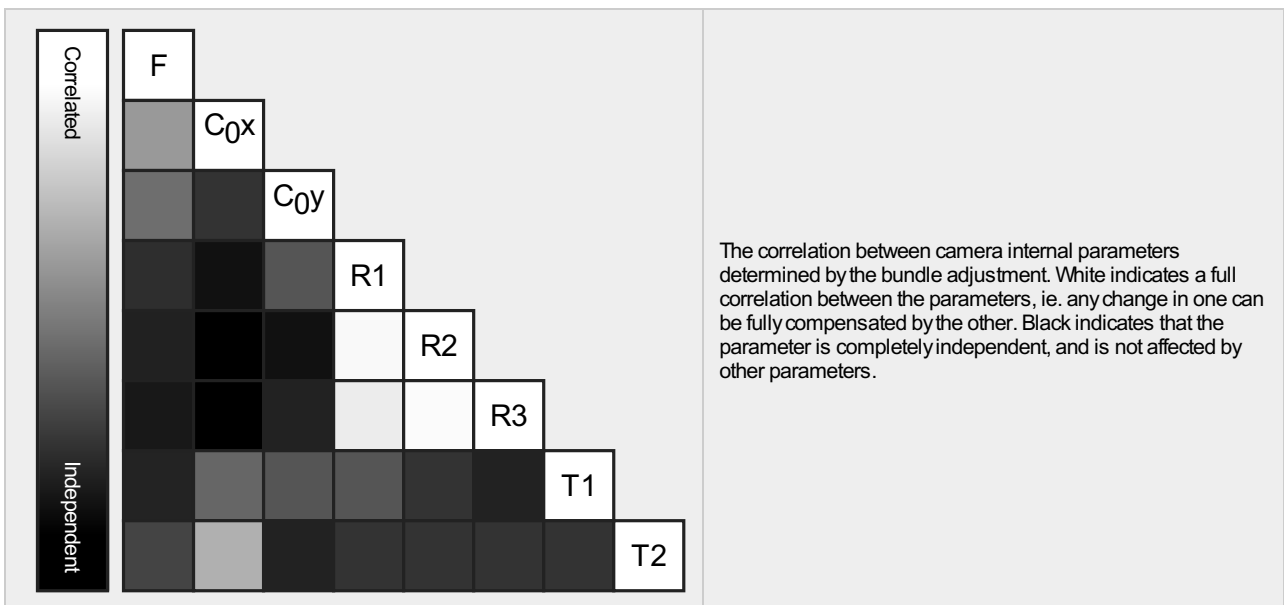
Internal Camera Parameters

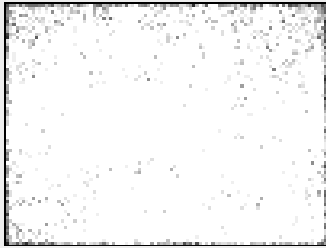
RedEdge-M_5.5_1280x960 (NIR). Sensor Dimensions: 4.800 [mm] x 3.600 [mm]



EXIF ID: RedEdge-M_5.5_1280x960

	Focal Length	Principal Point x	Principal Point y	R1	R2	R3	T1	T2
Initial Values	1446.530 [pixel] 5.424 [mm]	642.352 [pixel] 2.409 [mm]	480.243 [pixel] 1.801 [mm]	-0.125	0.250	-0.251	-0.000	-0.000
Optimized Values	1448.653 [pixel] 5.432 [mm]	642.142 [pixel] 2.408 [mm]	480.491 [pixel] 1.802 [mm]	-0.104	0.132	0.005	-0.000	-0.000
Uncertainties (Sigma)	0.459 [pixel] 0.002 [mm]	0.177 [pixel] 0.001 [mm]	0.176 [pixel] 0.001 [mm]	0.001	0.007	0.015	0.000	0.000





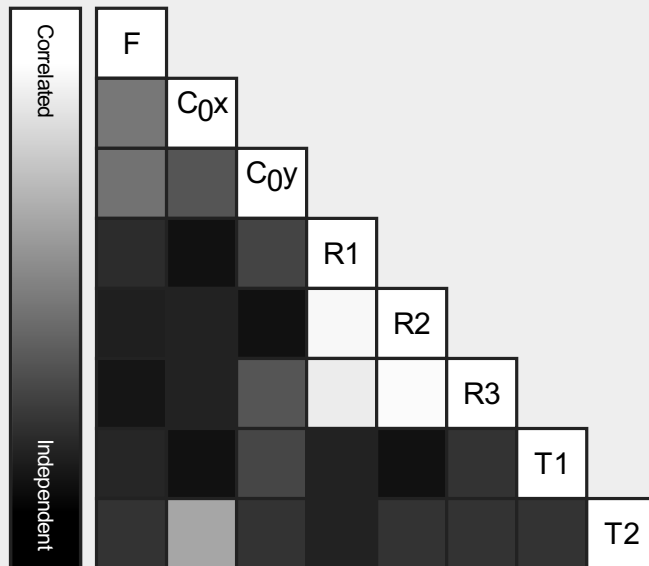
The number of Automatic Tie Points (ATPs) per pixel, averaged over all images of the camera model, is color coded between black and white. White indicates that, on average, more than 16 ATPs have been extracted at the pixel location. Black indicates that, on average, 0 ATPs have been extracted at the pixel location. Click on the image to see the average direction and magnitude of the re-projection error for each pixel. Note that the vectors are scaled for better visualization. The scale bar indicates the magnitude of 1 pixel error.

Internal Camera Parameters

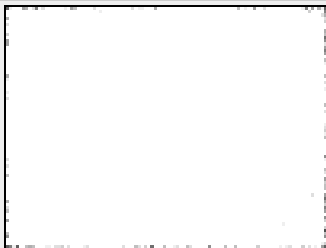
RedEdge-M_5.5_1280x960 (Red edge). Sensor Dimensions: 4.800 [mm] x 3.600 [mm]

EXIF ID: RedEdge-M_5.5_1280x960

	Focal Length	Principal Point x	Principal Point y	R1	R2	R3	T1	T2
Initial Values	1446.530 [pixel] 5.424 [mm]	635.456 [pixel] 2.383 [mm]	490.851 [pixel] 1.841 [mm]	-0.118	0.215	-0.165	0.001	-0.001
Optimized Values	1451.905 [pixel] 5.445 [mm]	635.949 [pixel] 2.385 [mm]	491.188 [pixel] 1.842 [mm]	-0.101	0.142	-0.019	0.000	-0.000
Uncertainties (Sigma)	0.460 [pixel] 0.002 [mm]	0.165 [pixel] 0.001 [mm]	0.169 [pixel] 0.001 [mm]	0.001	0.006	0.014	0.000	0.000



The correlation between camera internal parameters determined by the bundle adjustment. White indicates a full correlation between the parameters, ie. any change in one can be fully compensated by the other. Black indicates that the parameter is completely independent, and is not affected by other parameters.



The number of Automatic Tie Points (ATPs) per pixel, averaged over all images of the camera model, is color coded between black and white. White indicates that, on average, more than 16 ATPs have been extracted at the pixel location. Black indicates that, on average, 0 ATPs have been extracted at the pixel location. Click on the image to see the average direction and magnitude of the re-projection error for each pixel. Note that the vectors are scaled for better visualization. The scale bar indicates the magnitude of 1 pixel error.

Camera Rig «RedEdge-M» Relatives. Images: 3560

	Transl X[m]	Transl Y[m]	Transl Z[m]	Rot X[degree]	Rot Y[degree]	Rot Z[degree]
RedEdge-M_5.5_1280x960 (Green)	Reference Camera					
RedEdge-M_5.5_1280x960 (Blue)						
Initial Values	0.030	0.000	0.000	0.000	0.000	0.000
Optimized values	0.030	0.000	0.000	0.511	-0.109	0.036
Uncertainties (sigma)				0.004	0.005	0.000
RedEdge-M_5.5_1280x960 (Red)						
Initial Values	0.030	-0.021	0.000	0.113	-0.404	-0.004
Optimized values	0.030	-0.021	0.000	-0.079	-0.449	-0.015

Uncertainties (sigma)				0.004	0.005	0.000
RedEdge-M_5.5_1280x960 (NIR)						
Initial Values	0.000	-0.021	0.000	0.134	-0.099	-0.197
Optimized values	0.000	-0.021	0.000	0.063	0.007	-0.196
Uncertainties (sigma)				0.005	0.006	0.000
RedEdge-M_5.5_1280x960 (Red edge)						
Initial Values	0.015	-0.011	0.000	0.025	-0.123	-0.050
Optimized values	0.015	-0.011	0.000	0.022	-0.152	-0.056
Uncertainties (sigma)				0.004	0.005	0.000

? 2D Keypoints Table



	Number of 2D Keypoints per Image	Number of Matched 2D Keypoints per Image
Median	10000	6106
Min	10000	701
Max	10000	8511
Mean	10000	5959

2D Keypoints Table for Camera RedEdge-M_5.5_1280x960 (Blue)

	Number of 2D Keypoints per Image	Number of Matched 2D Keypoints per Image
Median	10000	5037
Min	10000	2753
Max	10000	7459
Mean	10000	5083

2D Keypoints Table for Camera RedEdge-M_5.5_1280x960 (Green)

	Number of 2D Keypoints per Image	Number of Matched 2D Keypoints per Image
Median	10000	6574
Min	10000	701
Max	10000	8511
Mean	10000	6430

2D Keypoints Table for Camera RedEdge-M_5.5_1280x960 (Red)

	Number of 2D Keypoints per Image	Number of Matched 2D Keypoints per Image
Median	10000	5267
Min	10000	3178
Max	10000	7815
Mean	10000	5260

2D Keypoints Table for Camera RedEdge-M_5.5_1280x960 (NIR)

	Number of 2D Keypoints per Image	Number of Matched 2D Keypoints per Image
Median	10000	3736
Min	10000	2362
Max	10000	6781
Mean	10000	3958

2D Keypoints Table for Camera RedEdge-M_5.5_1280x960 (Red edge)

	Number of 2D Keypoints per Image	Number of Matched 2D Keypoints per Image
Median	10000	4703
Min	10000	2811
Max	10000	7526
Mean	10000	4887

Median / 75% / Maximal Number of Matches Between Camera Models

	RedEdge-M_5.5_... (Blue)	RedEdge-M_5.5_... (Green)	RedEdge-M_5.5_1... (Red)	RedEdge-M_5.5_1...(NIR)	RedEdge-M_...(Red edge)
RedEdge-M_5.5_1280x960 (Blue)	622 / 2080 / 4912	376 / 966 / 5360	846 / 1684 / 4396	371 / 757 / 3551	721 / 1435 / 4278
RedEdge-M_5.5_1280x960 (Green)		479 / 1212 / 6012	366 / 950 / 5152	161 / 470 / 4213	332 / 865 / 5098
RedEdge-M_5.5_1280x960 (Red)			748 / 2360 / 5508	456 / 929 / 4366	908 / 1732 / 4982
RedEdge-M_5.5_1280x960 (NIR)				679 / 2087 / 4994	489 / 1077 / 4473
RedEdge-M_5.5_1280x960 (Red edge)					651 / 2040 / 5246

3D Points from 2D Keypoint Matches

	Number of 3D Points Observed
In 2 Images	627077
In 3 Images	226308
In 4 Images	126889
In 5 Images	88386
In 6 Images	67854
In 7 Images	51619
In 8 Images	44384
In 9 Images	37023
In 10 Images	24028
In 11 Images	19572
In 12 Images	16414
In 13 Images	11456
In 14 Images	8844
In 15 Images	7627
In 16 Images	6255
In 17 Images	5201
In 18 Images	3582
In 19 Images	2942
In 20 Images	2569
In 21 Images	1896
In 22 Images	1533
In 23 Images	1345
In 24 Images	1092
In 25 Images	805
In 26 Images	670
In 27 Images	489
In 28 Images	368
In 29 Images	299
In 30 Images	158
In 31 Images	157
In 32 Images	97
In 33 Images	79
In 34 Images	47
In 35 Images	21
In 36 Images	31
In 37 Images	9
In 38 Images	8
In 39 Images	5
In 40 Images	2
In 41 Images	3

2D Keypoint Matches

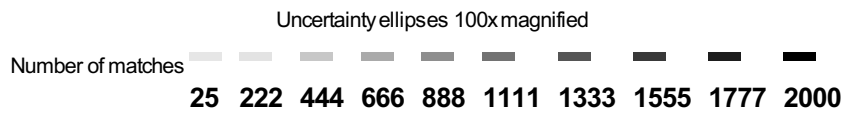
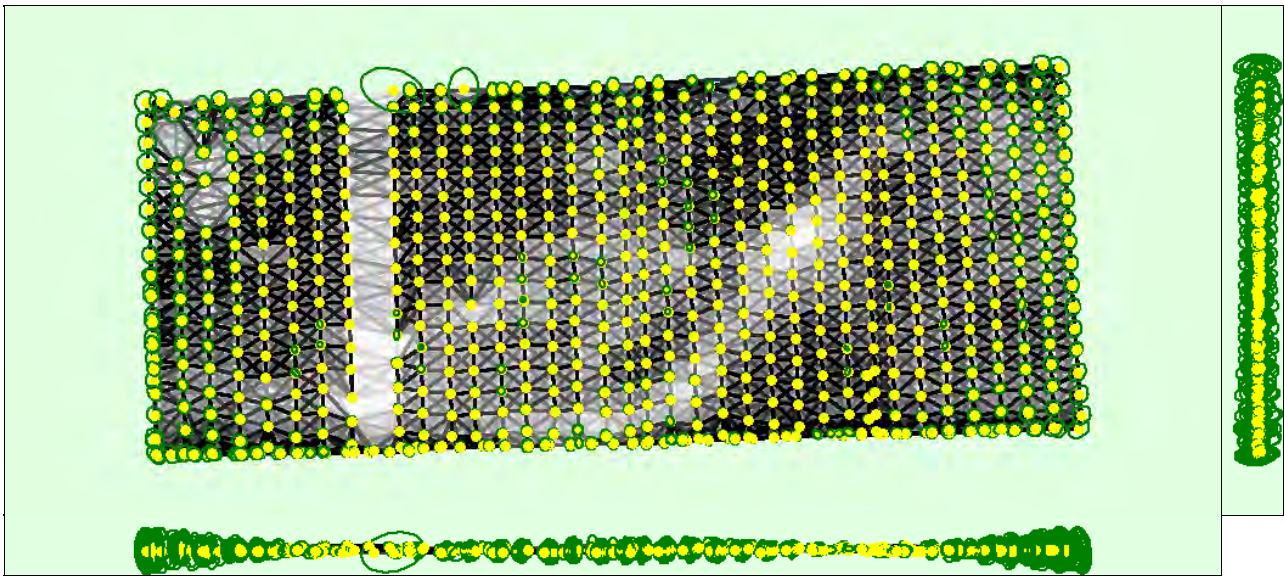


Figure 5: Computed image positions with links between matched images. The darkness of the links indicates the number of matched 2D keypoints between the images. Bright links indicate weak links and require manual tie points or more images. Dark green ellipses indicate the relative camera position uncertainty of the bundle block adjustment result.

Relative camera position and orientation uncertainties

	X [m]	Y [m]	Z [m]	Omega [degree]	Phi [degree]	Kappa [degree]
Mean	0.052	0.056	0.096	0.027	0.042	0.016
Sigma	0.020	0.019	0.051	0.009	0.020	0.009

Geolocation Details

Ground Control Points

GCP Name	Accuracy XYZ [m]	Error X [m]	Error Y [m]	Error Z [m]	Projection Error [pixel]	Verified/Marked
VR01 (3D)	0.020/ 0.020	-0.016	0.011	-0.244	0.293	5 / 5
VR02 (3D)	0.020/ 0.020	-0.009	-0.007	-0.336	0.202	5 / 5
VR03 (3D)	0.020/ 0.020	-0.007	0.017	-0.209	0.126	5 / 5
VR04 (3D)	0.020/ 0.020	0.025	-0.032	0.027	0.173	5 / 5
VR05 (3D)	0.020/ 0.020	-0.012	-0.019	-0.195	0.131	5 / 5
VR06 (3D)	0.020/ 0.020	-0.023	-0.006	0.305	0.245	5 / 5
VR07 (3D)	0.020/ 0.020	-0.064	-0.014	0.552	0.244	5 / 5
Mean [m]		-0.015205	-0.006983	-0.014339		
Sigma [m]		0.024221	0.015605	0.304969		
RMS Error [m]		0.028598	0.017096	0.305306		

Localisation accuracy per GCP and mean errors in the three coordinate directions. The last column counts the number of calibrated images where the GCP has been automatically verified vs. manually marked.

Absolute Geolocation Variance

Mn Error [m]	Max Error [m]	Geolocation Error X [%]	Geolocation Error Y [%]	Geolocation Error Z [%]
--------------	---------------	-------------------------	-------------------------	-------------------------

-	-2.37	0.14	4.33	14.61
-2.37	-1.89	2.25	7.75	11.38
-1.89	-1.42	0.28	9.52	8.57
-1.42	-0.95	1.83	5.14	8.57
-0.95	-0.47	20.22	9.41	8.85
-0.47	0.00	15.34	15.39	14.89
0.00	0.47	37.36	12.95	11.10
0.47	0.95	18.29	10.39	5.76
0.95	1.42	3.88	8.40	4.02
1.42	1.89	0.28	7.87	3.15
1.89	2.37	0.14	6.52	1.12
2.37	-	0.00	2.33	8.01
Mean [m]		-1.069615	2.841031	-5.675336
Sigma [m]		0.645776	1.363108	2.205713
RMS Error [m]		1.249441	3.151114	6.088892

Min Error and Max Error represent geolocation error intervals between -1.5 and 1.5 times the maximum accuracy of all the images. Columns X, Y, Z show the percentage of images with geolocation errors within the predefined error intervals. The geolocation error is the difference between the initial and computed image positions. Note that the image geolocation errors do not correspond to the accuracy of the observed 3D points.

Geolocation Bias	X	Y	Z
Translation [m]	-1.080543	2.901750	-5.323084

Bias between image initial and computed geolocation given in output coordinate system.

Relative Geolocation Variance

Relative Geolocation Error	Images X[%]	Images Y[%]	Images Z[%]
[-1.00, 1.00]	87.81	45.00	47.61
[-2.00, 2.00]	97.33	72.33	80.65
[-3.00, 3.00]	100.00	97.75	92.56
Mean of Geolocation Accuracy [m]	0.857357	0.857357	1.206954
Sigma of Geolocation Accuracy [m]	0.060203	0.060203	0.148413

Images X, Y, Z represent the percentage of images with a relative geolocation error in X, Y, Z.

Initial Processing Details

System Information

Hardware	CPU: Intel(R) Core(TM) i7-6700 CPU @ 3.40GHz RAM: 16GB GPU: NVIDIA GeForce GT 730 (Driver: 25.21.14.1701)
Operating System	Windows 10 Home, 64-bit

Coordinate Systems

Image Coordinate System	WGS 84 (EGM96 Geoid)
Ground Control Point (GCP) Coordinate System	WGS 84 / UTMzone 11N (EGM96 Geoid)
Output Coordinate System	WGS 84 / UTMzone 11N (EGM96 Geoid)

Processing Options

Detected Template	No Template Available
Keypoints Image Scale	Full, Image Scale: 2
Advanced: Matching Image Pairs	Aerial Grid or Corridor

Advanced: Matching Strategy	Use Geometrically Verified Matching: yes
Advanced: Keypoint Extraction	Targeted Number of Keypoints: Custom, Number of Keypoints: 10000
Advanced: Calibration	Calibration Method: Alternative Internal Parameters Optimization: All External Parameters Optimization: All Rematch: Custom, yes
Rig «RedEdge-M» processing	optimize relative rotation using a subset of secondary cameras

Point Cloud Densification details



Processing Options



Image Scale	multiscale, 1/2 (Half image size, Default)
Point Density	Low (Fast)
Minimum Number of Matches	3
3D Textured Mesh Generation	yes
3D Textured Mesh Settings:	Resolution: Medium Resolution (default) Color Balancing: no
LOD	Generated: no
Advanced: 3D Textured Mesh Settings	Sample Density Divider: 1
Advanced: Image Groups	Blue, Green, Red, NIR, Red edge
Advanced: Use Processing Area	yes
Advanced: Use Annotations	yes
Time for Point Cloud Densification	03m:45s
Time for Point Cloud Classification	25s
Time for 3D Textured Mesh Generation	05m:27s

Results



Number of Generated Tiles	1
Number of 3D Densified Points	1681354
Average Density (per m ³)	2.33

DSM, Orthomosaic and Index Details



Processing Options



DSM and Orthomosaic Resolution	1 x GSD (7.36 [cm/pixel])
DSM Filters	Noise Filtering: yes Surface Smoothing: yes, Type: Sharp
Raster DSM	Generated: yes Method: Inverse Distance Weighting Merge Tiles: yes
Orthomosaic	Generated: yes Merge Tiles: yes GeoTIFF Without Transparency: no Google Maps Tiles and KML: no
Raster DTM	Generated: yes Merge Tiles: yes
DTM Resolution	5 x GSD (7.36 [cm/pixel])
Contour Lines Generation	Generated: yes Contour Base [m]: 0 Elevation Interval [m]: 0.5 Resolution [cm]: 100 Minimum Line Size [vertices]: 20
Radiometric calibration with reflectance target	yes
Index Calculator: Reflectance Map	Generated: yes Resolution: 1 x GSD (7.36 [cm/pixel]) Merge Tiles: yes

Index Calculator: Indices	ndvi, GNDVI
Index Calculator: Index Values	Polygon Shapefile [cm/grid]: 400
Time for DSM Generation	03m:20s
Time for Orthomosaic Generation	46m:34s
Time for DTM Generation	01m:50s
Time for Contour Lines Generation	01s
Time for Reflectance Map Generation	01h:06m:01s
Time for Index Map Generation	03m:13s

Camera Radiometric Correction



Camera Name	Band	Radiometric Correction Type	Reflectance target
RedEdge-M_5.5_1280x960	Blue	Camera, Sun Irradiance and Sun Angle using DLS IMU	✓
RedEdge-M_5.5_1280x960	Green	Camera, Sun Irradiance and Sun Angle using DLS IMU	✓
RedEdge-M_5.5_1280x960	Red	Camera, Sun Irradiance and Sun Angle using DLS IMU	✓
RedEdge-M_5.5_1280x960	NIR	Camera, Sun Irradiance and Sun Angle using DLS IMU	✓
RedEdge-M_5.5_1280x960	Red edge	Camera, Sun Irradiance and Sun Angle using DLS IMU	✓

- !** **Important:** Click on the different icons for:
- ?** Help to analyze the results in the Quality Report
 - i** Additional information about the sections

💡 Click [here](#) for additional tips to analyze the Quality Report

Summary



Project	VR-ms-20210408
Processed	2021-05-17 23:36:05
Camera Model Name(s)	RedEdge-M_5.5_1280x960 (Blue), RedEdge-M_5.5_1280x960 (Green), RedEdge-M_5.5_1280x960 (Red), RedEdge-M_5.5_1280x960 (NIR), RedEdge-M_5.5_1280x960 (Red edge)
Rig name(s)	«RedEdge-M»
Average Ground Sampling Distance (GSD)	7.36 cm / 2.90 in
Area Covered	0.534 km ² / 53.3897 ha / 0.21 sq. mi. / 131.9972 acres
Time for Initial Processing (without report)	41m:51s

Quality Check



? Images	median of 10000 keypoints per image	
? Dataset	2860 out of 2995 images calibrated (95%), all images enabled, 3 blocks	
? Camera Optimization	0.58% relative difference between initial and optimized internal camera parameters	
? Matching	median of 5645.29 matches per calibrated image	
? Georeferencing	yes, 5 GCPs (5 3D), mean RMS error = 0.01 m	

? Preview

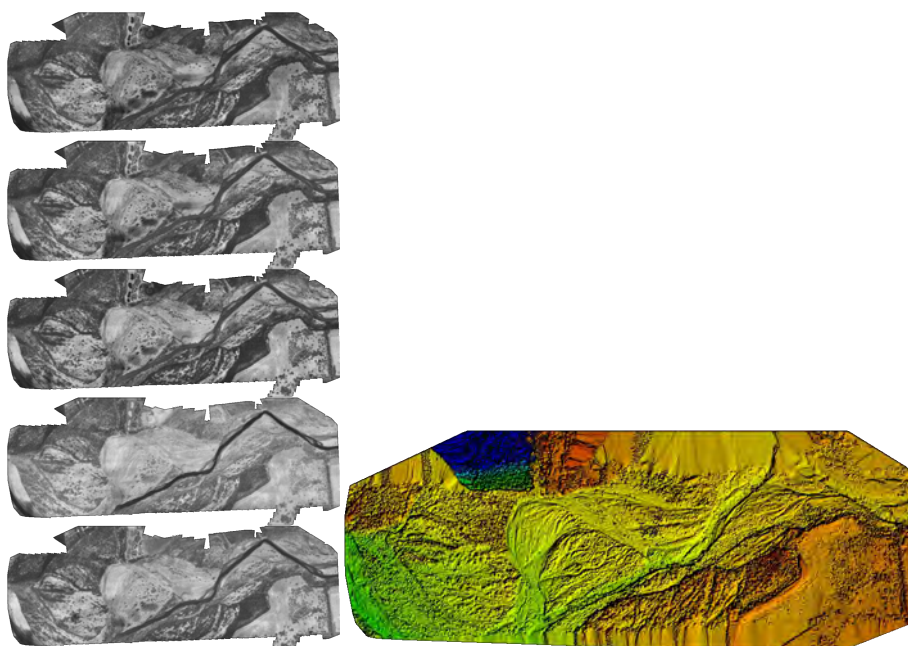


Figure 1: Orthomosaic and the corresponding sparse Digital Surface Model (DSM) before densification.

Calibration Details



Number of Calibrated Images	2860 out of 2995
Number of Geolocated Images	2995 out of 2995

Initial Image Positions

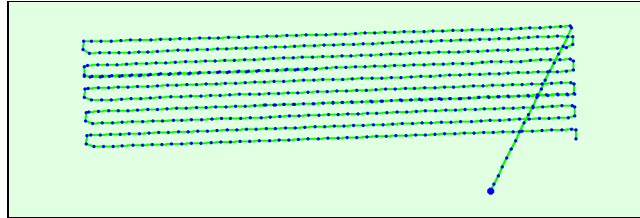
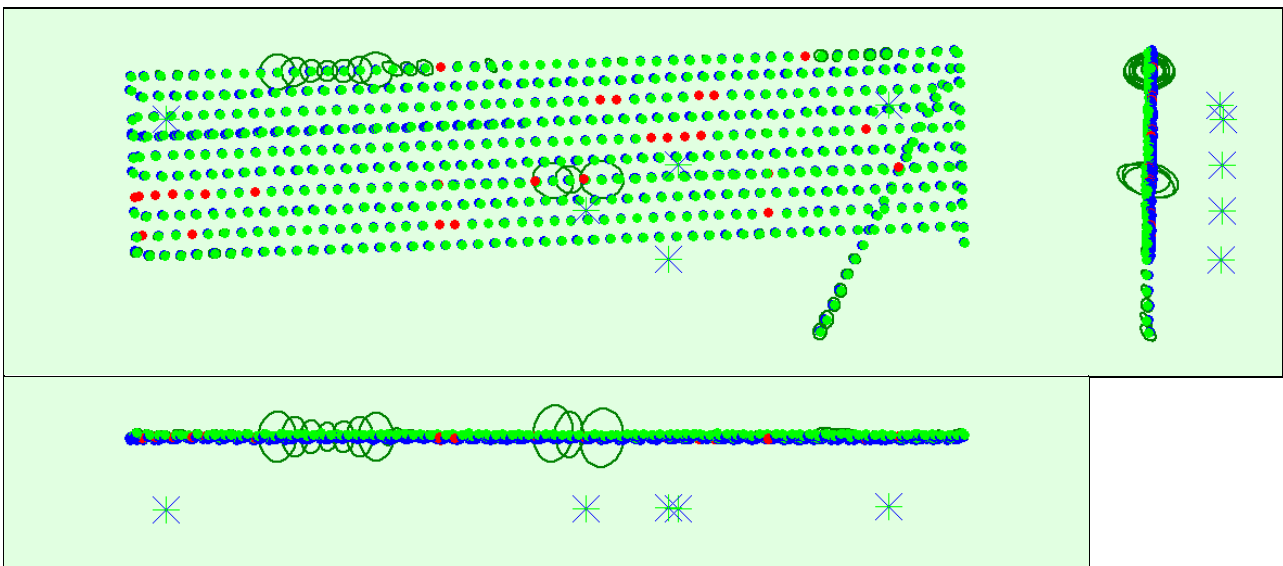


Figure 2: Top view of the initial image position. The green line follows the position of the images in time starting from the large blue dot.

Computed Image/GCPs/Manual Tie Points Positions



Uncertainty ellipses 100x magnified

Figure 3: Offset between initial (blue dots) and computed (green dots) image positions as well as the offset between the GCPs initial positions (blue crosses) and their computed positions (green crosses) in the top-view (XY plane), front-view (XZ plane), and side-view (YZ plane). Red dots indicate disabled or uncalibrated images. Dark green ellipses indicate the absolute position uncertainty of the bundle block adjustment result.

Absolute camera position and orientation uncertainties



	X[m]	Y[m]	Z[m]	Omega [degree]	Phi [degree]	Kappa [degree]
Mean	0.047	0.045	0.043	0.036	0.029	0.020
Sigma	0.028	0.026	0.040	0.181	0.042	0.135

Overlap

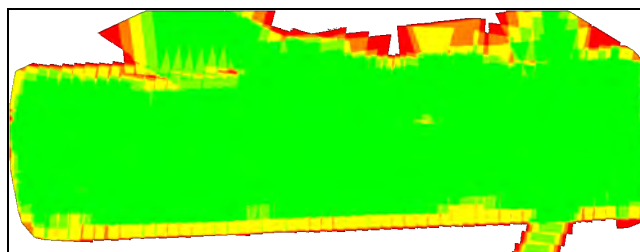




Figure 4: Number of overlapping images computed for each pixel of the orthomosaic. Red and yellow areas indicate low overlap for which poor results may be generated. Green areas indicate an overlap of over 5 images for every pixel. Good quality results will be generated as long as the number of keypoint matches is also sufficient for these areas (see Figure 5 for keypoint matches).

Bundle Block Adjustment Details

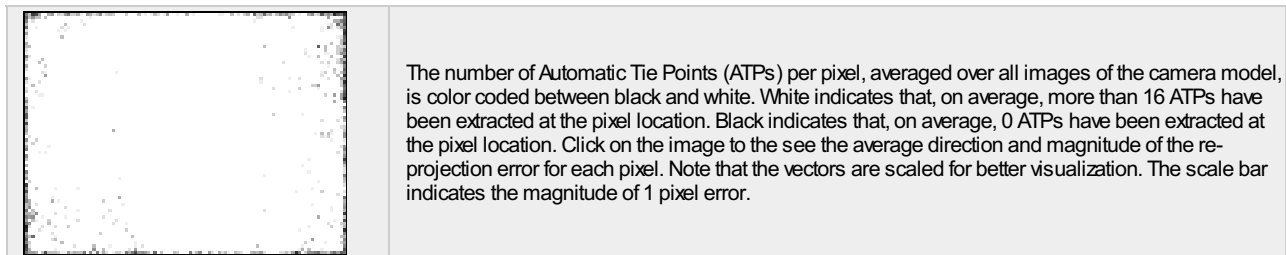
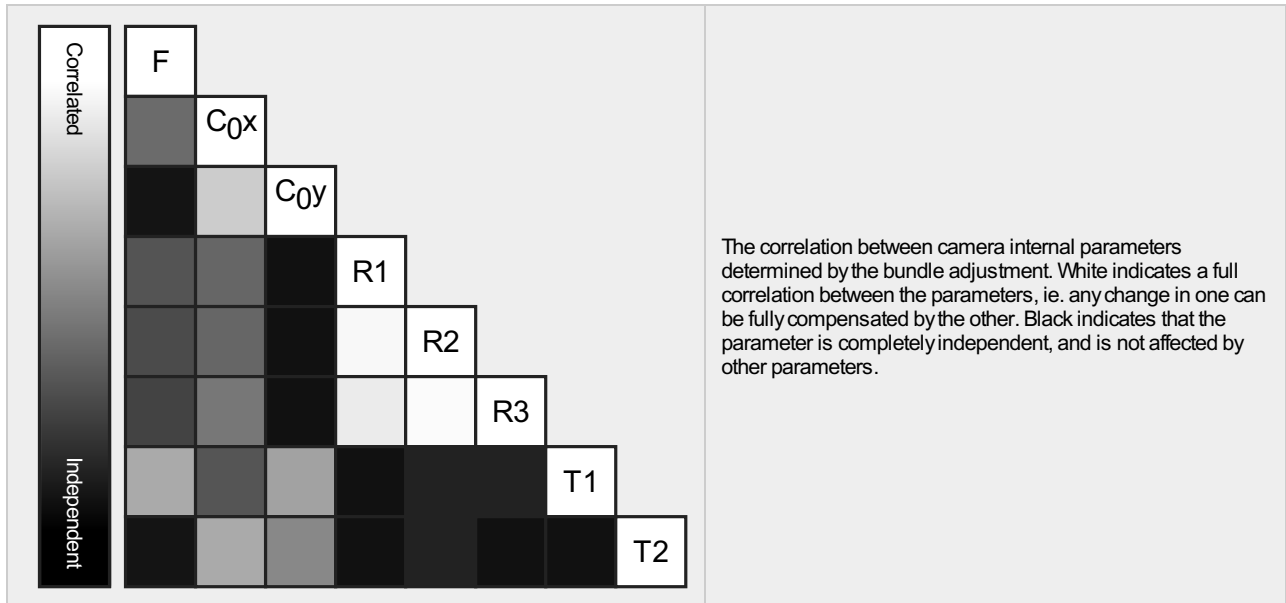
Number of 2D Keypoint Observations for Bundle Block Adjustment	4403725
Number of 3D Points for Bundle Block Adjustment	1074145
Mean Reprojection Error [pixels]	0.216

Internal Camera Parameters

RedEdge-M_5.5_1280x960 (Blue). Sensor Dimensions: 4.800 [mm] x 3.600 [mm]

EXIF ID: RedEdge-M_5.5_1280x960

	Focal Length	Principal Point x	Principal Point y	R1	R2	R3	T1	T2
Initial Values	1446.530 [pixel] 5.424 [mm]	669.584 [pixel] 2.511 [mm]	489.632 [pixel] 1.836 [mm]	-0.114	0.232	-0.214	0.001	-0.000
Optimized Values	1460.517 [pixel] 5.477 [mm]	667.908 [pixel] 2.505 [mm]	488.296 [pixel] 1.831 [mm]	-0.096	0.135	-0.003	0.001	-0.000
Uncertainties (Sigma)	0.226 [pixel] 0.001 [mm]	0.233 [pixel] 0.001 [mm]	0.168 [pixel] 0.001 [mm]	0.001	0.008	0.018	0.000	0.000

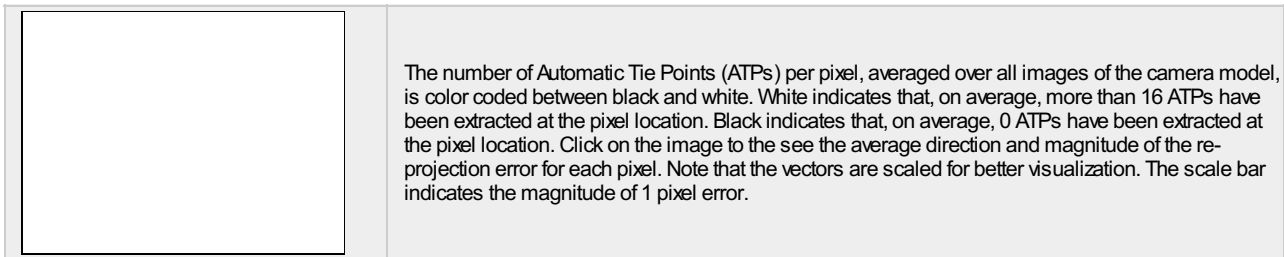
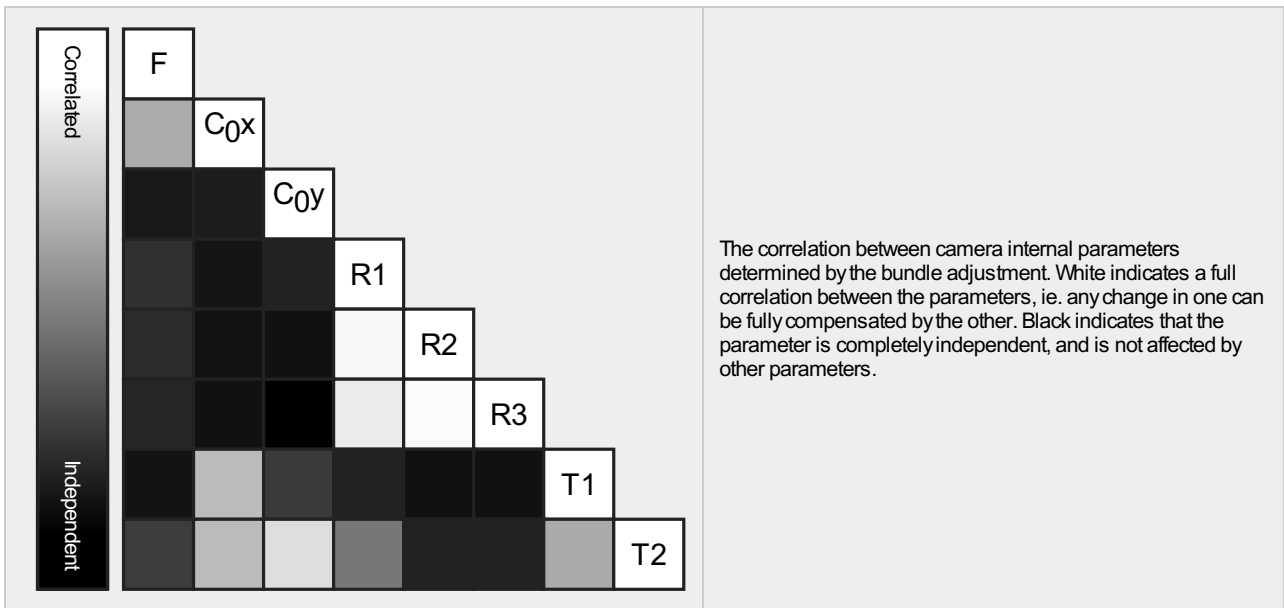


Internal Camera Parameters

RedEdge-M_5.5_1280x960 (Green). Sensor Dimensions: 4.800 [mm] x 3.600 [mm]

EXIF ID: RedEdge-M_5.5_1280x960

	Focal Length	Principal Point x	Principal Point y	R1	R2	R3	T1	T2
Initial Values	1446.530 [pixel] 5.424 [mm]	654.936 [pixel] 2.456 [mm]	480.704 [pixel] 1.803 [mm]	-0.119	0.237	-0.215	0.000	-0.000
Optimized Values	1448.201 [pixel] 5.431 [mm]	654.460 [pixel] 2.454 [mm]	479.659 [pixel] 1.799 [mm]	-0.101	0.146	-0.024	-0.000	0.000
Uncertainties (Sigma)	0.213 [pixel] 0.001 [mm]	0.156 [pixel] 0.001 [mm]	0.106 [pixel] 0.000 [mm]	0.000	0.003	0.006	0.000	0.000



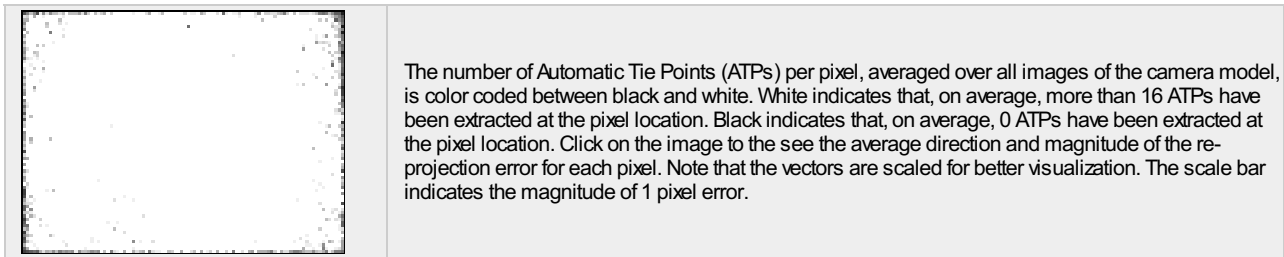
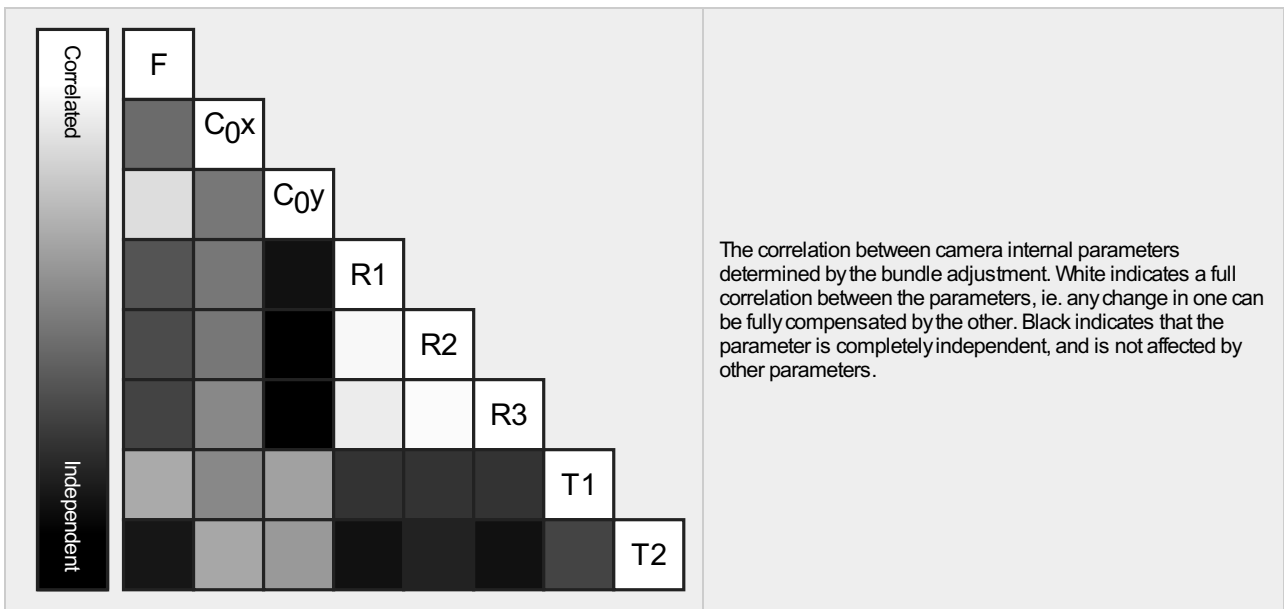
Internal Camera Parameters

RedEdge-M_5.5_1280x960 (Red). Sensor Dimensions: 4.800 [mm] x 3.600 [mm]



EXIF ID: RedEdge-M_5.5_1280x960

	Focal Length	Principal Point x	Principal Point y	R1	R2	R3	T1	T2
Initial Values	1446.530 [pixel] 5.424 [mm]	659.416 [pixel] 2.473 [mm]	484.059 [pixel] 1.815 [mm]	-0.118	0.233	-0.219	0.001	-0.000
Optimized Values	1456.563 [pixel] 5.462 [mm]	659.340 [pixel] 2.473 [mm]	484.112 [pixel] 1.815 [mm]	-0.098	0.124	0.016	0.001	0.000
Uncertainties (Sigma)	0.226 [pixel] 0.001 [mm]	0.229 [pixel] 0.001 [mm]	0.168 [pixel] 0.001 [mm]	0.001	0.009	0.018	0.000	0.000



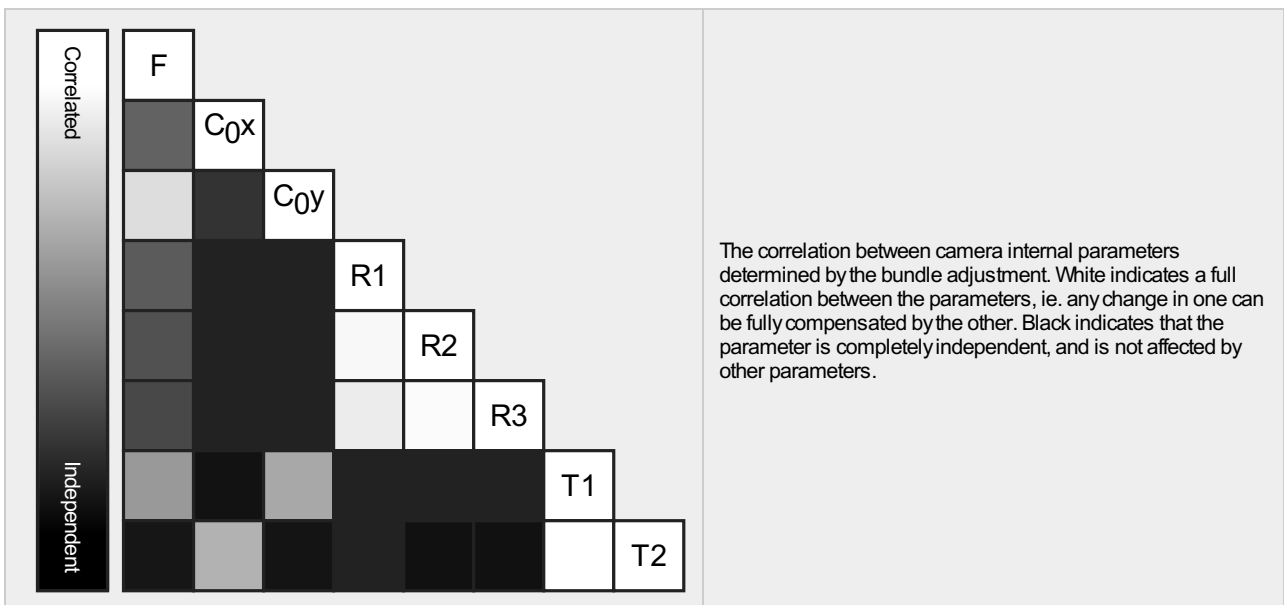
Internal Camera Parameters

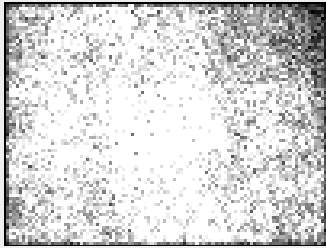
RedEdge-M_5.5_1280x960 (NIR). Sensor Dimensions: 4.800 [mm] x 3.600 [mm]



EXIF ID: RedEdge-M_5.5_1280x960

	Focal Length	Principal Point x	Principal Point y	R1	R2	R3	T1	T2
Initial Values	1446.530 [pixel] 5.424 [mm]	642.352 [pixel] 2.409 [mm]	480.243 [pixel] 1.801 [mm]	-0.125	0.250	-0.251	-0.000	-0.000
Optimized Values	1453.381 [pixel] 5.450 [mm]	641.168 [pixel] 2.404 [mm]	478.711 [pixel] 1.795 [mm]	-0.107	0.155	-0.046	-0.000	-0.000
Uncertainties (Sigma)	0.228 [pixel] 0.001 [mm]	0.252 [pixel] 0.001 [mm]	0.183 [pixel] 0.001 [mm]	0.001	0.010	0.022	0.000	0.000





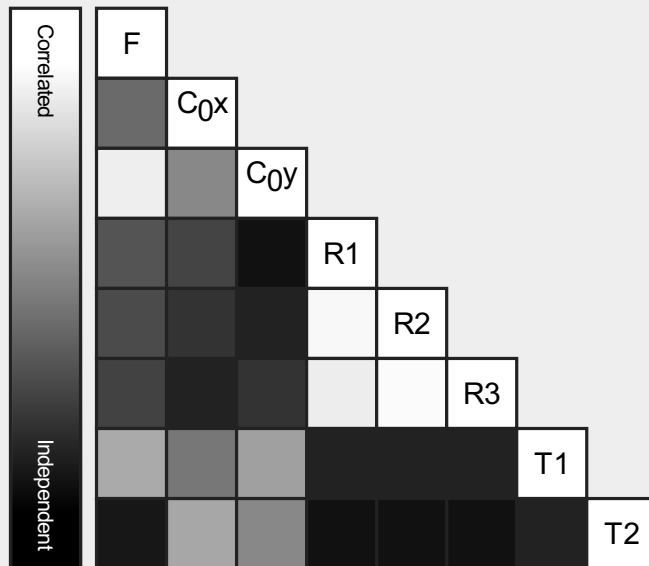
The number of Automatic Tie Points (ATPs) per pixel, averaged over all images of the camera model, is color coded between black and white. White indicates that, on average, more than 16 ATPs have been extracted at the pixel location. Black indicates that, on average, 0 ATPs have been extracted at the pixel location. Click on the image to see the average direction and magnitude of the re-projection error for each pixel. Note that the vectors are scaled for better visualization. The scale bar indicates the magnitude of 1 pixel error.

Internal Camera Parameters

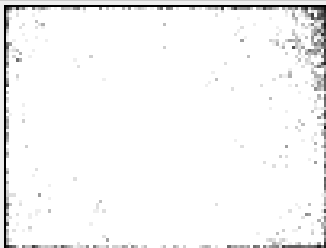
RedEdge-M_5.5_1280x960 (Red edge). Sensor Dimensions: 4.800 [mm] x 3.600 [mm]

EXIF ID: RedEdge-M_5.5_1280x960

	Focal Length	Principal Point x	Principal Point y	R1	R2	R3	T1	T2
Initial Values	1446.530 [pixel] 5.424 [mm]	635.456 [pixel] 2.383 [mm]	490.851 [pixel] 1.841 [mm]	-0.118	0.215	-0.165	0.001	-0.001
Optimized Values	1456.517 [pixel] 5.462 [mm]	634.746 [pixel] 2.380 [mm]	489.909 [pixel] 1.837 [mm]	-0.101	0.134	-0.001	0.000	-0.000
Uncertainties (Sigma)	0.226 [pixel] 0.001 [mm]	0.232 [pixel] 0.001 [mm]	0.168 [pixel] 0.001 [mm]	0.001	0.009	0.020	0.000	0.000



The correlation between camera internal parameters determined by the bundle adjustment. White indicates a full correlation between the parameters, ie. any change in one can be fully compensated by the other. Black indicates that the parameter is completely independent, and is not affected by other parameters.



The number of Automatic Tie Points (ATPs) per pixel, averaged over all images of the camera model, is color coded between black and white. White indicates that, on average, more than 16 ATPs have been extracted at the pixel location. Black indicates that, on average, 0 ATPs have been extracted at the pixel location. Click on the image to see the average direction and magnitude of the re-projection error for each pixel. Note that the vectors are scaled for better visualization. The scale bar indicates the magnitude of 1 pixel error.

Camera Rig «RedEdge-M» Relatives. Images: 2995

	Transl X[m]	Transl Y[m]	Transl Z[m]	Rot X[degree]	Rot Y[degree]	Rot Z[degree]
RedEdge-M_5.5_1280x960 (Green)	Reference Camera					
RedEdge-M_5.5_1280x960 (Blue)						
Initial Values	0.030	0.000	0.000	0.000	0.000	0.000
Optimized values	0.030	0.000	0.000	0.516	-0.129	0.036
Uncertainties (sigma)				0.006	0.007	0.001
RedEdge-M_5.5_1280x960 (Red)						
Initial Values	0.030	-0.021	0.000	0.113	-0.404	-0.004
Optimized values	0.030	-0.021	0.000	-0.082	-0.453	-0.016

Uncertainties (sigma)				0.006	0.007	0.001
RedEdge-M_5.5_1280x960 (NIR)						
Initial Values	0.000	-0.021	0.000	0.134	-0.099	-0.197
Optimized values	0.000	-0.021	0.000	0.080	0.014	-0.194
Uncertainties (sigma)				0.006	0.008	0.001
RedEdge-M_5.5_1280x960 (Red edge)						
Initial Values	0.015	-0.011	0.000	0.025	-0.123	-0.050
Optimized values	0.015	-0.011	0.000	0.020	-0.151	-0.056
Uncertainties (sigma)				0.006	0.007	0.001

? 2D Keypoints Table



	Number of 2D Keypoints per Image	Number of Matched 2D Keypoints per Image
Median	10000	5645
Min	10000	1144
Max	10000	8246
Mean	10000	5505

2D Keypoints Table for Camera RedEdge-M_5.5_1280x960 (Blue)

	Number of 2D Keypoints per Image	Number of Matched 2D Keypoints per Image
Median	10000	4627
Min	10000	1474
Max	10000	6638
Mean	10000	4441

2D Keypoints Table for Camera RedEdge-M_5.5_1280x960 (Green)

	Number of 2D Keypoints per Image	Number of Matched 2D Keypoints per Image
Median	10000	6155
Min	10000	1756
Max	10000	8246
Mean	10000	6010

2D Keypoints Table for Camera RedEdge-M_5.5_1280x960 (Red)

	Number of 2D Keypoints per Image	Number of Matched 2D Keypoints per Image
Median	10000	4581
Min	10000	1618
Max	10000	6694
Mean	10000	4642

2D Keypoints Table for Camera RedEdge-M_5.5_1280x960 (NIR)

	Number of 2D Keypoints per Image	Number of Matched 2D Keypoints per Image
Median	10000	3455
Min	10000	1144
Max	10000	6184
Mean	10000	3513

2D Keypoints Table for Camera RedEdge-M_5.5_1280x960 (Red edge)

	Number of 2D Keypoints per Image	Number of Matched 2D Keypoints per Image
Median	10000	4501
Min	10000	1561
Max	10000	6488
Mean	10000	4357

Median / 75% / Maximal Number of Matches Between Camera Models

	RedEdge-M_5.5_... (Blue)	RedEdge-M_5.5_... (Green)	RedEdge-M_5.5_1... (Red)	RedEdge-M_5.5_1...(NIR)	RedEdge-M_...(Red edge)
RedEdge-M_5.5_1280x960 (Blue)	674 / 2215 / 3339	295 / 873 / 4271	741 / 1643 / 3903	367 / 716 / 2914	690 / 1346 / 3576
RedEdge-M_5.5_1280x960 (Green)		392 / 1103 / 5472	292 / 856 / 4294	133 / 390 / 3290	263 / 779 / 4133
RedEdge-M_5.5_1280x960 (Red)			708 / 2423 / 3479	455 / 803 / 3113	850 / 1731 / 3990
RedEdge-M_5.5_1280x960 (NIR)				590 / 1938 / 3043	505 / 1012 / 3343
RedEdge-M_5.5_1280x960 (Red edge)					736 / 2152 / 3192

3D Points from 2D Keypoint Matches



	Number of 3D Points Observed
In 2 Images	499939
In 3 Images	188923
In 4 Images	100046
In 5 Images	65408
In 6 Images	50427
In 7 Images	35487
In 8 Images	28465
In 9 Images	23281
In 10 Images	16459
In 11 Images	13864
In 12 Images	11382
In 13 Images	8391
In 14 Images	6896
In 15 Images	5388
In 16 Images	4350
In 17 Images	3520
In 18 Images	2703
In 19 Images	2056
In 20 Images	1730
In 21 Images	1308
In 22 Images	901
In 23 Images	722
In 24 Images	757
In 25 Images	525
In 26 Images	290
In 27 Images	233
In 28 Images	211
In 29 Images	136
In 30 Images	118
In 31 Images	91
In 32 Images	69
In 33 Images	44
In 34 Images	19
In 35 Images	4
In 36 Images	2

2D Keypoint Matches



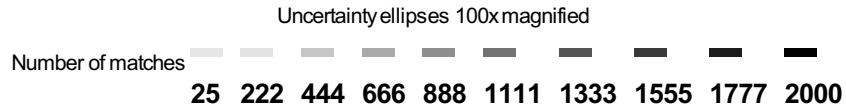
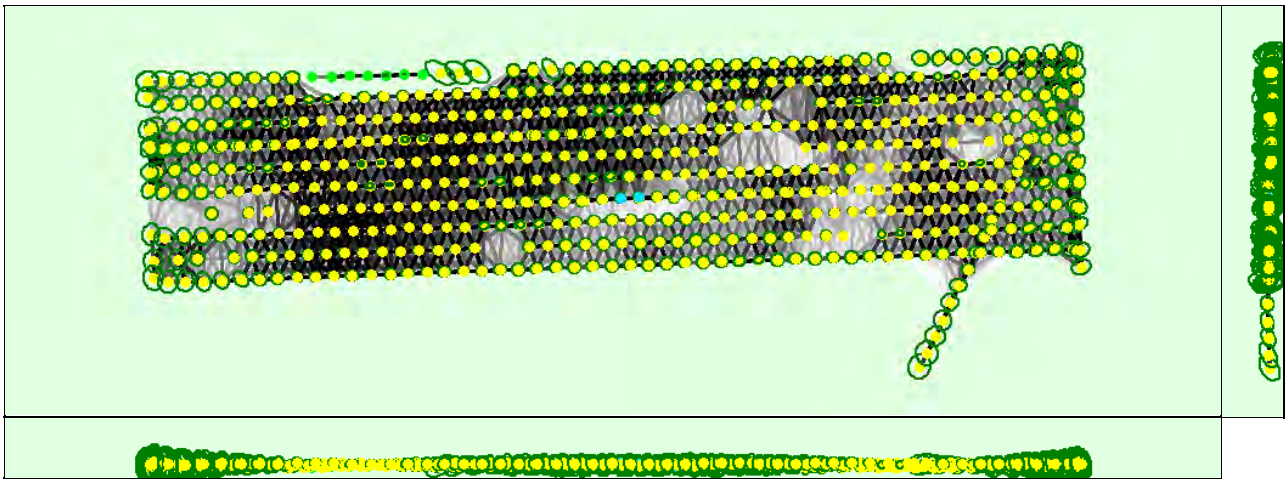


Figure 5: Computed image positions with links between matched images. The darkness of the links indicates the number of matched 2D keypoints between the images. Bright links indicate weak links and require manual tie points or more images. Dark green ellipses indicate the relative camera position uncertainty of the bundle block adjustment result.

Relative camera position and orientation uncertainties

	X [m]	Y [m]	Z [m]	Omega [degree]	Phi [degree]	Kappa [degree]
Mean	0.073	0.066	0.102	0.027	0.045	0.023
Sigma	0.026	0.028	0.048	0.043	0.017	0.027

Geolocation Details

Ground Control Points

GCP Name	Accuracy XYZ [m]	Error X [m]	Error Y [m]	Error Z [m]	Projection Error [pixel]	Verified/Marked
VR03 (3D)	0.020/ 0.020	-0.002	-0.004	-0.020	0.149	5 / 5
VR04 (3D)	0.020/ 0.020	-0.010	0.000	-0.039	0.163	6 / 6
VR05 (3D)	0.020/ 0.020	0.003	-0.004	0.008	0.177	5 / 5
VR06 (3D)	0.020/ 0.020	0.010	0.005	0.020	0.277	6 / 6
VR09 (3D)	0.020/ 0.020	0.002	-0.000	0.017	0.265	7 / 7
Mean [m]		0.000604	-0.000576	-0.002749		
Sigma [m]		0.006335	0.003138	0.023079		
RMS Error [m]		0.006364	0.003190	0.023242		

Localisation accuracy per GCP and mean errors in the three coordinate directions. The last column counts the number of calibrated images where the GCP has been automatically verified vs. manually marked.

Absolute Geolocation Variance

Mn Error [m]	Max Error [m]	Geolocation Error X [%]	Geolocation Error Y [%]	Geolocation Error Z [%]
-	-2.32	0.00	0.00	0.00
-2.32	-1.85	0.56	0.00	0.17
-1.85	-1.39	12.38	0.00	1.40
-1.39	-0.93	9.90	0.52	4.55
-0.93	-0.46	13.99	10.91	12.24

-0.46	0.00	11.64	37.69	34.93
0.00	0.46	12.06	38.32	29.51
0.46	0.93	14.34	11.71	12.66
0.93	1.39	12.03	0.49	2.45
1.39	1.85	10.00	0.35	1.40
1.85	2.32	3.04	0.00	0.70
2.32	-	0.07	0.00	0.00
Mean [m]		-2.066234	1.055837	-3.259650
Sigma [m]		1.085081	0.390719	0.582742
RMS Error [m]		2.333822	1.125812	3.311330

Min Error and Max Error represent geolocation error intervals between -1.5 and 1.5 times the maximum accuracy of all the images. Columns X, Y, Z show the percentage of images with geolocation errors within the predefined error intervals. The geolocation error is the difference between the initial and computed image positions. Note that the image geolocation errors do not correspond to the accuracy of the observed 3D points.

Geolocation Bias	X	Y	Z
Translation [m]	-2.120930	1.052510	-3.242580

Bias between image initial and computed geolocation given in output coordinate system.

Relative Geolocation Variance

Relative Geolocation Error	Images X[%]	Images Y[%]	Images Z[%]
[-1.00, 1.00]	49.51	97.34	95.10
[-2.00, 2.00]	94.02	100.00	100.00
[-3.00, 3.00]	100.00	100.00	100.00
Mean of Geolocation Accuracy [m]	0.883643	0.883643	1.286844
Sigma of Geolocation Accuracy [m]	0.053570	0.053570	0.152039

Images X, Y, Z represent the percentage of images with a relative geolocation error in X, Y, Z.

Initial Processing Details

System Information

Hardware	CPU: Intel(R) Core(TM) i7-6700 CPU @ 3.40GHz RAM: 16GB GPU: NVIDIA GeForce GT 730 (Driver: 25.21.14.1701)
Operating System	Windows 10 Home, 64-bit

Coordinate Systems

Image Coordinate System	WGS 84 (EGM96 Geoid)
Ground Control Point (GCP) Coordinate System	WGS 84 / UTMzone 11N (EGM96 Geoid)
Output Coordinate System	WGS 84 / UTMzone 11N (EGM96 Geoid)

Processing Options

Detected Template	No Template Available
Keypoints Image Scale	Full, Image Scale: 2
Advanced: Matching Image Pairs	Aerial Grid or Corridor
Advanced: Matching Strategy	Use Geometrically Verified Matching: yes
Advanced: Keypoint Extraction	Targeted Number of Keypoints: Custom, Number of Keypoints: 10000
Advanced: Calibration	Calibration Method: Alternative Internal Parameters Optimization: All External Parameters Optimization: All Rematch: Custom, yes

Point Cloud Densification details



Processing Options



Image Scale	multiscale, 1/2 (Half image size, Default)
Point Density	Optimal
Minimum Number of Matches	3
3D Textured Mesh Generation	yes
3D Textured Mesh Settings:	Resolution: Medium Resolution (default) Color Balancing: no
LOD	Generated: no
Advanced: 3D Textured Mesh Settings	Sample Density Divider: 1
Advanced: Image Groups	Blue, Green, Red, NIR, Red edge
Advanced: Use Processing Area	yes
Advanced: Use Annotations	yes
Time for Point Cloud Densification	06m:49s
Time for Point Cloud Classification	01m:21s
Time for 3D Textured Mesh Generation	08m:23s

Results



Number of Generated Tiles	1
Number of 3D Densified Points	5220789
Average Density (per m ³)	7.91

DSM, Orthomosaic and Index Details



Processing Options



DSM and Orthomosaic Resolution	1 x GSD (7.36 [cm/pixel])
DSM Filters	Noise Filtering: yes Surface Smoothing: yes, Type: Sharp
Raster DSM	Generated: yes Method: Inverse Distance Weighting Merge Tiles: yes
Orthomosaic	Generated: yes Merge Tiles: yes GeoTIFF Without Transparency: no Google Maps Tiles and KML: no
Grid DSM	Generated: yes, Spacing [cm]: 100
Raster DTM	Generated: yes Merge Tiles: yes
DTM Resolution	5 x GSD (7.36 [cm/pixel])
Contour Lines Generation	Generated: yes Contour Base [m]: 0 Elevation Interval [m]: 0.5 Resolution [cm]: 100 Minimum Line Size [vertices]: 20
Radiometric calibration with reflectance target	yes
Index Calculator: Reflectance Map	Generated: yes Resolution: 1 x GSD (7.36 [cm/pixel]) Merge Tiles: no
Index Calculator: Indices	ndvi, GNDVI
Index Calculator: Index Values	Polygon Shapefile [cm/grid]: 400
Time for DSM Generation	03m:45s
Time for Orthomosaic Generation	43m:43s

Time for DTM Generation	01m:36s
Time for Contour Lines Generation	02s
Time for Reflectance Map Generation	55m:49s
Time for Index Map Generation	03m:05s

Camera Radiometric Correction



Camera Name	Band	Radiometric Correction Type	Reflectance target
RedEdge-M_5.5_1280x960	Blue	Camera, Sun Irradiance and Sun Angle using DLS IMU	✓
RedEdge-M_5.5_1280x960	Green	Camera, Sun Irradiance and Sun Angle using DLS IMU	✓
RedEdge-M_5.5_1280x960	Red	Camera, Sun Irradiance and Sun Angle using DLS IMU	✓
RedEdge-M_5.5_1280x960	NIR	Camera, Sun Irradiance and Sun Angle using DLS IMU	✓
RedEdge-M_5.5_1280x960	Red edge	Camera, Sun Irradiance and Sun Angle using DLS IMU	✓

Quality Report



Generated with Pix4Dmapper version 4.6.4



Important: Click on the different icons for:



Help to analyze the results in the Quality Report



Additional information about the sections



Click [here](#) for additional tips to analyze the Quality Report

Summary



Project	Clark_County_210413
Processed	2021-04-14 10:54:14
Camera Model Name(s)	FC6310_8.8_5472x3648 (RGB)
Average Ground Sampling Distance (GSD)	2.30 cm / 0.91 in
Area Covered	0.433 km ² / 43.3121 ha / 0.17 sq. mi. / 107.0819 acres

Quality Check



Images	median of 5499 keypoints per image	
Dataset	696 out of 696 images calibrated (100%), all images enabled	
Camera Optimization	4.41% relative difference between initial and optimized internal camera parameters	
Matching	median of 1768.65 matches per calibrated image	
Georeferencing	yes, 8 GCPs (8 3D), mean RMS error = 0.005 US survey foot	

Preview



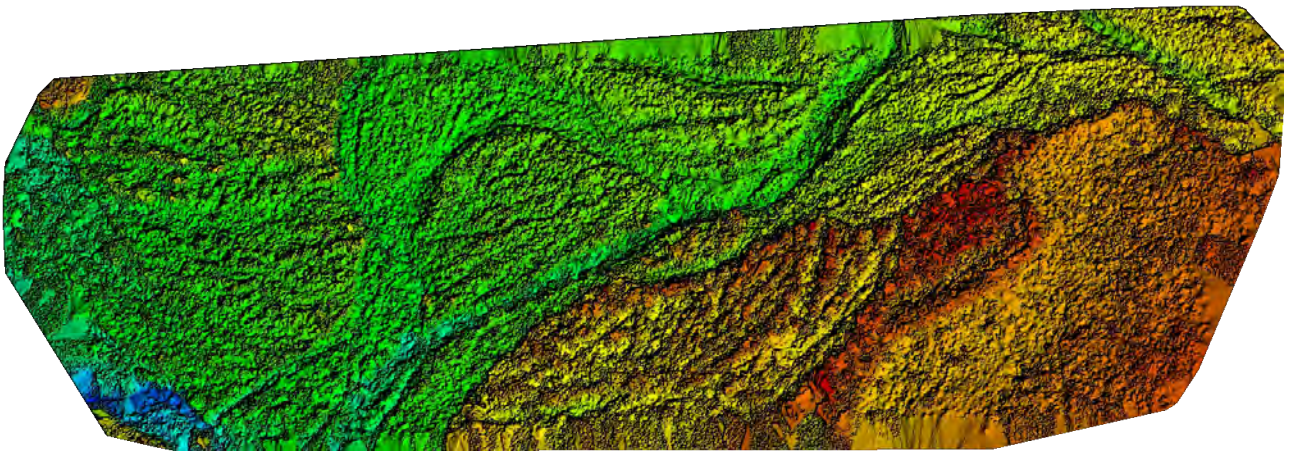


Figure 1: Orthomosaic and the corresponding sparse Digital Surface Model (DSM) before densification.

Calibration Details

Number of Calibrated Images	696 out of 696
Number of Geolocated Images	696 out of 696

Initial Image Positions

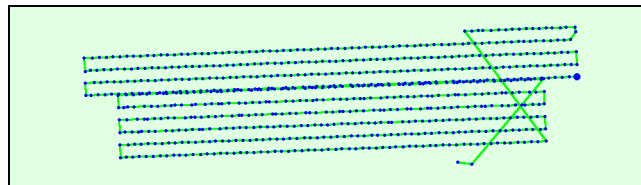
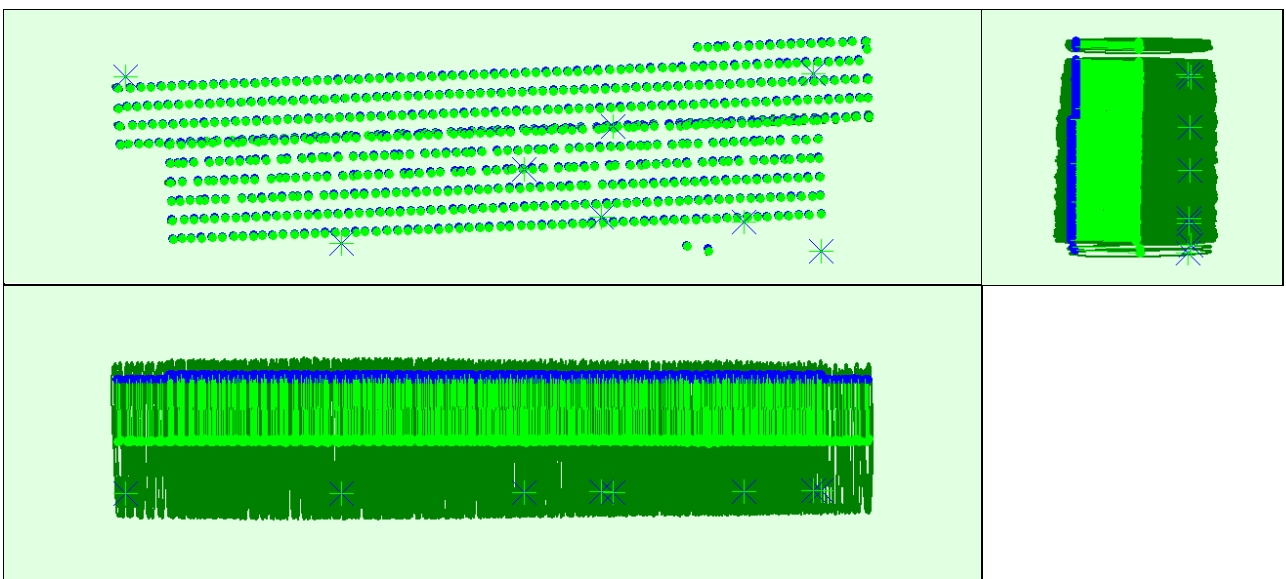


Figure 2: Top view of the initial image position. The green line follows the position of the images in time starting from the large blue dot.

Computed Image/GCPs/Manual Tie Points Positions



Uncertainty ellipses 100x magnified

Figure 3: Offset between initial (blue dots) and computed (green dots) image positions as well as the offset between the GCPs initial positions (blue crosses) and their computed positions (green crosses) in the top-view (XY plane), front-view (XZ plane), and side-view (YZ plane). Dark green ellipses indicate the absolute position uncertainty of the bundle block adjustment result.

🔍 Absolute camera position and orientation uncertainties



	X [US survey foot]	Y [US survey foot]	Z [US survey foot]	Omega [degree]	Phi [degree]	Kappa [degree]
Mean	0.124	0.117	3.843	0.018	0.024	0.006
Sigma	0.017	0.022	0.117	0.003	0.004	0.001

🔍 Overlap

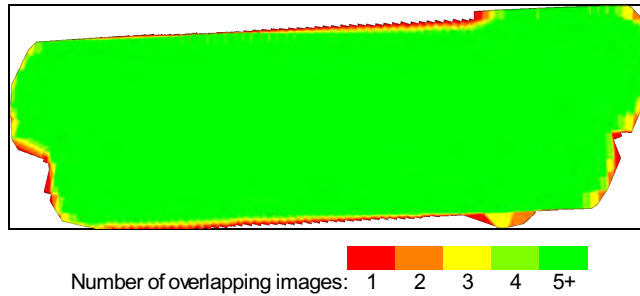


Figure 4: Number of overlapping images computed for each pixel of the orthomosaic. Red and yellow areas indicate low overlap for which poor results may be generated. Green areas indicate an overlap of over 5 images for every pixel. Good quality results will be generated as long as the number of keypoint matches is also sufficient for these areas (see Figure 5 for keypoint matches).

Bundle Block Adjustment Details



Number of 2D Keypoint Observations for Bundle Block Adjustment	1274533
Number of 3D Points for Bundle Block Adjustment	365009
Mean Reprojection Error [pixels]	0.100

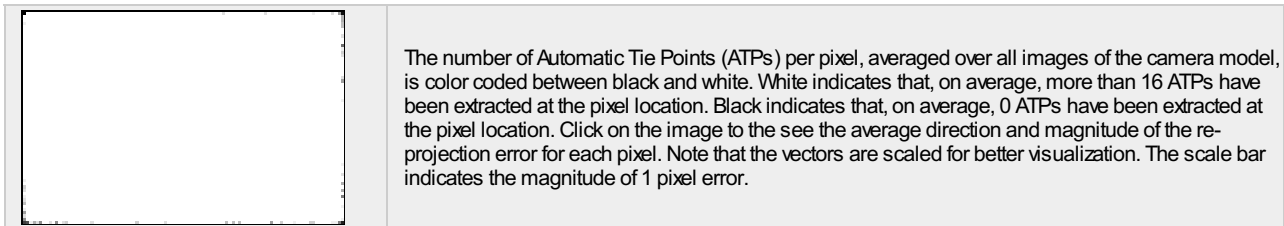
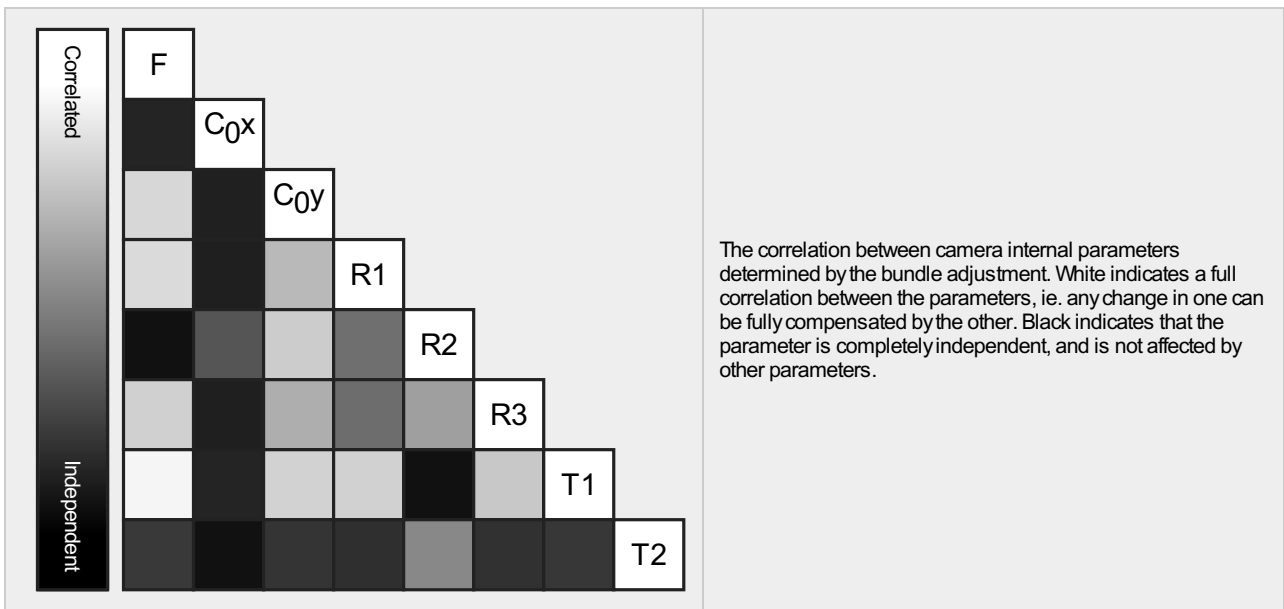
🔍 Internal Camera Parameters

📷 FC6310_8.8_5472x3648 (RGB). Sensor Dimensions: 12.833 [mm] x 8.556 [mm]



EXIF ID: FC6310S_8.8_5472x3648

	Focal Length	Principal Point x	Principal Point y	R1	R2	R3	T1	T2
Initial Values	3668.759 [pixel] 8.604 [mm]	2736.001 [pixel] 6.417 [mm]	1823.999 [pixel] 4.278 [mm]	0.003	-0.008	0.008	-0.000	0.000
Optimized Values	3506.625 [pixel] 8.224 [mm]	2739.359 [pixel] 6.425 [mm]	1806.828 [pixel] 4.237 [mm]	-0.011	-0.001	0.007	-0.002	0.000
Uncertainties (Sigma)	50.851 [pixel] 0.119 [mm]	0.859 [pixel] 0.002 [mm]	1.490 [pixel] 0.003 [mm]	0.000	0.001	0.001	0.000	0.000



2D Keypoints Table

	Number of 2D Keypoints per Image	Number of Matched 2D Keypoints per Image
Median	5499	1769
Mn	3503	585
Max	6896	3516
Mean	5376	1831

3D Points from 2D Keypoint Matches

	Number of 3D Points Observed
In 2 Images	198565
In 3 Images	67309
In 4 Images	33217
In 5 Images	20172
In 6 Images	11380
In 7 Images	7845
In 8 Images	5568
In 9 Images	4256
In 10 Images	3347
In 11 Images	2395
In 12 Images	1931
In 13 Images	1528
In 14 Images	1389
In 15 Images	1345
In 16 Images	1000
In 17 Images	653
In 18 Images	491
In 19 Images	527
In 20 Images	467
In 21 Images	401
In 22 Images	317
In 23 Images	235

In 24 Images	207
In 25 Images	181
In 26 Images	135
In 27 Images	59
In 28 Images	52
In 29 Images	24
In 30 Images	11
In 31 Images	1
In 32 Images	1

? 2D Keypoint Matches

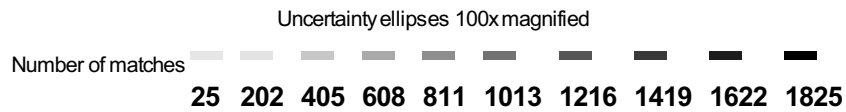
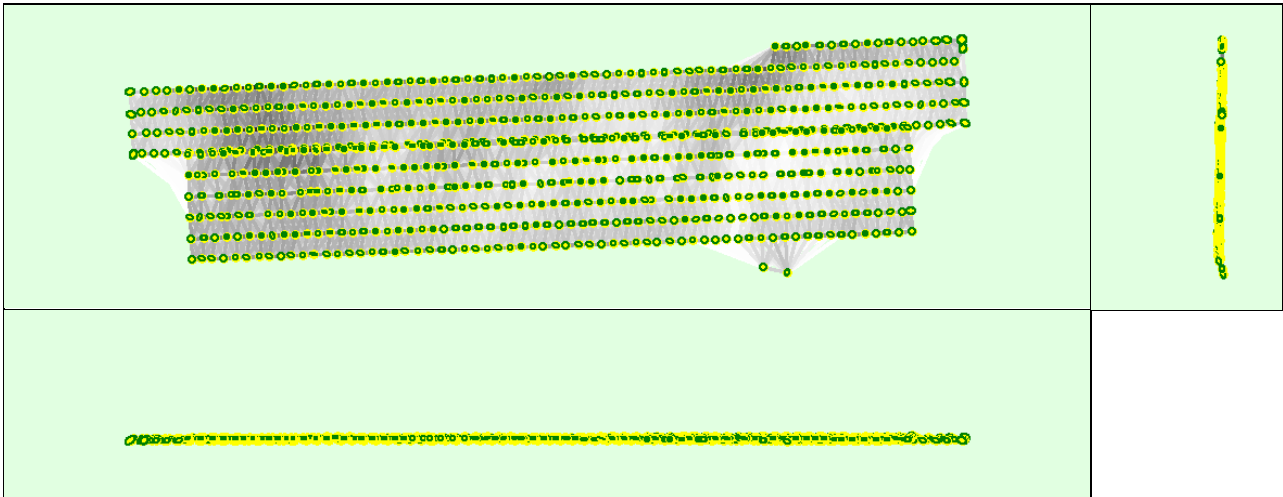


Figure 5: Computed image positions with links between matched images. The darkness of the links indicates the number of matched 2D keypoints between the images. Bright links indicate weak links and require manual tie points or more images. Dark green ellipses indicate the relative camera position uncertainty of the bundle block adjustment result.

? Relative camera position and orientation uncertainties



	X [US survey foot]	Y [US survey foot]	Z [US survey foot]	Omega [degree]	Phi [degree]	Kappa [degree]
Mean	0.121	0.105	0.070	0.015	0.020	0.008
Sigma	0.018	0.016	0.020	0.003	0.004	0.002

Geolocation Details



? Ground Control Points



GCP Name	Accuracy XYZ [US survey foot]	Error X [US survey foot]	Error Y [US survey foot]	Error Z [US survey foot]	Projection Error [pixel]	Verified/Marked
301 (3D)	0.020/0.020	0.006	-0.018	-0.023	0.028	3 / 3
302 (3D)	0.020/0.020	0.002	0.000	-0.000	0.097	11 / 11
303 (3D)	0.020/0.020	-0.001	-0.001	0.000	0.106	12 / 12
304 (3D)	0.020/0.020	-0.001	0.003	-0.000	0.197	14 / 14
305 (3D)	0.020/0.020	0.000	0.001	-0.000	0.086	12 / 12
306 (3D)	0.020/0.020	-0.001	-0.002	0.001	0.100	14 / 14
307 (3D)	0.020/0.020	0.002	-0.001	-0.001	0.074	12 / 12
309 (3D)	0.020/0.020	-0.001	0.002	-0.003	0.031	7 / 7

Mean [US survey foot]		0.000791	-0.002079	-0.003398		
Sigma [US survey foot]		0.002322	0.006136	0.007610		
RMS Error [US survey foot]		0.002453	0.006479	0.008334		

Localisation accuracy per GCP and mean errors in the three coordinate directions. The last column counts the number of calibrated images where the GCP has been automatically verified vs. manually marked.

🔍 Absolute Geolocation Variance



Mn Error [US survey foot]	Max Error [US survey foot]	Geolocation Error X [%]	Geolocation Error Y [%]	Geolocation Error Z [%]
-	-49.21	0.00	0.00	0.00
-49.21	-39.37	0.00	0.00	0.00
-39.37	-29.53	0.00	0.00	0.00
-29.53	-19.68	0.00	0.00	0.00
-19.68	-9.84	0.00	0.00	16.38
-9.84	0.00	52.73	42.39	29.02
0.00	9.84	47.27	57.61	45.98
9.84	19.69	0.00	0.00	8.62
19.69	29.53	0.00	0.00	0.00
29.53	39.37	0.00	0.00	0.00
39.37	49.21	0.00	0.00	0.00
49.21	-	0.00	0.00	0.00
Mean [US survey foot]		-2.737791	6.078725	318.304690
Sigma [US survey foot]		1.043746	1.042829	8.184375
RMS Error [US survey foot]		2.930001	6.167527	318.409892

Min Error and Max Error represent geolocation error intervals between -1.5 and 1.5 times the maximum accuracy of all the images. Columns X, Y, Z show the percentage of images with geolocation errors within the predefined error intervals. The geolocation error is the difference between the initial and computed image positions. Note that the image geolocation errors do not correspond to the accuracy of the observed 3D points.

Geolocation Bias	X	Y	Z
Translation [US survey foot]	-2.737791	6.078725	318.304727

Bias between image initial and computed geolocation given in output coordinate system.

🔍 Relative Geolocation Variance



Relative Geolocation Error	Images X [%]	Images Y [%]	Images Z [%]
[-1.00, 1.00]	100.00	100.00	100.00
[-2.00, 2.00]	100.00	100.00	100.00
[-3.00, 3.00]	100.00	100.00	100.00
Mean of Geolocation Accuracy [US survey foot]	16.404167	16.404167	32.808333
Sigma of Geolocation Accuracy [US survey foot]	0.000002	0.000002	0.000004

Images X, Y, Z represent the percentage of images with a relative geolocation error in X, Y, Z.

Geolocation Orientational Variance	RMS [degree]
Omega	0.460
Phi	0.890
Kappa	13.951

Geolocation RMS error of the orientation angles given by the difference between the initial and computed image orientation angles.

Initial Processing Details



System Information



Hardware	CPU: Intel(R) Core(TM) i7-3770 CPU @ 3.40GHz RAM: 16GB GPU: AMD FirePro W5100 (Driver: 21.19.154.1280)
Operating System	Windows 10 Pro, 64-bit

Coordinate Systems



Image Coordinate System	WGS 84 (EGM96 Geoid)
Ground Control Point (GCP) Coordinate System	NAD83(2011) / Nevada East (ftUS) (EGM96 Geoid)
Output Coordinate System	NAD83(2011) / Nevada East (ftUS) (EGM96 Geoid)

Processing Options



Detected Template	No Template Available
Keypoints Image Scale	Rapid, Image Scale: 0.25
Advanced: Matching Image Pairs	Aerial Grid or Corridor
Advanced: Matching Strategy	Use Geometrically Verified Matching: no
Advanced: Keypoint Extraction	Targeted Number of Keypoints: Automatic
Advanced: Calibration	Calibration Method: Standard Internal Parameters Optimization: All External Parameters Optimization: All Rematch: Auto, no

Point Cloud Densification details



Processing Options



Image Scale	multiscale, 1/2 (Half image size, Default)
Point Density	Optimal
Minimum Number of Matches	3
3D Textured Mesh Generation	yes
3D Textured Mesh Settings:	Resolution: Medium Resolution (default) Color Balancing: no
LOD	Generated: no
Advanced: 3D Textured Mesh Settings	Sample Density Divider: 1
Advanced: Image Groups	group1
Advanced: Use Processing Area	yes
Advanced: Use Annotations	yes
Time for Point Cloud Densification	03h:22m:02s
Time for Point Cloud Classification	NA
Time for 3D Textured Mesh Generation	39m:11s

Results



Number of Processed Clusters	3
Number of Generated Tiles	4
Number of 3D Densified Points	83178902
Average Density (per US survey foot ³)	8.38

DSM, Orthomosaic and Index Details



Processing Options



DSM and Orthomosaic Resolution	1 x GSD (2.3 [cm/pixel])
DSM Filters	Noise Filtering: yes Surface Smoothing: yes, Type: Sharp
Raster DSM	Generated: yes Method: Inverse Distance Weighting Merge Tiles: yes
Orthomosaic	Generated: yes Merge Tiles: yes GeoTIFF Without Transparency: no Google Maps Tiles and KML: no
Grid DSM	Generated: yes, Spacing [cm]: 20
Time for DSM Generation	01h:26m:34s
Time for Orthomosaic Generation	02h:21m:43s
Time for DTM Generation	00s
Time for Contour Lines Generation	00s
Time for Reflectance Map Generation	00s
Time for Index Map Generation	00s

Aerial LiDAR Accuracy Statement

Instrument Datasheet Accuracy:

Alta's Trimble and CHC GNSS base stations are rated at 1-cm RMSE accuracy while operating in static logging modes. The GNSS receivers and Velodyne LiDAR sensor deployed by Alta for our airborne mapping are rated at 2-cm RMSE accuracy for their individual components during kinematic operational modes. The system accuracy of the LidarUSA Snoopy A-Series LiDAR Scanner is rated at 3-cm RMSE within the typical operational range of data collection.

Typical Operational Accuracy:

After performing a least squares adjustment constrained to our fixed ground targets, the remaining unconstrained control points are within the typical survey grade accuracy required for topography mapping and civil design projects. Sampled control and transect points tested against the National Map Accuracy Standards (NMAS) and National Standard for Spatial Data Accuracy (NSSDA) criteria easily meet or exceed the statistical requirements for 1-foot contour intervals typically specified for civil design requirements even prior to adjustment.

Observed Operational Accuracy:

After performing a least squares adjustment constrained to our fixed ground targets, the remaining unconstrained control points are within 7.1 cm RMSE.

Observed LiDAR Data Density:

Our Velodyne LiDAR sensor uses 32 individual lasers arranged within a 40-degree field of view and produces 700,000 points per second in a 360-degree coverage to an effective range of 100 meters. Observed point density on the ground surface ranges from 100 to 500 points per square meter

LiDAR Data Classification:

Each LiDAR return processed within the final point cloud typically represents the surface or object that it hits. Classification is the process that categorizes each of the data points into a class that represents the ground, trees, other vegetation, buildings, utility lines, etc. This automated process can be refined manually and further segregated into sub-classes of data based on elevation, intensity, slope, image colorization, and other algorithms or manual methods depending on the project requirements. The bare earth surface was used to construct contours, profiles and cross sections.